The Role of the Neural Cell Adhesion Molecule Ncam1b during Development and Regeneration of the Zebrafish Lateral Line System

---

Die Rolle des Neuronalen Zelladhäsionsmoleküls Ncam1b während der Entwicklung und Regeneration des Seitenliniensystems im Zebrafisch

Zur Erlangung des akademischen Grades einer

DOKTORIN DER NATURWISSENSCHAFTEN

(Dr. rer. nat.)

von der KIT-Fakultät für Chemie und Biowissenschaften

des Karlsruher Instituts für Technologie (KIT)

genehmigte

DISSERTATION

von

M. Sc. Annemarie Lange

1. Referent: Prof. Dr. Martin Bastmeyer
2. Referent: Prof. Dr. Nicholas S. Foulkes
Tag der mündlichen Prüfung: 16.07.2024

Selbstständigkeitserklärung

Der experimentelle Teil der vorliegenden Arbeit wurde von Januar 2020 bis Juni 2024 am Zoologischen Institut in der Abteilung für Zell- und Neurobiologie des Karlsruher Instituts für Technologie (KIT) durchgeführt. Hiermit erkläre ich, dass ich die vorliegende Arbeit selbstständig und ohne fremde Hilfe verfasst und keine anderen Hilfsmittel als angegeben verwendet habe. Insbesondere versichere ich, dass ich alle wörtlichen und sinngemäßen Übernahmen aus anderen Werken als solche kenntlich gemacht habe. Die Satzung zur Sicherung guter wissenschaftlicher Praxis am Karlsruher Institut für Technologie (KIT) habe ich in der gültigen Fassung beachtet. Diese Arbeit wurde in keiner Form einer anderen Prüfungsbehörde vorgelegt. Ich versichere außerdem, dass die beigelegte elektronische Version der Arbeit mit der schriftlichen Version der Arbeit übereinstimmt.

Karlsruhe, den 11. Juni 2024 _____

Abstract

Sensory hair cells (HCs) are essential for sound perception and transmission in the mammalian ear. The inability of the adult mammalian inner ear to regenerate HCs after damage leads to irreversible hearing loss. Unlocking the mechanisms of HC development and regeneration is therefore a key goal for developing therapies to restore hearing. HCs of the mammalian inner ear are functionally homologous to the HCs found in the mechanosensory lateral line system of aquatic vertebrates like zebrafish, which detects water movements and vibrations. The zebrafish provides a powerful model system in this regard, as it possesses an amazing ability to regenerate HCs in the superficially located posterior lateral line organ (pLLO).

The present study focuses on the role of the neural cell adhesion molecule Ncam1b in the development and regeneration of the posterior lateral line system (pLLS). NCAM in general is essential for neuronal development; it facilitates cell-cell contacts that enable organized cell migration, axon growth, and fasciculation. In zebrafish, Ncam1 has two paralogs, Ncam1a and Ncam1b, which arose from a genome duplication event. Previous studies in our lab have demonstrated that a morpholino knockdown of *ncam1b* has severe consequences for the development of the pLLS [Dries et al., 2021]. Reductions in primordium size, neuromast numbers, and migration distance were observed. These anomalies are attributed to the fact that Ncam1b interacts with FGF receptor Fgfr1a in the Trailing Zone of the primordium. After *ncam1b* knockdown, FGF signaling is reduced in this area, leading to disrupted proliferation. These findings underscore the central role of Ncam1b in the formation of pLLS in zebrafish.

In the current study, CRISPR/Cas9-induced *ncam1b* mutants were generated, because of ongoing controversies surrounding the reliability of morpholino knockdown approaches. Surprisingly, the knockout of *ncam1b* did not cause the same effects as the knockdown with morpholinos. This discrepancy is likely attributed to genetic compensation mechanisms, evidenced by the upregulation of genes like the *ncam1a* paralog or *l1cam* in *ncam1b* mutants. While *ncam1b* mutants did not show severe morphological defects during pLLS development, molecular analyses revealed that Ncam1b orchestrates the balance between Wnt and FGF signaling pathways within the primordium. This was obvious by a disrupted spatial distribution of proliferating cells in the primordium. The total number of proliferating cells, however, remained unaltered.

Although Ncam1b is expressed in HCs during pLLO development, HC development proceeded unaffected in *ncam1b* mutants. Ncam1b is, however, crucial for HC regeneration after neomycin-induced damage. The absence of *ncam1b* led to an accumulation of proliferating support cells that failed to differentiate properly into HCs. Since the *ncam1b* mutant phenotype could be rescued by DAPT-mediated Notch inhibition, it is assumed that Ncam1b modulates the Notch signaling pathway to coordinate the balance between support cell proliferation and HC differentiation. This may be achieved via Ncam1b binding to Fgfr1a. In contrast to pLLS development, where Ncam1a likely plays a key role in genetic compensation, Ncam1a did not appear to be involved in compensating for the loss of Ncam1b during regeneration in *ncam1b* mutants.

The mutant analyses suggest that Ncam1b serves two distinct functions in the pLLS of zebrafish. On one hand, it regulates cell proliferation during development, while on the other hand, it triggers HC differentiation during regeneration in mature neuromast structures.

Zusammenfassung

Haarsinneszellen (HSZ) sind für die Schallwahrnehmung und -weiterleitung unerlässlich. Allerdings sind diese Zellen im adulten Säugerinnenohr normalerweise nicht regenerationsfähig, was zu irreversiblem Hörverlust führt. Die Entschlüsselung der Mechanismen der Haarzellentwicklung und -regeneration ist daher ein wichtiges Ziel für die Entwicklung von Therapien zur Wiederherstellung des Gehörs. Die HSZ des adulten Säugerinnenohrs sind funktionell homolog zu den HSZ des mechanosensorischen Seitenlinienorgans aquatischer Wirbeltiere wie dem Zebrafisch, das Wasserbewegungen und Vibrationen wahrnimmt. Der Zebrafisch erweist sich als äußerst gutes Modellsystem, da er über die bemerkenswerte Fähigkeit verfügt, Haarzellen im oberflächennahen posterioren Seitenlinienorgan zu regenerieren.
Die vorliegende Studie konzentrierte sich auf die Rolle des neuronalen Zelladhäsionsmoleküls Ncam1b in der Entwicklung und Regeneration des posterioren Seitenlinienorgans (pSLO). NCAM, im Allgemeinen, ist essentiell für die neuronale Entwicklung und ermöglicht organisierte Zellmigration, Axonwachstum und Faszikulation. Infolge einer Genomduplikation im Zebrafisch entstanden die Paraloge Ncam1a und Ncam1b. Frühere Studien zeigten, dass ein Morpholino-*Knockdown* von *ncam1b* schwerwiegende Auswirkungen auf die pSLO-Entwicklung hat, wie reduzierte Primordiumgröße, Neuromastenzahlen und Migrationsdistanz. Dies wird auf die Interaktion von Ncam1b mit dem FGF-Rezeptor Fgfr1a im Primordium und die daraus resultierende gestörte Proliferation zurückgeführt.
In der aktuellen Studie wurden CRISPR/Cas9-induzierte *ncam1b*-Mutanten im Zebrafisch erzeugt und analysiert, da anhaltende Zweifel an der Aussagekraft von Morpholino-*Knockdown*-Ansätzen bestehen. Überraschenderweise verursachte der *Knockout* von *ncam1b* nicht die gleichen Effekte wie der *Knockdown*. Diese Diskrepanz ist wahrscheinlich auf genetische Kompensationsmechanismen zurückzuführen, die durch die Hochregulation von Genen wie dem *ncam1a*-Paralog oder *l1cam* in *ncam1b*-Mutanten belegt wurden. Obwohl *ncam1b*-Mutanten während der pSLO-Entwicklung keine schweren morphologischen Defekte aufwiesen, zeigten molekulare Analysen, dass Ncam1b das Gleichgewicht zwischen den Wnt- und FGF-Signalwegen innerhalb des pSLO-Primordiums orchestriert. Dies äußerte sich lokal in einer gestörten räumlichen Verteilung proliferierender Zellen, während die Gesamtzahl unverändert blieb. Ncam1b wird zwar während der pSLO-Entwicklung in HSZ exprimiert, *ncam1b*-Mutanten zeigten jedoch keine Probleme in der Entwicklung von HSZ. Allerdings führte der *ncam1b Knockout* zu einer beeinträchtigten Regeneration von HSZ nach Neomycin-induzierter Schädigung. *ncam1b* Mutanten zeigten eine Ansammlung proliferierender Stützzellen, die sich nicht ordnungsgemäß zu HSZ differenzierten. Aus der Tatsache, dass dieser *ncam1b*-Mutanten-Phänotyp durch DAPT-vermittelte Notch-Inhibition gerettet werden konnte, wird vermutet, dass Ncam1b den Notch-Signalweg moduliert, um das Gleichgewicht zwischen Stützzellproliferation und Differenzierung von HSZ zu koordinieren. Dies könnte über die Bindung von Ncam1b an Fgfr1a erreicht werden. Im Gegensatz zur pSLO-Entwicklung, bei der Ncam1a wahrscheinlich eine Schlüsselrolle bei der genetischen Kompensation spielt, schien Ncam1a nicht als Kompensator während der Regeneration in *ncam1b*-Mutanten beteiligt gewesen zu sein.
Zusammenfassend deuten die Mutantenanalysen auf zwei unterschiedliche Funktionen von Ncam1b im pSLO des Zebrafischs hin. Während es an der Regulation der Zellproliferation während der embryonalen Entwicklung beteiligt ist, spielt es eine Rolle bei der Initiierung der Differenzierung von HSZ während des Regenerationsprozesses in reifen Neuromasten.

Contents

1 Introduction

Hair cells in the inner ear can be damaged by excessive noise, aging, and ototoxic drugs, often resulting in permanent hearing loss and balance disorders [Forge and Schacht, 2000, Petit et al., 2001, Seidman et al., 2002, Chen and Fechter, 2003, Matsui and Cotanche, 2004, Yorgason et al., 2006, Bielefeld et al., 2010, Oishi and Schacht, 2011, Kidd and Bao, 2012]. Unlike mammals, which have limited or no ability to regenerate damaged hair cells in the inner ear, non-mammalian vertebrates including fish [Harris et al., 2003, Hernández et al., 2006], birds [Corwin and Cotanche, 1988, Ryals and Rubel, 1988], and amphibians [Taylor and Forge, 2005], replace degenerated hair cells through proliferation and differentiation of support cells throughout their lifespan. The zebrafish lateral line, a sensory system for detecting water movements, contains hair cells that share structural and functional similarities with cochlear hair cells in mammals. These hair cells are optically and pharmacologically more accessible and examinable within an intact organism, making the zebrafish an excellent model for investigating hair cell development and regeneration. Additionally, the ability to easily manipulate zebrafish embryos allows the investigation of different types of mutations. The development and regeneration of the zebrafish lateral line require the formation of cell clusters, which strongly depend on cell adhesion proteins. Calcium-dependent cell adhesion molecules like cadherins [Kerstetter et al., 2004, Matsuda and Chitnis, 2010, Colak-Champollion et al., 2019], but also calcium-independent proteins, like the neural cell adhesion molecule 1 (Ncam1) play a crucial role in this process [Hinsby et al., 2004, Dries et al., 2021]. NCAM1 is considered the first and most extensively characterized cell surface glycoprotein [Jørgensen and Bock, 1974, Hinsby et al., 2004]. It plays a crucial role in mediating cell-cell contacts and promoting cell adhesion, processes that are vital for the development, maintenance, and regeneration of the nervous system, including the lateral line system [Rutishauser et al., 1982]. Ncam1 is expressed in the posterior lateral line system of zebrafish [Langhauser et al., 2012] and plays a crucial role in the development of the lateral line organ [Dries et al., 2021].

In the present study, the role of Ncam1b, a specific isoform of Ncam1, was investigated during development and regeneration of the posterior lateral line organ using different *ncam1b* knockout lines.

1.1 The lateral line system: a vital sensory modality in fish and amphibians

The lateral line is a sensory system present in fish and amphibians, responsible for the detection of pressure changes and water disturbances in the vicinity of the animal's body [Dykgraaf, 1933]. This "touch-at-a-distance" sense is vital for the performance of complex motor behaviors, including navigation, prey tracking, predator avoidance, rheotaxis, schooling, and sexual courtship [Dykgraaf, 1963, Montgomery et al., 1997, Coombs and Montgomery, 1999, Montgomery et al., 2000]. The lateral line system consists of two major branches: the anterior lateral line, extending towards the head [Raible and Kruse, 2000], and the posterior lateral line running along the trunk to the tip of the tail [Gompel et al., 2001]. Both systems comprise a number of sensory organs called neuromasts, which are distributed on the surface of the animal's skin in a species-specific pattern. The distribution of those sensory neuromasts over the entire body of the fish allows the fish to assign signals to their direction.

1.2 The development of the posterior lateral line system

The posterior lateral line system (pLLS) of zebrafish originates from the primary sensory lateral line placode (pLLP), an ectodermal thickening posterior to the otic placode [Ghysen and Dambly-Chaudière, 2007]. The otic placode will develop into the otic vesicle - the precursor of the inner ear structures (Fig. 1.1 A (ov) + Fig. 1.2 A + B). Prior to 10 hours post fertilization (hpf), Fibroblast growth factor (FGF) signaling inhibits pLLP specification, maintaining a uniform population of undifferentiated cells. Towards the end of gastrulation, retinoic acid begins to inhibit FGF signaling, allowing the pLLP to initiate its differentiation process [Nikaido et al., 2017]. Around 18 hpf, the pLLP divides into two distinct cell clusters: the anterior group of around 20 cells forms the posterior lateral line ganglion (pLLG), while the posterior group of around 100 cells becomes the primary posterior lateral line primordium (Fig. 1.1 A + Fig. 1.2 D) [Metcalfe et al., 1985, Kimmel et al., 1995]. After segregating from the ganglion, the primordium starts migrating caudally along the horizontal myoseptum beneath the epidermis, reaching the tail tip by 40-48 hpf (Fig. 1.1 A) [Metcalfe et al., 1985, Kimmel et al., 1995]. During its migration, the primordium periodically deposits primary proneuromasts (pnms) every 5-7 somites, with the first pnm (L1) forming around 26 hpf (Fig. 1.1 B + Fig.1.2 C).

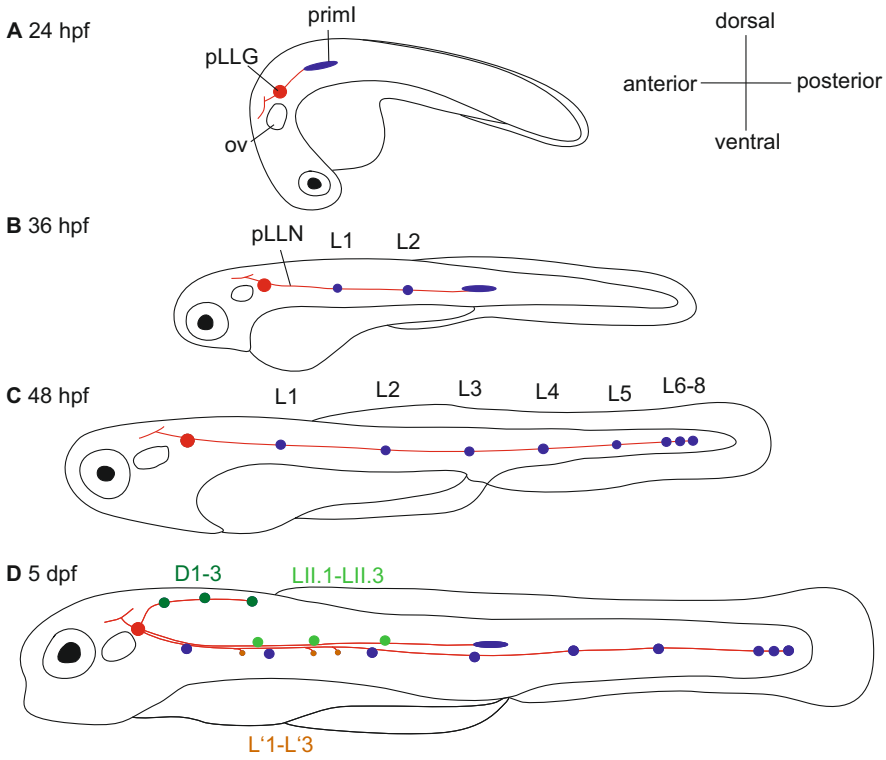

Figure 1.1: Development of the posterior lateral line system. (A) The primordium (primI) starts its migration rostral of the posterior lateral line ganglion (pLLG) and the otic vesicle (ov) along the horizontal myoseptum. **(B)** During migration, proneuromasts are formed within primI, which are deposited along the migration path and differentiate into neuromasts (L1, L2,...). **(C)** At 48 hpf, primI reaches the tip of the tail and breaks into three terminal proneuromasts (L6-L8). **(D)** The second posterior primordium (primII) migrates along the same route as primI and deposits additional neuromasts (LII.1-LII.3). The dorsal primordium primD (not shown) migrates anteriorly and deposits additional dorsal neuromasts (D1-3). Interneuromast cells form intercalary neuromasts (L'1-L'3). Modified from Pujol-Martí and López-Schier (2013).

This process continues until the primordium reaches the tail, where it breaks into three terminal proneuromasts (Fig. 1.1 C). Each pnm consists of approximately 20 cells and serves as a sensory organ precursor that will differentiate into a mature primary neuromast (Fig. 1.2) [Ghysen and Dambly-Chaudière, 2007]. These mechanosensory units are embedded in stable epithelia and are functionally analogous to the inner ear [Ghysen and Dambly-Chaudière, 2007]. In addition to neuromast cells, the primordium also releases interneuromast cells, which act as progenitors for additional neuromasts [Grant et al., 2005]. Peripheral axons extending from the pLLG and following the migrating primordium innervate the sensory hair cells of the deposited neuromasts [Metcalfe et al., 1985]. To form the posterior lateral line nerve (pLLN), these axons are bundled together by Schwann cells, which wrap around them to create a compact bundle [Gilmour et al., 2002].
Around 38 hpf, a secondary placode forms near the primary pLLP, splitting into three groups of cells [Sapède et al., 2002]. One group directly differentiates into the D1 neuromast at the location of the placode, while two other groups form the secondary posterior primordium (primII) and the dorsal primordium (primD) (Fig. 1.1 D). At 48 hpf, primII follows the path of the primordium and deposits up to three proneuromasts (LII.1-LII.3) between the previously deposited neuromasts [Sapède et al., 2002]. PrimD migrates to the dorsal side of the embryo and releases two proneuromasts (D2 and D3) between the head and the dorsal fin. These later-born neuromasts form the secondary posterior lateral line, with bipolar nerve cells originating from the secondary pLLG and neural crest-derived glial cells connecting primary and secondary neuromasts [Ledent, 2002, Pujol-Martí and López-Schier, 2013]. The posterior lateral line organ (pLLO) undergoes complete development and differentiation in 21 days, during which lateral neuromasts derived from primI and primII migrate from the horizontal myoseptum to the ventral region of the zebrafish [Sapède et al., 2002, Ledent, 2002, Nuñez et al., 2009]. This mechanism allows the lateral line to expand and adapt as the fish matures.

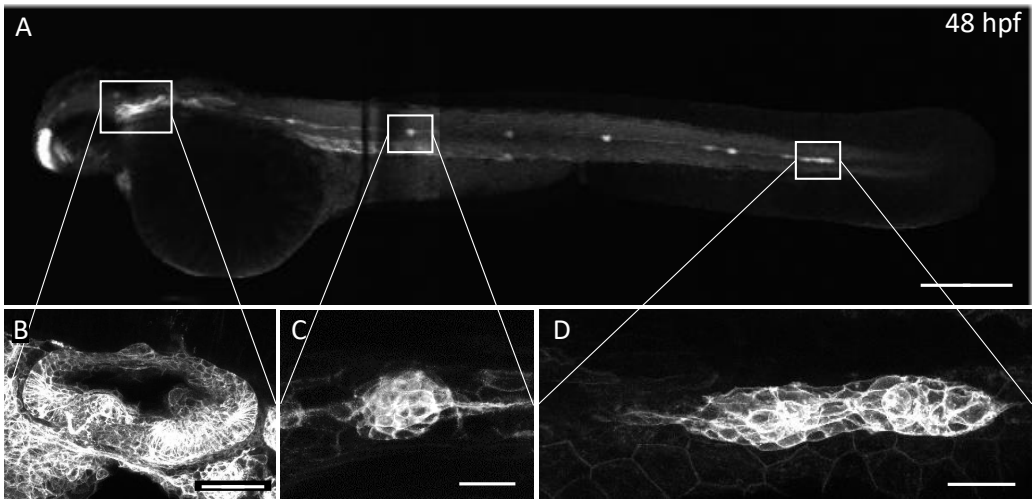

Figure 1.2: Prominent structures during the development of the lateral line organ. (A) A lateral view of a *Tg(ClaudinB::lynGFP)* embryo expressing GFP under the control of the ClaudinB promoter allows visualization of the lateral line system, 48 hpf. **(D)** The primordium (primI) begins its migration near **(B)** the otic vesicle (ov) and deposits **(C)** proneuromasts (pnms) along the way to the tip of the tail. These proneuromasts will differentiate into the sensory organs known as neuromasts. Scale bars **(A)** 200 µm, **(B)** 40 µm, **(C - D)** 20 µm.

1.3 Signaling in the developing and migrating lateral line primordium

The posterior lateral line primordium exhibits a distinct anterior-posterior polarity, characterized by morphological and signaling differences between the Leading Zone at the posterior end and the Trailing Zone at the anterior end (Fig. 1.3). In the Leading Zone of the primordium, Wnt signaling triggers the expression of its target gene protein Lymphoid Enhancer-binding Factor 1 (Lef1). Lef1 is a transcription factor that stimulates the proliferation of primorial pseudomesenchymal cells [Lecaudey et al., 2008, Gamba et al., 2010]. Additionally, the expression of the diffusible FGF ligands, Fgf 3 and Fgf 10 (Fgf 3/10), as well as of the cytoplasmic membrane-associates FGF-inhibitor Sef, are initiated in this region [Aman and Piotrowski, 2008, Lecaudey et al., 2008]. Sef prevents the binding of Fgf 3/10 to the weakly expressed Fibroblast Growth Factor Receptor 1a (Fgfr1a) in the Leading Zone, protecting leading mesenchymal cells from acquiring epithelial morphology [Aman and Piotrowski, 2008, Lecaudey et al., 2008]. Fgf 3/10 utilize heparan sulfate proteoglycans as carriers to facilitate their diffusion from the Leading Zone to the Trailing Zone [VeneroGalanternik et al., 2015]. Once they reach the Trailing Zone, Fgf 3/10 activate Fgfr1a, thereby establishing an FGF signaling center in the rostral region of the primordium [Aman and Piotrowski, 2008]. FGF signaling orchestrates rosette formation and proliferation in the Trailing Zone [Aman and Piotrowski, 2008, Lecaudey et al., 2008]. In addition, it triggers expression of FGF target genes, such as *pea3* and the Wnt inhibitor *dickkopf 1* (*dkk1*). This establishes two antagonistic signal systems in the primordium - FGF signaling in the Trailing Zone and Wnt signaling in the Leading Zone [Aman and Piotrowski, 2008].

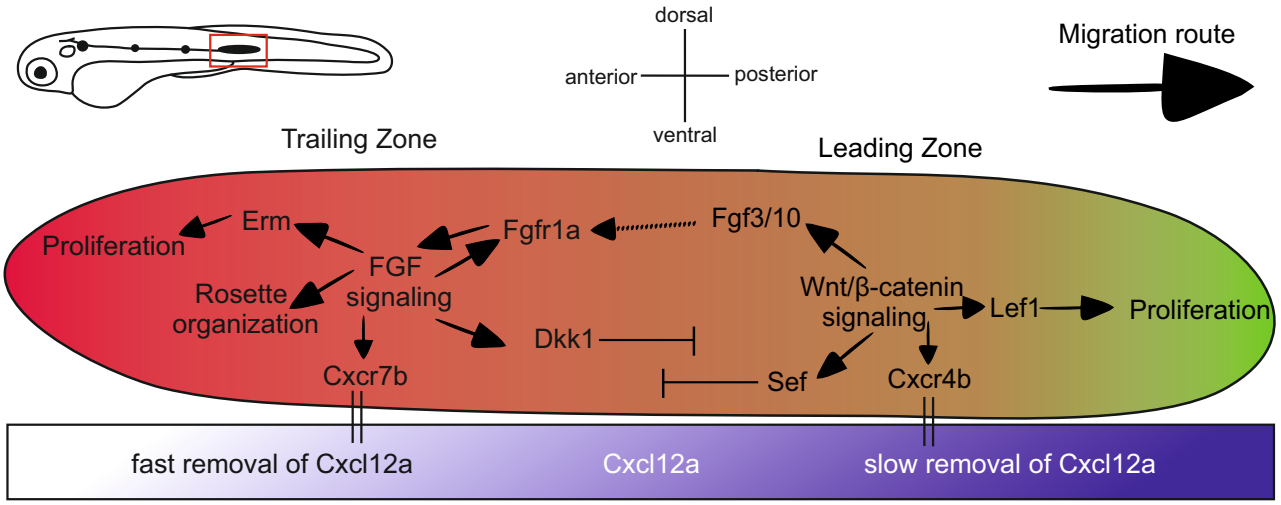

Figure 1.3: Signaling in the posterior lateral line primordium. The lateral line primordium is divided into two distinct zones: the Leading Zone and the Trailing Zone. The Leading Zone is located caudally, in the direction of the primordium migration. In this region, Wnt signaling induces the expression of the transcription factor Lef1, which stimulates the proliferation of the pseudomesenchymal cells. Additionally, Wnt signaling leads to the expression of Fgf 3/10 and the FGF inhibitor Sef. In the Trailing Zone, the diffusible Fgf 3/10 ligands bind to Fgfr1a, activating FGF signaling. This FGF signaling promotes the differentiation of the pseudomesenchymal cells into epithelial cells, which then organize into rosettes. In addition, FGF signaling regulates local proliferation. In the Trailing Zone, Wnt signaling is inhibited by the FGF-dependent inhibitor Dickkopf 1 (Dkk 1). In addition, the polarized activity of the Wnt and FGF signaling pathways establishes a polarized chemokine gradient (Cxcr 4b vs. Cxcr 7b). The Cxcr 7b receptor binds and internalizes the Cxcl 12a ligand, thereby generating a gradient of Cxcl 12a (turquoise). The primordium is then able to migrate towards this Cxcl 12a gradient. Modified from Ma and Raible (2009).

Precise regulation of these two signaling pathways is essential for the normal directional migration of the primordium and deposition of proneuromasts [Aman and Piotrowski, 2008]. Inhibition of either Wnt or FGF signaling can severely impair cell proliferation in the primordium, with FGF inhibition having the most dramatic effect in completely abolishing proliferation [Aman et al., 2011]. This underscores the crucial role that these developmental signaling pathways play in enabling the development and migration of the primordium. As the primordium migrates from the otic vesicle along the horizontal myoseptum towards the tail, it utilizes a complex signaling network, with chemokine signaling to play a crucial role in guiding this directional movement (bottom part of Fig. 1.3). Chemokines, known for their chemotactic properties, are secreted proteins that signal through G-protein coupled receptors. They function in diverse tissues such as leukocytes, blood vessels, and neurons [Raman et al., 2011]. Adjacent muscle cells along the horizontal myoseptum release the chemokine ligand Cxcl 12a (Sdf1a) to guide the migration process [David et al., 2002]. To ensure this directed migration, the primordium exhibits an asymmetric expression pattern of the chemokine receptors Cxcr 4b and Cxcr 7b. Cxcr 4b is broadly expressed throughout the primordium, with decreasing levels towards the rostral end. In contrast, Cxcr 7b is specifically expressed in the Trailing Zone [Valentin et al., 2007]. Cxcr 7b binds the Cxcl 12a chemokine, leading to internalization and the establishment of a chemokine gradient. This Cxcl 12a gradient guides the primordium by chemoattraction, directing it towards higher chemokine concentration [Haas and Gilmour, 2006, Dambly-Chaudière et al., 2007, Valentin et al., 2007]. The asymmetric expression of Cxcr 4b and Cxcr 7b is tightly regulated by antagonistic interactions between Wnt/β-Catenin signaling in the Leading Zone and FGF signaling in the Trailing Zone [Aman and Piotrowski, 2008, Breau et al., 2012]. This indicates an interplay of chemokine signaling, receptor expression patterning, and cross-regulation between key signaling pathways orchestrating the directed migration of the primordium during zebrafish embryogenesis.

1.4 Neuromast formation and specification of hair cell precursors

pLLS development involves a complex interplay of signaling pathways orchestrating the formation and patterning of neuromasts - the mechanosensory organs that house the hair cells. During the migration of the primordium, proneuromasts are formed as the migration of pseudomesenchymal cells slows down once they move from the Leading to the Trailing Zone. Here, FGF signaling replaces Wnt signaling causing the pseudomesenchymal cells to differentiate into epithelial cells. At regular intervals, however, single cells retain their mesenchymal character. These cells subsequently differentiate into hair cells. They become surrounded by epithelial cells, which express increased levels of tight junction proteins, adherens junctions, and desmosomes. This causes apical constriction leading to the rosette appearance of the proneuromasts [Lecaudey et al., 2008]. Aman et al. (2011) hypothesized that chemokine signaling is also involved in the deposition process.

The specification of the first hair cells in newly deposited neuromasts depends on FGF receptor activation by FGF ligands diffusing from the Leading Zone to the Trailing Zone (Fig. 1.4). This FGF signaling triggers activation of *atonal homolog 1a* (*atoh1a*) in a central progenitor cell [Lecaudey et al., 2008, Nechiporuk and Raible, 2008]. The *atoh1a* signal induces the expression of the ligands Fgf 3/10, as well as of the membrane-bound Notch ligand, Delta D. Delta D activates the Notch 3 receptor in nearby potential non-sensory support cells, preventing them from expressing *atoh1a* and thereby enabling their differentiation into support cells [Matsuda and Chitnis, 2010]. The initial hair cell progenitor maintains the expression of *atoh1a* and becomes an independent FGF ligand source,

increasing Fgf 3/10 levels while suppressing its own receptor Fgfr1a [Lecaudey et al., 2008, Matsuda and Chitnis, 2010]. As hair cell progenitors mature, their identity becomes determined by intrinsic self-regulatory mechanisms rather than extrinsic FGF signaling [Matsuda and Chitnis, 2010]. This is facilitated by the *atoh1a*-dependent activation of the expression of another key transcription factor, *atoh1b*. *atoh1b* helps to maintain the expression of *atoh1a* through a cross-activation mechanism, allowing the hair cell progenitor to sustain its own differentiation program. The continued expression of Fgfr1a in the surrounding cells maintains their competence to receive FGF activation signals, enabling the formation of stable epithelial rosettes.

The ability of *atoh1a* to drive Fgf 3/10 and Delta D expression in the central hair cell progenitor is crucial for proneuromast formation. By expressing Fgf 3/10 and Delta D, the progenitor maintains FGF and Notch signaling in neighboring support cells. As an Fgf 3/10 source, it can induce *atoh1a* expression and generate additional hair cell progenitors in nearby cells. Simultaneously, Notch signaling tightly regulates this induction, inhibiting *atoh1a* expression to prevent excess hair cell progenitor production until needed. In summary, the hair cell progenitor promotes new progenitor formation via Fgf 3/10, while Notch signaling prevents uncontrolled hair cell differentiation in neighboring cells. This balanced FGF-Notch interplay enables ordered patterning and differentiation of hair cells and support cells within the developing neuromast [Chitnis et al., 2012].

The newly formed hair cell progenitor, now an independent source of both, FGF ligands and the Notch ligand Delta D, can activate *atoh1a* expression in its neighboring cells. This allows the progenitor to promote the specification of additional hair cell progenitors in its vicinity. Through this interplay between FGF and Notch signaling, the hair cell progenitor and its surrounding support cell precursors become specified, marking the first major event of cell diversification in the developing neuromast. This transition to FGF-independent hair cell progenitor identity, driven by the cross-regulatory relationship between *atoh1a* and *atoh1b*, is a crucial step in establishing the proper patterning and differentiation of hair cells and support cells in the posterior lateral line system.

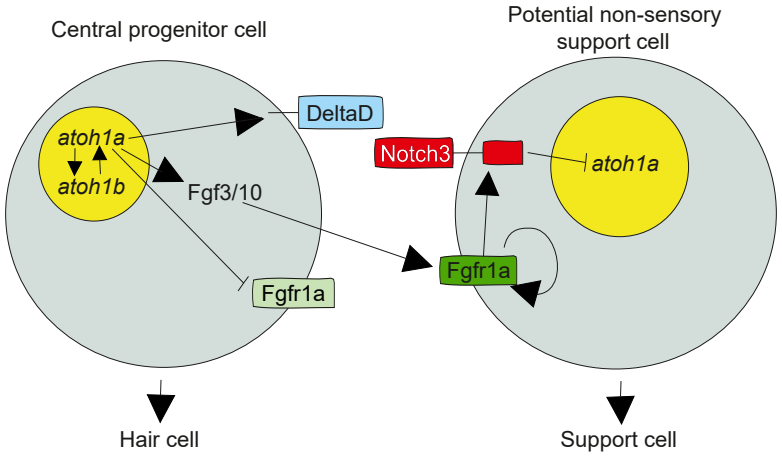

Figure 1.4: Signaling during specification of hair cells and support cells. The central progenitor hair cell expresses *atoh1a*, which then initiates the expression of *atoh1b*. These two transcription factors drive each other's expression, creating a positive feedback loop. As a result of the *atoh1a*/*atoh1b* expression, the central cell starts to express Fgf 3/10 and Delta D. Additionally, the expression of Fgfr1a is inhibited in the central cell, leading to decreased FGF signaling in this cell. In contrast, the surrounding potential non-sensory support cells encounter heightened FGF signaling due to the Fgf 3/10 ligand secreted from the central cell. Increased FGF signaling in these cells activates Notch signaling, which prevents the support cells from expressing *atoh1a* and differentiating into hair cells. Modified from Matsuda and Chitnis (2010).

1.5 Neuromast structure

The posterior lateral line system is composed of rosette-shaped structures called neuromasts consisting of three major cell types: the mechanosensory hair cells, surrounded by support and mantle cells (Fig. 1.5). The hair cells in the neuromasts extend actin-based stereocilia and a single microtubule-based kinocilium into the water. The tips of the stereocilia are connected by molecular strands of Cadherin 23 and Protocadherin 15, known as tip links [Kazmierczak et al., 2007]. Support cells are located around and underneath the hair cells and serve as a source of progenitors that replace hair cells during homeostasis and regeneration. Mantle cells are the outermost cells of the neuromast. They form the gelatinous cupula, which encloses the neuromast and protects it from mechanical influences [Romero-Carvajal et al., 2015]. Water movements cause mechanical deflection of stereocilia and kinocilia. If the deflection of stereocilia is towards the kinocilium the cell depolarizes, while deflection away from the kinocilium hyperpolarizes it [Hudspeth, 1989]. This stimulus can be transmitted from the neuromast to the brain by the pLLN, whose afferent nerve fibers innervate the mature neuromasts. Bipolar nerve cells of the pLLN project to neurons in the *media octavolateralis nuclei* in the hindbrain, from where signal transmission proceeds to the *torus semicircularis*, the center of the auditory system [Bleckmann, 2008]. Additionally, axons from the primary pLLN project to the neuronal mauthner cells, which are located in the fourth rhombomere of the hindbrain. Their stimulation triggers "fast escape responses" [Pujol-Martí and López-Schier, 2013].

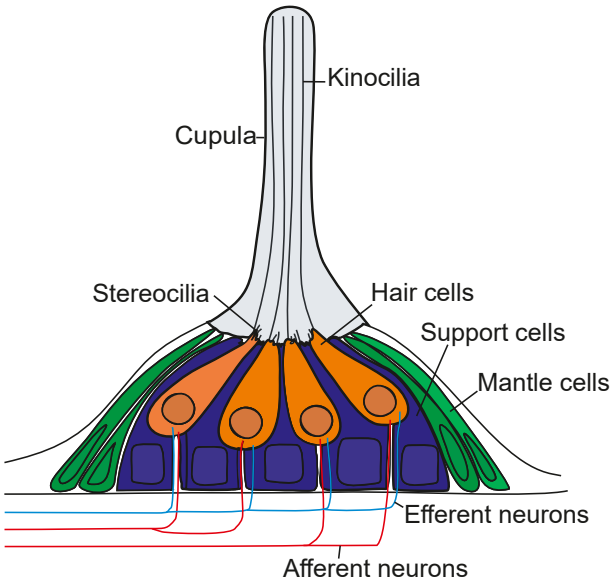

Figure 1.5: Illustration of a side view of a neuromast. A neuromast consists of several mechanosensory hair cells (orange) in the center, surrounded by support cells (blue) and mantle cells (green). The hair cells are innervated by afferent neurons (red) that are localized in the pLLG. In addition, efferent neurons (blue) carry motor informations from the central nervous system to the hair cells. The stereocilia and kinocillia of the hair cells are extended into the water, and covered with a gelatinous cupula (gray). Modified from Ma and Raible (2009).

1.6 Sensory hair cell regeneration in zebrafish

Sensory hair cells in the auditory and vestibular systems are essential for hearing and balance in vertebrates. The homeostasis and survival of these hair cells are crucial for the lifelong function of these mechanosensory organs. However, hair cells can be damaged by various factors, including infection, excessive noise, traumatic injury, and age [Yorgason et al., 2006, Bielefeld et al., 2010, Oishi and Schacht, 2011, Kidd and Bao, 2012]. In mammals, hair cells are almost exclusively produced during embryogenesis and display very limited regenerative capacity. Hence, the postembryonic loss of these cells leads to irreversible hearing loss and balance disorders [Davis et al., 1989, Chardin et al., 1995]. Contrary to mammals, a variety of non-mammalian vertebrates, such as salamanders, sharks, reptiles, birds, and bony fish, can regenerate hair cells throughout their lifetime [Corwin, 1981, Corwin and Cotanche, 1988, Ryals and Rubel, 1988, Corwin and Warchol, 1991, Burns and Corwin, 2013, Rubel et al., 2013, Cruz et al., 2015]. The postembryonic addition of hair cells was first observed in amphibians and cartilaginous fish as part of their continuous growth process [Corwin, 1981, Corwin, 1985, Balak et al., 1990]. Hair cell regeneration after damage was first discovered in chicken, making it a widely used model for studying this phenomenon [Cotanche, 1987, Cruz et al., 1987]. Chickens require 3-4 weeks to fully regenerate their hair cells after gentamicin treatment, with the regenerative process beginning around day 10 [Cruz et al., 1987]. In contrast, the zebrafish lateral line system develops rapidly, and its accessible sensory organs, the neuromasts, mature in the first week of development. In addition, lateral line hair cells share cellular, physiological, and molecular characteristics with those found in the inner ear [Coombs and Montgomery, 1999, Whitfield, 2002, Nicolson, 2005]. Notably, mutations that impact lateral line hair cells in fish have also been implicated in causing deafness in humans [Nicolson, 2005]. A further key advantage of the zebrafish lateral line system is the rapid and efficient induction of hair cell death, which can be achieved within 15-20 minutes through exposure to ototoxic agents, such as antibiotics like neomycin [Harris et al., 2003]. Furthermore, the initiation of hair cell regeneration in the zebrafish lateral line system occurs within 3-5 hours following neomycin damage, and the hair cells are fully regenerated in both, form and function within 2-3 days [Song et al., 1995, Williams and Holder, 2000, Murakami et al., 2003, Hernández et al., 2006, Linbo et al., 2006, Romero-Carvajal et al., 2015]. Regenerating hair cells are also properly reinnervated by directionally sensitive neurons [Nagiel et al., 2008, Faucherre et al., 2009]. This makes the zebrafish lateral line system an excellent model to investigate hair cell regeneration.

Aminoglycosides like neomycin can harm sensory hair cells even at low concentrations, leading to cell death [Harris et al., 2003, Hernández et al., 2007]. It is, however, not clearly understood, how neomycin treatment leads to hair cell death. It may act by inducing transient increases in calcium levels and mitochondrial swelling [Owens et al., 2007, Esterberg et al., 2013, Esterberg et al., 2014]. BrdU assays and proliferation-blocking-experiments have demonstrated that the regeneration of damaged hair cells is primarily achieved through the induction of proliferation in the inner support cells, followed by their subsequent differentiation into new hair cells [López-Schier and Hudspeth, 2006, Ma et al., 2008, Wibowo et al., 2011, Mackenzie and Raible, 2012, Namdaran et al., 2012]. Some hair cells are not produced via cell division, but through direct transdifferentiation of support cells into hair cells without an intervening cell division (Fig. 1.6) [Hernández et al., 2007]. Unlike the proliferative support cells, the quiescent mantle cells lining the neuromast periphery fail to respond to neomycin-induced hair

cell death. These mantle cells, however, can robustly regenerate neuromasts if more support and hair cells are eliminated, or they generate entirely new neuromasts, for example during tail regeneration [Romero-Carvajal et al., 2015]. Due to the homology between the human inner ear hair cells and zebrafish lateral line hair cells, continued research into sensory hair cell regeneration may reveal novel strategies for promoting hair cell regeneration, offering hope for treating hearing and balance disorders.

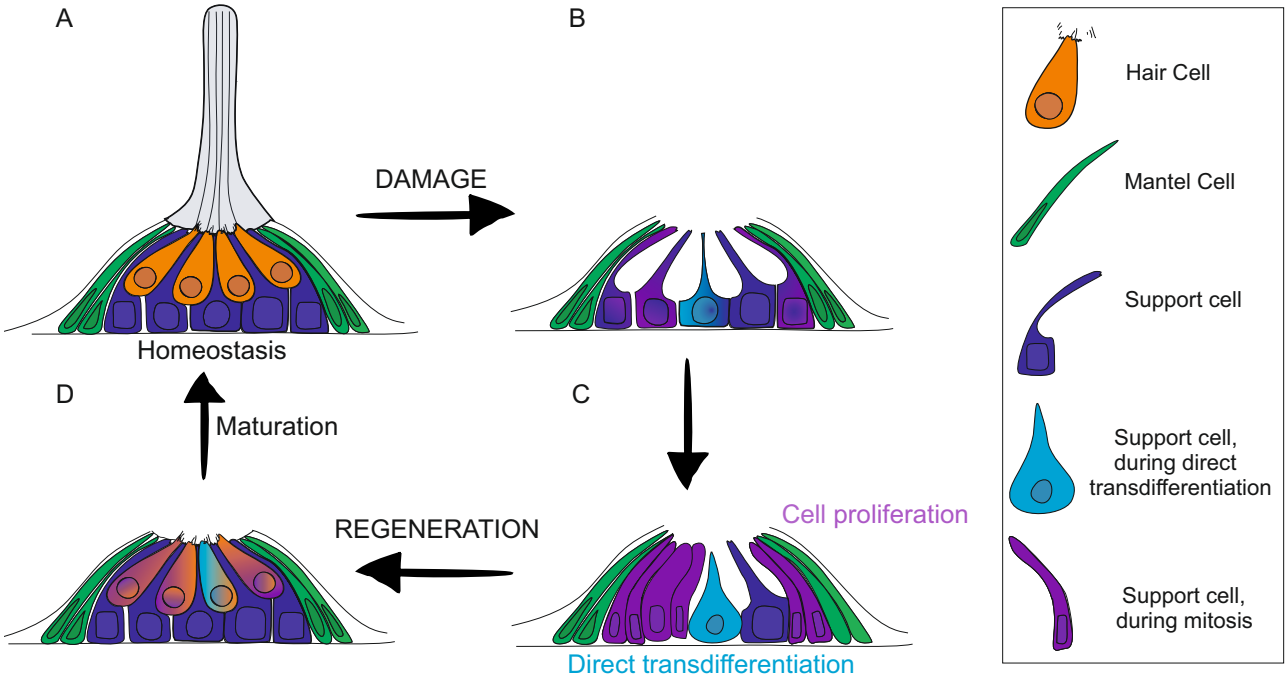

Figure 1.6: Lateral line hair cells are regenerated by two distinct cellular processes. **(A)** Neuromast during homeostasis with mature sensory hair cells (orange). **(B)** Neomycin treatment leads to hair cell damage. **(C)** The two types of hair cell regeneration after damage in zebrafish: The more rarely direct transdifferentiation of hair cells and the major mechanism of regeneration through mitosis. Direct transdifferentiation: The support cell is converted into a precursor hair cell (turquoise) and then becomes a new hair cell (orange). Mitosis: The support cell divides and the newly formed support cell becomes a hair cell precursor (light purple), **(D)** The regeneration of the neuromast leads to the restoration of its fully functional, differentiated structure.

1.7 Signaling pathways regulating hair cell regeneration in the zebrafish lateral line

Hair cell damage triggers alterations in signaling cascades, and these modifications persist dynamically throughout the regenerative phase [Baek et al., 2022]. Notch signaling, one of the most thoroughly investigated pathways, plays a crucial role in various stages of hair cell development and regeneration, particularly in the zebrafish inner ear and lateral line. Immediately after hair cell damage, Notch is downregulated to allow Wnt-dependent support cell proliferation and initiate hair cell differentiation [Ma et al., 2008, Wibowo et al., 2011, Romero-Carvajal et al., 2015, Lush et al., 2019, Baek et al., 2022]. However, between 3-5 hours post damage, Notch signaling is then upregulated to ensure a balanced ratio of hair cells and support cells via lateral inhibition [Ma et al., 2008, Romero-Carvajal et al., 2015, Baek et al., 2022]. Interestingly, while Notch inhibition enhances hair cell regeneration, it has minimal effects on proliferation during homeostasis [Romero-Carvajal et al., 2015]. Similar to Notch, Fgf-induced FGF signaling also has an inhibitory effect on proliferation [Romero-Carvajal et al., 2015, Lush et al., 2019]. Therefore, directly after hair cell death, Ffg signaling is downregulated to allow support cell proliferation [Lush et al., 2019, Baek et al., 2022]. In contrast to Notch and FGF, Wnt activation stimulates support cell proliferation, leading to an increase in hair cells during both homeostasis and regeneration [Jacques et al., 2014, Romero-Carvajal et al., 2015]. Wnt pathway genes are, however, not expressed during homeostasis and are only upregulated after the initial phase of regeneration [Jiang et al., 2014, Baek et al., 2022], suggesting that other signals trigger the initial proliferative response.

1.8 The neural cell adhesion molecule NCAM1

The current work aims to elucidate the role of the neural cell adhesion molecule Ncam1b in regulating development and regeneration processes within the lateral line system. Cell adhesion molecules, such as the neural cell adhesion molecule 1 (NCAM1), play a crucial role in regulating interactions between cells and their surrounding extracellular matrix as well as promoting homophilic and heterophilic cell-cell connections during the development of the nervous system [Smith et al., 1993]. NCAM1 is prominently expressed in both, the embryonic and adult nervous systems and is involved in various processes, including cell adhesion, proliferation, migration, neuritogenesis, axon guidance, synaptic plasticity, and regeneration [Jørgensen and Bock, 1974, Covault and Sanes, 1985, Rutishauser, 1996, Gascon et al., 2007, Rutishauser, 2008]. The extracellular part of NCAM1 consists of five Immunoglobulin-like (Ig) domains and two Fibronectin (FN) domains (Fig. 1.7) [Cunningham et al., 1987]. Due to alternative splicing, vertebrates express multiple isoforms of NCAM1, including NCAM1-120, NCAM1-140, and NCAM1-180, which vary in terms of membrane anchorage and the structure and length of their cytoplasmic domain [Murray et al., 1986, Gower et al., 1988, Thompson et al., 1989, Fields and Itoh, 1996]. NCAM1-180 and NCAM1-140 have transmembrane and cytoplasmic domains, while NCAM1-120 lacks an intracellular region and is tethered to the cell membrane through a glycophosphosphatidylinositol (GPI) anchor [Gennarini et al., 1984, Hemperly et al., 1986]. Soluble isoforms of NCAM1 are also known [He et al., 1986, Gower et al., 1988].

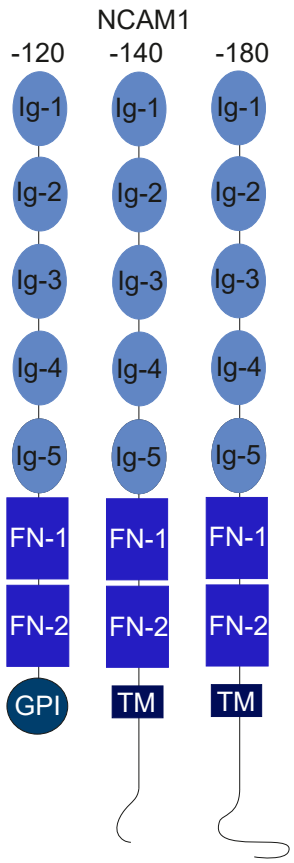

Figure 1.7: Schema of the three isoforms of NCAM1. The Neural Cell Adhesion Molecule 1 (NCAM1) is a glycoprotein expressed as 120, 140 and 180 kDa isoforms, all derived through alternative splicing of a single gene. It consists of five Immunoglobulin-like domains (Ig 1–5) and two Fibronectin type III repeats (FN 1–2). NCAM1-140 and -180 have a transmembrane domain, while NCAM1-120 is glycophosphosphatidylinositol (GPI)-anchored. NCAM1-120 contains no intracellular domain, whereas NCAM1-140 and -180 have different lengths of cytoplasmic tails.

NCAM1 can engage in both, homophilic and heterophilic interactions, to regulate various signaling pathways. Homophilic NCAM1 interactions occur in a three-step process, where NCAM1 molecules first form cis-dimers, then interact in trans and finally can form larger clusters [Soroka et al., 2003, Kiselyov et al., 2005]. The interaction between NCAM1 and FGFR1 plays a crucial role in the development of the nervous system, particularly in axon outgrowth and pathfinding [Williams et al., 1994a]. NCAM acts as a non-canonical ligand for FGFR1 and stimulates an FGFR1-mediated cellular response that is distinct from that elicited by FGF [Francavilla et al., 2009]. This interaction leads to the activation of FGFR1 by phosphorylation and triggers two important signaling pathways: a calcium increase via PLCγ, which promotes neurite outgrowth and cell adhesion, as well as the activation of Src and Erk1/2, which stimulates cell migration [Williams et al., 1994b, Francavilla et al., 2009].

1.9 Ncam1 during the development of zebrafish lateral line

The zebrafish expresses three different Ncam1 molecules: Ncam1a, Ncam1b, and Ncam2, with this study focusing on the two Ncam1 paralogs. These Ncam1 paralogs arose from a gene duplication event in teleosts and have 66 % homology in their amino acid sequence, with the differences mainly located in the intracellular domain [Mizuno et al., 2001]. Previous protein expression studies showed that both, Ncam1a and Ncam1b, are expressed in the pLLO [Langhauser et al., 2012]. During embryonic development, Ncam1a and Ncam1b can be detected in pLLG, pLLN, the primordium, as well as in interneuromast and neuromast cells [Langhauser et al., 2012, Heiny, 2013, Dries et al., 2021]. A more detailed examination of the primordium by Heiny (2013) and Dries (2018) showed that Ncam1a is expressed in both, the Leading and Trailing Zone, while Ncam1b staining was only found in the Trailing Zone [Heiny, 2013, Dries, 2018]. Furthermore, Dries (2014) demonstrated that Ncam1b is expressed throughout the otic vesicle, whereas Ncam1a was detectable only in the anterior region [Dries, 2014]. These overlapping, but also temporally and spatially distinct expression patterns, suggest a subfunctionalization of the two paralogs, as also discussed by Mizuno et al. (2001), Heiny (2013) and Langhauser (2012). The distinct functions of Ncam1a and Ncam1b during the development of pLLS are also reflected in the distinctly pronounced phenotypes after a morpholino knockdown (Fig. 1.8) [Dries et al., 2021]. A knockdown of *ncam1a* affects pLLS development, by reducing the migration distance of the primordium and the number of deposited proneuromasts. The loss of *ncam1b* resulted in a more severe phenotype characterized by a slowed, partially misdirected migration of a drastically smaller primordium. The formation and deposition of proneuromasts were rarely observed, and proliferation was decreased in the Trailing Zone. According to the authors, the lack of interaction between Ncam1b and Fgfr1a in the Trailing Zone is responsible for this phenomenon, leading to reduced FGF signaling and thus decreased proliferation. Furthermore, Cxcr 7b expression is markedly downregulated in *ncam1b* morphants, which could also contribute to the disrupted migration.
In the present study, two independent *ncam1b* mutants were generated to supplement, expand and critically scrutinize the morphant experiments.

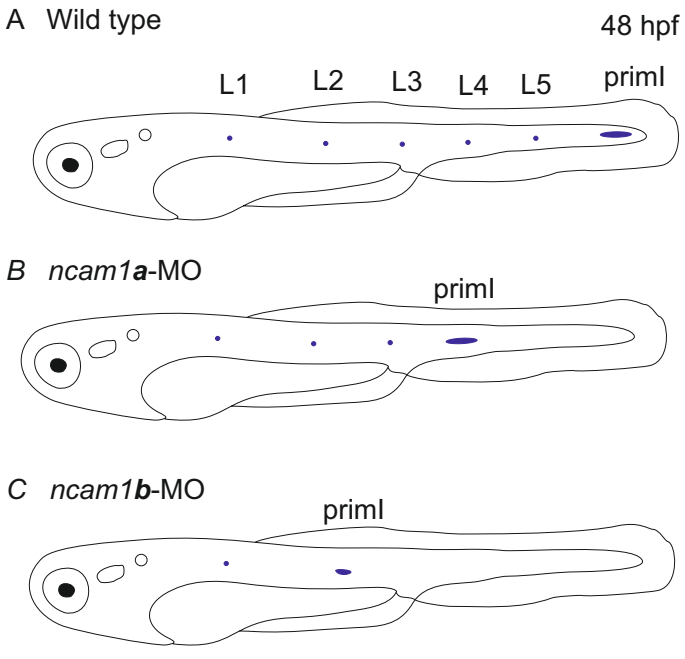

Figure 1.8: Illustration of posterior lateral line phenotypes after *ncam1a* and *ncam1b* morpholino knockdown respectively. (A) At 48 hpf, the wild type primordium (primI) is near the tip of the tail, shortly before it breaks up into the three terminal proneuromasts. During migration, 5 proneuromasts (L1-L5) were deposited. **(B)** *ncam1a*-morphants show only weak migration defects, but primI length is not affected. **(C)** *ncam1b*-knockdown induces migration defects as well as a reduction in the number of deposited proneuromasts and reduced size of primI.

1.10 Ncam1 during regeneration of zebrafish lateral line

The differential expression patterns of the paralogous genes *ncam1a* and *ncam1b* suggest that they have undergone subfunctionalization during the development and maintenance of the zebrafish lateral line system [Mizuno et al., 2001, Langhauser et al., 2012]. Ncam1a appears to be more important for the initial development and patterning of the pLLS as its expression is downregulated in mature neuromasts 5 dpf [Dries, 2018]. In contrast, Ncam1b maintains a more persistent expression, being present in both developing and differentiated hair cells. Shortly after neomycin-induced damage to zebrafish sensory hair cells, Ncam1b expression begins to increase in the support cells and remains upregulated throughout the regeneration process (Fig. 1.9). This rapid upregulation of Ncam1b following hair cell damage implies that it may play a crucial role in hair cell differentiation during regeneration in the lateral line system. After regeneration is complete, Ncam1b is expressed in both hair cells and support cells, mirroring its expression pattern during pLLO development. Inhibition of Notch signaling by DAPT not only accelerates regeneration as expected but also leads to an increased number of Ncam1b-expressing support cells. This finding supports the hypothesis that Ncam1b is involved in the differentiation of support cells into sensory hair cells.

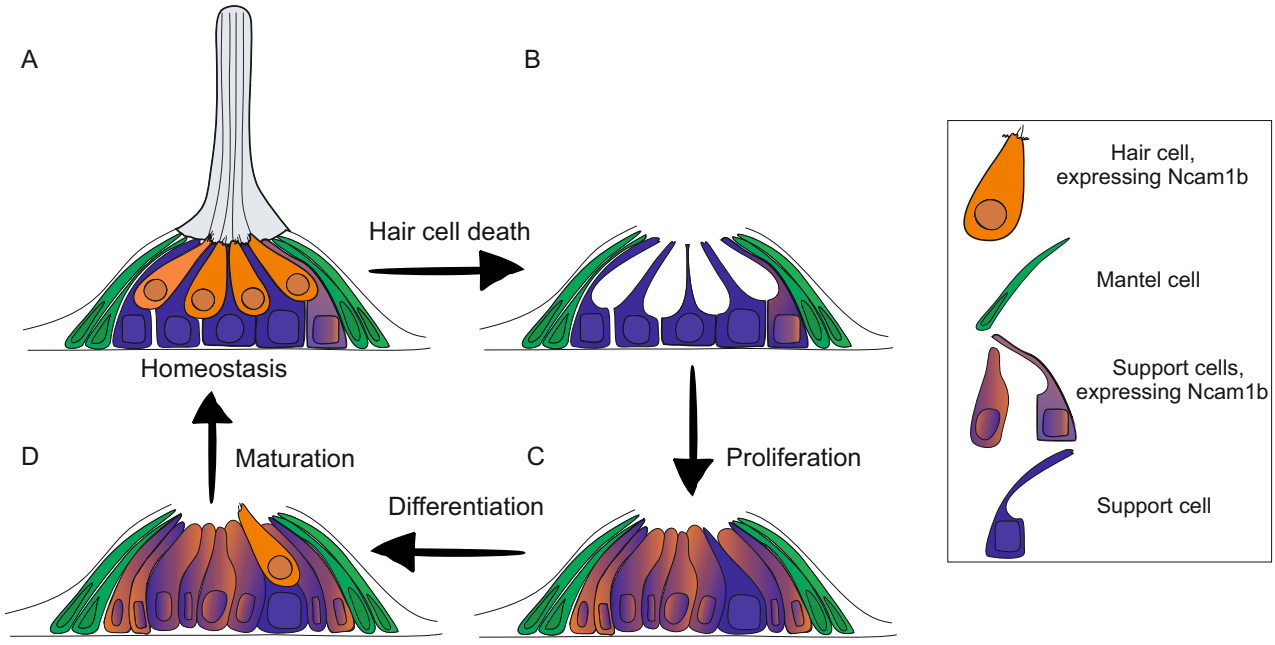

Figure 1.9: Ncam1b is expressed in regenerating neuromasts. (A) Ncam1b (orange) is expressed in hair cells and in single support cells during homeostasis. **(B)** Neomycin treatment leads to hair cell damage. **(C)** Support cells, expressing Ncam1b, begin to proliferate and then differentiate into hair cells. **(D)** The regeneration of the neuromast leads to the restoration of its fully functional, differentiated structure.

2 Aim of the Thesis

The ability of the zebrafish to regenerate sensory hair cells presents a unique opportunity to investigate the cellular and molecular mechanisms underlying this process. Mammals cannot regenerate hair cells in the inner ear as adults, which leads to permanent sensorineural hearing loss after hair cell damage or loss [Chardin et al., 1995]. Elucidating the mechanisms underlying hair cell development and regeneration could pave the way for devising therapeutic strategies to restore hearing in humans affected by hearing loss. Previous studies in our lab have highlighted the crucial role that Ncam1b plays in the development of the posterior lateral line system (pLLS) [Dries et al., 2021]. Morpholino knockdown of *ncam1b* resulted in severe developmental defects, including reduced primordium size, fewer neuromasts, and impaired migration, attributed to disrupted FGF signaling and proliferation. While these findings underscore the importance of Ncam1b during pLLS development, the consequences of a complete *ncam1b* loss through genetic knockout remained unexplored.

Therefore, a primary aim of this thesis was to generate and characterize two distinct types of *ncam1b* mutant zebrafish lines using CRISPR/Cas9 technology, one carrying a classical premature point mutation, the other by deleting nearly the entire *ncam1b* gene sequence. Generating these two different mutant lines would enable ruling out potential off-target effects. These mutants were used to elucidate whether the developmental phenotypes observed in *ncam1b* morphants could be recapitulated. Surprisingly, the *ncam1b* mutants did not exhibit overt developmental defects in the pLLS, contrasting with the severe phenotypes observed in morphants. This discrepancy on the one hand prompted an investigation into potential genetic compensation mechanisms that could mask the effects of *ncam1b* loss in mutants. On the other hand, the molecular pathways underlying the Ncam1b regulatory functions during pLLS development were studied. The main focus was laid on the Ncam1b impact on key signaling cascades like Wnt and FGF, as well as on its influence on cell proliferation.

Ncam1b is known to be expressed in differentiated hair cells. After hair cell damage, Ncam1b expression increases in support cells that subsequently differentiate into new hair cells. This suggests a potential role for Ncam1b in the differentiation process during regeneration. In this context, the current work investigated whether the absence of Ncam1b affects hair cell regeneration in zebrafish. Specifically, it was to be determined if a loss of *ncam1b* impacts the proliferation of support cells or their differentiation into hair cells. To address this, *ncam1b* mutant zebrafish lines were analyzed following neomycin-induced hair cell damage.

3 Materials and Methods

3.1 Materials

3.1.1 Chemicals, buffers, solutions, media, antibiotics

Chemicals

All chemicals were obtained, unless otherwise stated, in the highest analytical purity (p.a.) from the companies Carl Roth GmbH & Co. KG (Karlsruhe, Germany), Merck KGaA (Darmstadt, Germany), and Sigma-Aldrich Chemie GmbH (Taufkirchen, Germany). Double-distilled water (ddH_2O) was obtained from the Ultrapure Water System PURELAB flex from Elga Veolia (Celle, Germany) and subsequently autoclaved. All chemicals used are listed in Table 3.1.

Table 3.1: Used chemicals and reagents.

Chemical	Supplier	Application
Agarose NEEO ultra-quality	Carl Roth	Preparation of agarose gels
BrdU	Sigma-Aldrich	Proliferation assay
BSA	Sigma-Aldrich	Blocking IHC
DAPT	Sigma-Aldrich	Inhibition of γ-sekretase
Diethyl pyrocarbonate (DEPC)	Carl Roth	Inactivation of RNases
DIG RNA Labeling Mix, 10x	Sigma-Aldrich	FISH
Dimethyl sulfoxide (DMSO)	Sigma Aldrich	IHC, BrdU, DAPT
DNA Gel loading dye	Thermo Fisher Scientfic	DNA gel electrophoresis
Fluorescein RNA Labeling Mix	Roche	FISH
Formamide	Carl Roth	FISH
Mowiol 4-88	Merck Millipore	Medium for embedding
n-Propyl gallate	Sigma-Aldrich	Supplement for embedding
PFA	Merk Millipore	Fixing embryos
Phenol Red	Sigma Aldrich	Dye to visualize injection
Propylthiouracil (PTU)	Sigma-Aldrich	Depigmentation
Roti® GelStain	Carl Roth	Staining of nucleic acids
Sodium borohydride ($NaBH_4$)	Carl Roth	Reduction of background during IHC
Sodium hydroxide (NaOH)	Carl Roth	Lysis of DNA
Triton X-100	Carl Roth	Embryo permeabilization
TRIzol Reagent	Thermo Fisher Scientific	RNA extraction
t-RNA	Merck	Blocking during FISH
Tween 20	Carl Roth	Embryo permeabilization

Buffers and solutions

All self-prepared buffers and solutions were autoclaved or prepared from sterile stock solutions. Non-autoclavable buffers or solutions were filtered under sterile conditions. Solutions for work with RNA were pre-treated with diethyl pyrocarbonate (DEPC) (1:1000). Commercially purchased buffers are listed in Table 3.2. Self-prepared buffers and solutions are listed in Table 3.3. Media specifically for embryos (Table 3.4) and for bacteria (Table 3.5) are listed separately.

Table 3.2: Buffers.

Name	Supplier
Cas9 Reaction Buffer	New England Biolabs
Gel Loading Buffer	New England Biolabs and Thermo Fischer Scientific
Nuclease Free Duplex Buffer	Integrated DNA Technologies

Table 3.3: Self-prepared buffers and solutions.

Name		Compositions
Agarose gel (1.5 %)		Agarose in 1x TAE buffer
Borate buffer	pH 8.5	6.19 g Boric acid 3.7 ml 5 M NaOH ad 1 l ddH_2O-DEPC
BrdU (10 mM)		10 mM BrdU 15 % DMSO 85 % ddH_2O
BSA (1 %)		1 % BSA in 1x PBS (w/v)
Cas9 working buffer	pH 7.5	20 mM HEPES 150 mM KCl in ddH_2O
Glycin (100 mM)	pH 2 (HCl)	7.5 g Glycin ad 1 l ddH_2O-DEPC
H_2O-DEPC		add 1 ml DEPC to 1 l ddH_2O
Hyb -		25 ml Formamid 12.5 ml 20x SSC 11.5 ml H_2O-DEPC 250 µl 20 % Tween 20 260 µl 1 M Citric acid ad 50 ml ddH_2O-DEPC
Hyb +		250 µl t-RNA (20 mg/ml) 2.5 µl Heparin (100 mg/ml) ad 5 ml Hyb -

Table 3.3: Self-prepared buffers and solutions.

Name		Compositions
MAB	pH 7.5 (NaOH)	100 mM Maleic acid 150 mM NaCl in ddH_2O-DEPC
MABT		0.1 % Tween 20 in MAB
Mowiol (20 %)	pH 8.5	Mowiol 4-88 0.1 g/ml Glycerin 25 % (v/v) n-Propyl gallate 0.1 mg/ml Tris-HCl 0.1 M in PBS
PBD		1 % BSA 1 % DMSO in 1x PBS
PBS for FISH		add 1 ml DEPC to 1 l PBS
PBS(T)	pH 7.4	1.37 M NaCl 27 mM KCl 100 mM Na_2HPO_4 27 mM KCl (0.5 % Triton X-100 or 0.1 % Tween20) in ddH_2O
PFA in PBS		4 % PFA 10 % 10x DEPC-PBS 0.5 % 1 M NaOH in ddH_2O
PFA in phosphate buffer		4 % PFA 25 % Phosphate buffer (4x) 0.5 % 1 M NaOH in ddH_2O
Phosphate buffer (4x)	pH 7.4	5.32 g NaH_2PO_4 x 1 H_2O 52.11 g Na_2HPO_4 x 12 H_2O ad 500 ml ddH_2O-DEPC
PTU		0.003 % PTU in ddH_2O
Sodium borohydride		1 µg/ml $NaBH_4$ in 1x PBS
SSC (Saline Sodium Citrate) (20x)		3 M NaCl 0.3 M Na-Citrat-2-Hydrat in ddH_2O-DEPC

Table 3.3: Self-prepared buffers and solutions.

Name	Compositions
TAE Buffer (50x)	2 M Tris 1 M Acetic acid 50 mM EDTA ad 1 l ddH_2O
t-RNA	0.2 mg/ml in ddH_2O

Table 3.4: Media for the cultivation of embryos.

Chemical	Composition	Application
Danieau (50x)	58 mM NaCl 0.7 mM KCL 0.4 mM $MgSO_4$ 0.6 mM $Ca(NO_3)_2$ 5 mM HEPES 0.5 mg/l Methylene blue	Medium for injection
Embryo medium (E2)(0.5x)	7.5 mM NaCl 0.25 mM KCl 0.5 mM $MgSO_4$ 75 µM KH_2PO_4 25 µM Na_2HPO_4 0.5 mM $CaCl_2$ 0.35 mM $NaHCO_3$ 0.5 mg/l Methylene blue	Neomycin and DAPT treatment
Embryo medium (E3) (60x)	294 mM NaCl 10 mM KCL 26.1 mM $CaCl_2$ 41 mM $MgSO_4$ 0.5 mg/l Methylene blue	Medium for embryo raising

Table 3.5: Media for the cultivation of bacteria.

Chemical	Composition	Application
LB medium liquid	1 % Tryptone 0.5 % Yeast extract 1 % NaCl in ddH_2O pH 7 add antibiotic	Culture medium for bacteria
LB agar plates	1 % Tryptone 0.5 % Yeast extract 1 % NaCl in ddH_2O pH 7 add antibiotic add 13 g agar-agar to 1 l	Culture medium for bacteria

Antibiotics

All antibiotic solutions were either prepared under sterile conditions or acquired already in soluble, sterile form, and are listed in Table 3.6.

Table 3.6: Antibiotics.

Name	End concentration	Application	Supplier
Ampicillin	100 µg/ml	Bacterial selection	Sigma-Aldrich
Kanamycin	50 µg/ml	Bacterial selection	Carl Roth
Neomycin	300 µM	Hair cell damage	Carl Roth

3.1.2 Kit systems

All kit systems used were purchased in the highest analytical purity and stored and used according to the manufacturer's instructions. A list of the kits used is provided in Table 3.7.

Table 3.7: Kit-Systems.

Consumable	Supplier
DNA Clean and Concentrator®-5	Zymo Research
QIAquick Gel Extraction Kit	Qiagen
QIAprep Spin Miniprep Kit	Qiagen
QubitTM RNA BR Assay Kit	Thermo Fisher Scientific
RNeasy Micro Kit	Qiagen
Zero Blunt TOPO PCR Cloning Kit	Invitrogen

3.1.3 Consumables

All consumables used, such as pipette tips, reaction vessels, culture plates, etc., were generally purchased sterile and disposed of properly after use. A compilation of specific consumables used is listed in Table 3.8.

Table 3.8: Consumables.

Consumable	Supplier
Amplification Diluent	Perkin Elmer
ddPCR 96-well plates	Bio-Rad
ddPCR Droplet Reader Oil	Bio-Rad
DG32 Automated Droplet Generator Cartridges	Bio-Rad
Gibson Assembly® Master Mix	New England Biolabs
illustr ProbeQuantG-50 Micro Columns	GE HealthCare
MicroPulser Electroporation Cuvettes	Bio-Rad
NEB Stable Competent *E.coli* (High Efficiency)	New England Biolabs
PCR Plate Heat Seal foil	Bio-Rad
Pipet tips for the AutoDG System	Bio-Rad
SigmaSpin colums	Sigma-Aldrich
TSA-Plus Cyanine 5 System	Perkin Elmer
Thin-Wall Capillary (3", w/Fil, 1,00 mm)	World Precision Instruments
Needles for RNA extraction (21 G 0.80x40 mm)	Braun
Needles for RNA extraction (26 G 0.45x25 mm)	Braun
XL1-blue strain *E. coli* cells	Agilent Technologies

3.1.4 Antibodies and dye-conjugated affinities

All antibodies were dissolved according to the manufacturer's instructions, mixed with 50 % sterile glycerol and aliquoted. The added glycerol prevents the sensitive antibodies from freezing. Short-term storage was at 4 °C, and long-term storage was at -20 °C or -80 °C. Primary antibodies are listed in Table 3.9, secondary antibodies in Table 3.10 and fluorescent reagents in Table 3.11.

Table 3.9: Primary antibodies.

Antigen	Name	Organism/ isotype	End concentration	Dilution	Supplier
BrdU	BrdU	mouse	10 µg/ml	1:100	abcam (ab8039)

Table 3.9: Primary antibodies.

Antigen	Name	Organism/ isotype	End concentration	Dilution	Supplier
Digoxigenin-POD	Digoxigenin-POD	sheep	16.7 mU/ml	1:3000	Roche (11207733910)
Fluorescein-POD	Fluorescein-POD	sheep	16.7 mU/ml	1:3000	Roche (11426346910)
GFP	GFP	chicken IgG, pkl	2 µg/ml	1:1000	abcam (ab13970)
HCS-1	Otoferlin	mouse IgG, mkl	370 ng/ml	1:100	DSHB
Ncam1a	NCAM	rabbit IgG, pkl	400 ng/ml	1:1000	Y. Yoshihara
Ncam1b	PCAM	rabbit IgG, pkl	200 ng/ml	1:1000	Y. Yoshihara
Sox2	Sox2	rabbit IgG, pkl	1.6 µg/ml	1:300	GeneTex (GTX12447)

Table 3.10: Secondary antibodies.

Antigen	Organism	Conjugate	End concentration/ dilution	Supplier
chicken	goat	Alexa Fluor® 488 IgY, pkl	2 µg/ml 1:1000	abcam (ab150173)
mouse	goat	Cy3 IgG, pkl	1.4 µg/ml 1:1000	Jackson ImmunoResearch (115 165 164)
mouse	goat	Alexa Fluor® 647 IgG, pkl	1.5 µg/ml 1:1000	Jackson ImmunoResearch (115-606-062)
mouse	donkey	Alexa Fluor® 488 IgG, pkl	1.4 µg/ml 1:1000	Jackson ImmunoResearch (715 545 151)
rabbit	donkey	Alexa Fluor® Cy5 IgG, pkl	1.5 µg/ml 1:1000	Jackson ImmunoResearch (711-175-152)
rabbit	goat	Alexa Fluor® Cy3 IgG, pkl	1 µg/ml 1:1000	Dianova (111-165-144)

Table 3.11: Fluorescent reagents.

Antigen	Dilution/ end concentration	Supplier
TSA Cyanine 3	5 mM	Labintern production
TSA-Plus Cyanine 5	1:200	Perkin Elmer
DAPI	0.5 µg/ml (IHC), 1 µg/ml (BrdU)	Carl Roth

3.1.5 Enzymes, proteins and (ribo)nucleotides

All enzymes, proteins and (ribo)nucleotides were stored according to the manufacturer's instructions and used with the specified buffer systems. Enzymes and (ribo)nucleotides are listed in Table 3.12, polymerases are listed separately in Table 3.13 and RNAs in Table 3.14.

Table 3.12: Enzymes and (ribo)nucleotides.

Enzyme/ (ribo)nucleotides	Supplier
BamHI	Thermo Fisher
Cas9	Integrated DNA Technologies
Deoxyribonucleotides (dNTPs) 10 mM	Biozym
GeneRuler 1 kb DNA ladder	Thermo Fisher Scientific
NotI-HF	New England Biolabs
Oligo(dT) primer	Invitrogen
Proteinase K	Roche
Random hexamer primer	Invitrogen
RiboLock RNase Inhibitor	Thermo Fisher Scientific
RNase A (DNase-free)	Thermo Fisher Scientific
RNase H	Thermo Fisher Scientific
Shrimp alkaline phosphatase	Thermo Fisher Scientific
SuperScript IV reverse transcriptase	Thermo Fisher Scientific
TURBO DNase	Thermo Fisher Scientific
QX200™ ddPCR™ EvaGreen Supermix	Bio-Rad

Table 3.13: Polymerases.

Enzyme	Supplier	Application
HotStart Taq DNA Polymerase with antibody	Genaxxon	PCR
Phusion High-Fidelity PCR Master Mix	Thermo Fisher Scientific	PCR
T7 RNA Polymerase	Sigma-Aldrich	*in vitro* transcription
VeraSeq High Fidelity DNA Polymerase	Biozym	PCR
Q5® High-Fidelity DNA Polymerase	New England Biolabs	PCR

Table 3.14: RNAs.

Name	Sequence (5'→3') of target site	Supplier
crRNA Ncam1b exon 1	TCCGACCAAGGCGATAATCT	Integrated DNA Technologies
crRNA Ncam1b 3' UTR	GTTGGGTTCAAATCCTGCAT	Integrated DNA Technologies
tracrRNA	Standard tracrRNA	Integrated DNA Technologies

3.1.6 Primers and morpholino oligonucleotides

Primers

Primers were purchased from Eurofins Genomics (Ebersberg, Germany), dissolved in ddH_2O to a concentration of 100 µM and stored at -20 °C. The number before the primer name serves for internal lab numbering. Primers for genotyping via PCR are listed in Table 3.15, primers for sequencing in Table 3.16, primers for RT-PCR in Table 3.17, primers for ddPCR in Table 3.18, and primers for Gibson assembly in Table 3.19.

Table 3.15: Primers for genotyping of *ncam1b* via PCR.

Name	Sequence (5'→3')
75_n1b_ex1_404bpr	CCAGTGACACCAGCATCACC
76_n1b_ex1_minus165_f	CCTCTTTCTCGGTCAGATGG
121_N1b_Nullallel_3_r	GCTCGCCAATTCGCAAATAC
122_N1b_Nullallel_3'_f	ACACGTAACTGTTTTGCCTC
176_N1b_Nullallel_3'_rev_2	GCCCAGTCAATCGTTCAGTC
TS728116_n1b_f	GGCTTTGGTTCAGTGCTTCA

Table 3.16: Primers for sequencing.

Gene	Name	Sequence (5'→3')
ncam1b	63_N1b_ex1_for	TCAGCGCGCGACATATGGG
	121_N1b_Nullallel_3_r	GCTCGCCAATTCGCAAATAC
	143_N1b_Exon12_f	ATCCAGAGTCTCAGAGCGAC
	147_N1b_ATG_f	ATGTTTCCGACCAAGGCG
	150_N1b_Stop_direkt_r	TCATGCTTTACTTTCAATGTTTGTTT
	RD_inmut_n1b_13_rev	AGTACGGCTGCACTTCACCGA
TOPO Vector	M13rev-29	CAGGAAACAGCTATGACC

Table 3.17: Primers for RT PCR.

Primer	Supplier	Application
Oligo(dT) primer	Invitrogen	cDNA sequencing
Random hexamer primer	Invitrogen	ddPCR

Table 3.18: Primers for ddPCR.

Gene	Name	Sequence (5'→3')
β-Actin	112_β-Actin_f	TCAGCACTTTCACACCAGGTT
	118_β-Actin_r	AACCTGGTGTGAAAGTGCTGA
l1cam	208_L1cam_for_2	TTGAGTTTGAGGAGACGGGA
	209_L1cam_rev_2	GGGTCACTCTTGCCGATTTC
ncam1a	204_Ncam1a_Exon 17_f1	GCACCGACCCTAAACCTACT
	205_Ncam1a_Exon17_r1	GGAATTCTTGGCAGGGTCAC
ncam1b	123_N1b_Ig2_f	CGCCATTATCGTGTGTGATGT
	126_N1b_Ig2_r	CCACGGGCTTTAATACGACC

Table 3.19: Primers for Gibson assembly.

Name	Sequence (5'→3')
187_NA_5'N1b_fwd	GGGCCTCTTCAAATAATTACTGTAAAAAATATTGTAAATACAC
188_NA_5'N1b_rev	CCAATCAAATCCACTGCTATCATTATATAACTTTTTG
189_NA_3'N1b_fwd	ATAGCAGTGGATTTGATTGGTTGAAGTCTTTATTAGATCAGT TTTTACAGTTGTCGTGTATTTCTAATATCTGAG
190_NA_3'N1b_rev	TTGCTGGCCTCCGATTGGCTGGCCGCCC
191_Backbone_fwd	AGCCAATCGGAGGCCAGCAAAAGGCCAG
192_Backbone_rev	GTAATTATTTGAAGAGGCCCGCACCGAT

Morpholino oligonucleotides

All morpholino oligonucleotides were purchased in the highest purity, lyophilized form from Gene Tools, LLC (Oregon, USA) and dissolved in ddH_2O to 1 mM according to the manufacturer's instructions. Morpholinos are artificially synthesized oligonucleotides that bind complementarily to the target mRNA to be inhibited, thereby blocking its translation. In this study, morpholinos targeting *ncam1b*-5' UTR (ZfNcam1b-5'UTR) and *ncam1b*-start (ZfNcam1b-start) were used. The *ncam1b*-5' UTR morpholino binds to the 5' untranslated region upstream of the start codon, preventing the ribosome from binding to the mRNA. In contrast, *ncam1b*-ATG morpholino binds to the start codon itself, blocking the ribosome from translating the mRNA. Morpholino oligonucleotides are listed in Table 3.20. The complementary start codon is shown in bold.

Table 3.20: Morpholino oligonucleotides.

Name	Sequence (5'→3')	Amount/ Embryo
ZfNcam1b-5'UTR	GTTTACTGTTTGTTTTTGCCTTCCG	2 ng/embryo
ZfNcam1b-start	AGATTATCGCCTTGGTCGGAAA**CAT**	4 ng/embryo

3.1.7 Plasmids

Purchased plasmids that were used as cloning vectors are listed in Table 3.21. Plasmids that were cloned in the course of the present work are marked as A. Lange and are listed in Table 3.22. Plasmids for generating antisense probes for FISH are listed in Table 3.23. They were either available in the laboratory at the beginning of the work (R. Dries) or were provided by the research group of S. Scholpp, University of Exeter, UK. All plasmids for the antisense probes contain the complete coding sequence of the respective gene. All plasmid DNA was obtained by an alkaline lysis minipreparation and stored at -20 °C. Long-term storage of the plasmids was carried out in *E. coli* bacteria in glycerine stocks at -80 °C. The number in parentheses after the plasmid name serves for internal lab numbering.

Table 3.21: Plasmids as cloning vectors.

Name	Supplied by	Antibiotic resistance	Cloning vector for
pBS Bluescript I KS+	Agilent	Ampicilin	*n1b* -/- Del pos control
pCR-BluntII-TOPO	Thermo Fisher Scientific	Kanamycin	cDNA of *ncam1b*

Table 3.22: Self-generated plasmids.

Name (No.)	Insert	Supplied by
NA Deletion N1b_GA (140)	target site regions of *n1b* -/- Del	A. Lange
PMS N1b PCR1 in TOPO (129)	cDNA *n1b* -/- PMSC	A. Lange
WT N1b PCR1 in TOPO (126)	cDNA *n1b* WT	A. Lange

Table 3.23: Plasmids for antisense probes.

Name (No.)	Restriction enzyme/ promotor	Supplied by
Erm-pBS-IISK+ (21)	EcoR1 T7	S. Scholpp, University of Exeter, UK
Fgfr1a-IIIb-CDS-Exon9-SS-TOPO (4)	BamHI T7	R. Dries
Lef1 (Plasmid unknown)(20)	Not1 T7	S. Scholpp University of Exeter, UK

3.1.8 Technical equipment

Standard laboratory instruments and specialized equipment are listed in Table 3.21.

Table 3.24: Technical equipment.

Device	Supplier	Application
Amersham Imager 600	GE Healthcare	Documentation of gels
C1000 Touch Thermal Cycler	Bio-Rad	PCR after ddPCR
E.coli Pulser	Bio-Rad	Electroporation
Micropipette Puller	Sutter Instrument Company	Generation of injection needles
Nanodrop 1000 Spectrophotometer	Peqlab	Measurement DNA concentration
PCR Thermocycler	Biometra TAdvanced	PCR
PCR Thermocycler	VWR	PCR
Pneumatic Pico Pump	WPI	Microinjection
PURELAB flex	Elga Veolia	Production of ddH_2O
Qubit 3 Fluorometer	Thermo Fisher Scientific	Measurement RNA concentration
QX200 Automated Droplet Generator	Bio-Rad	Droplet generation for ddPCR
QX200 Droplet Reader	Bio-Rad	Droplet reader for dPCR
ZebTec	Tecniplast	Zebrafish facility

3.1.9 Microscopes and software

Microscopes and objectives were purchased from Carl Zeiss AG (Oberkochen, Germany) and are listed in Table 3.25. A range of specialized software tools were utilized at different stages of this research project, from initial data acquisition to final manuscript preparation. The specific software is listed in Table 3.26.

Table 3.25: Microscopes and objectives (supplied by Carl Zeiss).

Microscope	Objective
ApoTome	Fluar 5x/0.25 Fluar 10x/0.5
LSM 800 (confocal)	Plan Apochromat 5x/0.16 Plan Apochromat 10x/0.3 Plan Apochromat 20x/0.8 DICII C Apochromat 40x/1.2 water DICII C Apochromat 40x/1.4 oil DIC

Table 3.26: Software.

Device	Supplier
CLC Sequence Viewer 8	Qiagen
CorelDraw X7	Coral Corporation
CRISPOR	Concordet and Haeussler (2018)
Fiji is just ImageJ (Fiji)	Schindelin et al. (2012)
Inkscape	Inkscape Project
Latex	LaTeX Project Team
OriginPro 2021	OriginLab Corporation
QuantaSoft Software	Bio-Rad
SnapGene Viewer	SnapGene
Texmaker 5.0.4	Pascal Brachet
ZEN lite 2	Carl Zeiss

3.2 Methods

3.2.1 The experimental animal: the zebrafish

Zebrafish lines

In the present study, the development and regeneration of the posterior lateral line system (pLLS) in zebrafish (*Danio rerio*) were examined in two self-generated *ncam1b* mutant lines. The manipulation to generate the mutations was carried out in the transgenic zebrafish line *Tg(ClaudinB::lynGFP)*. This line expresses GFP under the ClaudinB promoter, which is predominantly found in the tight junctions of sensory placode organs, including the pLLS [Haas and Gilmour, 2006].

Zebrafish husbandry and embryo collection

Adult fish were maintained in a ZebTEC aquaculture system by Tecniplast (Buguggiate, Italy) under constant standard conditions (27 °C; pH 7.2; 360 µS; 0.3 bar; $NO_3 < 50$ mg/ml; NO_2 0 mg/ml). System water parameters such as nitrate, nitrite, and ammonia were continuously monitored. The natural day-night cycle was simulated using a timer, providing 14 hours of light and 10 hours of darkness. To collect embryos, adult fish were paired in breeding tanks with grid bottoms (1.0 liter, Tecniplast) the evening before. A partition separated the female and male. They were kept in temperature-controlled aquarium water. The following morning, pairs were transferred to fresh, temperature-controlled aquarium water, and the partition was removed. The spawned embryos fell through the grid bottom into a collection container, which prevents adult fish from eating them. The eggs were subsequently collected, washed, and transferred to a petri dish with E3 medium. Substances such as RNA, morpholinos, and proteins were injected into zebrafish eggs at the one-cell stage.

Fish breeding

After spawning, the embryos were transferred to petri dishes with E3 medium. To facilitate optimal development, these embryos were kept in an incubator at a constant temperature of 28.5 °C for seven days. Subsequently, larvae were transferred to a rearing tank in the system. They were initially fed more frequently (up to five times a day) compared to adult fish (two times a day). Zebrafish reached sexual maturity approximately three months later and were considered adults from that point onwards.

3.2.2 Microinjection of zebrafish embryos

For the microinjection injection needles were created from glass capillaries using a micropipette puller (Heat: 900, Pull: 400). Embryos were collected in Danieau medium and arranged on a plastic injection micro molding. Injections were performed using a compressed air microinjector (pressure: 0.2 psi (vent); duration: timed; range: 100 ms) into the yolk at the one-cell stage. The injection volume was calibrated to 4 nl per air pulse. After injection, the embryos were transferred to petri dishes with E3 medium.

Embryo rearing and staging

Embryos were staged according to the developmental criteria described by Kimmel et al. (1995), with the stage indicated as hours post fertilization (hpf) [Kimmel et al., 1995]. Immediately after spawning or microinjection, embryos were transferred to E3 medium and incubated at a constant temperature of 28.5 °C. After 24 hpf, the embryos were manually dechorionated using fine forceps. For experiments involving hair cell toxicity tests, embryos were allowed to hatch naturally and were fixed at the desired time point. To prevent pigmentation, embryos were treated with 0.3 % propylthiouracil (PTU) starting at approximately 24 hpf. The E3 medium was changed daily, and fresh PTU was added until the day of fixation. Embryos were maintained under these conditions throughout the experiment.

3.2.3 Generation of stable *ncam1b* mutant lines

Generation of a *ncam1b* Pre Mature Stop Codon mutant

The *ncam1b* **P**re **M**ature **S**top **C**odon (*n1b* -/- PMSC) mutant was generated using the CRISPR/Cas9 genomic editing system. Guide RNA (gRNA) was chosen using the CRISPOR web tool. It targets exon 1, relatively near to the *ncam1b* start codon. The gRNA and Cas9 protein (both from Integrated DNA Technologies) were co-injected into one-cell stage embryos. Mutation events in the targeted genomic region were identified by PCR amplification, followed by sequencing (Fig. 3.1 A). Injected siblings were grown to adulthood and outcrossed to identify those transmitting the mutation through the germline. A one-base deletion predicted to cause a frameshift and premature termination codon in exon 1 was isolated and propagated for further studies. *n1b* -/- PMSC mutant embryos were obtained by crossing homozygous mutant parents.

Sequencing of *ncam1b* mRNA of *n1b* -/- PMSC mutant embryos

Given that frameshift mutations with an early stop codon, as observed in the *n1b* -/- PMSC mutant, may lead to alternative mRNA splicing and the emergence of mRNA variants with restored open reading frames, the *ncam1b* mRNA was examined in detail. Total RNA was isolated from homozygous *n1b* -/- PMSC and wild type (WT) control embryos at 48 hpf using TRIzol reagent, as further described below. The mRNA was then purified using oligo(dT) primers and subjected to reverse transcriptase PCR (RT-PCR) to obtain the complete *ncam1b* mRNA sequence. RT-PCR was performed as described below. To amplify the complete *ncam1b* coding sequence, PCR was carried out with primers targeting the entire open reading frame. RT-PCR analysis revealed that the *n1b* -/- PMSC sample contained significantly less *ncam1b* template compared to the WT control, despite using equal amounts of cDNA input (Fig. 3.1 B). This suggests that the *n1b* -/- PMSC mutant mRNA is degraded to nonsense-mediated mRNA decay (NMD), which was further investigated in this study (Fig. 4.1). Sequencing of the amplified *ncam1b* cDNA fragments showed no other missing or altered sequences in the *n1b* -/- PMSC mutant, excluding alternative splicing or skipping of exon 1, where the premature stop codon is located (Fig. 3.1 C).

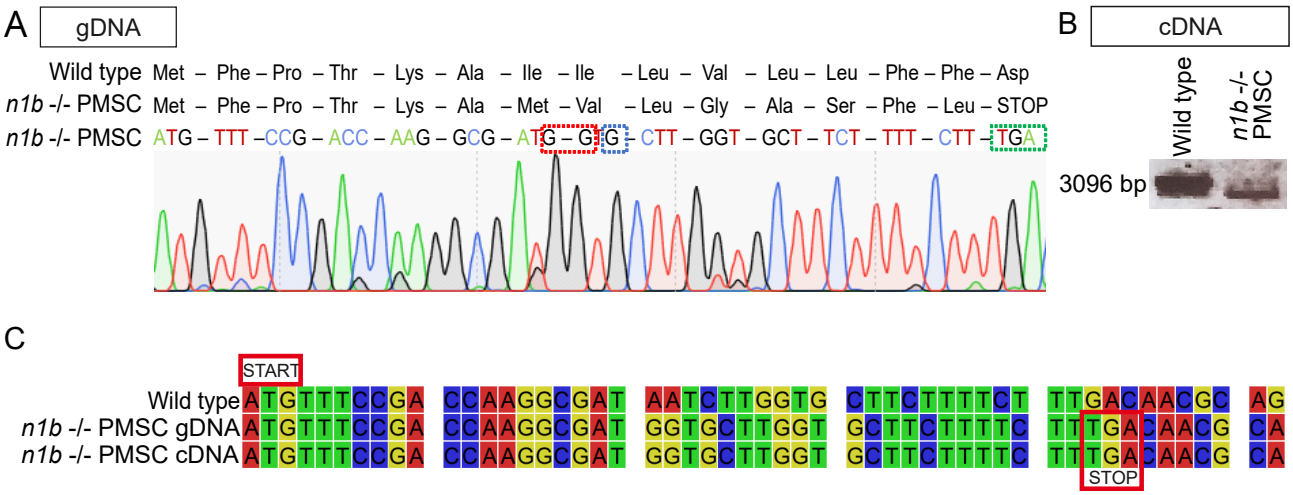

Figure 3.1: The *n1b* -/- PMSC mutant has a premature stop codon in exon 1. **(A)** Amino acid sequence of wild type and *n1b* -/- PMSC mutant in exon 1. The base sequences of the genomic DNA (gDNA)and the chromatogram show the following changes: red box: 2x inversion (adenine → guanine), blue box: insertion of guanine, green box: premature stop codon. **(B)** The reverse transcriptase PCR with cDNA as template shows a narrower band for the *n1b* -/- PMSC sample compared to the WT. **(C)** Representatively for the alignment of the complete sequence, the region of exon 1 is depicted here. Alignment of *ncam1b* sequences of gDNA of exon 1 of wild type, *n1b* -/- PMSC and cDNA of *n1b* -/- PMSC shows that stop codon is present in exon 1 in *n1b* -/- PMSC.

Generation of a *ncam1b* deletion mutant

The *ncam1b* **del**etion mutant (*n1b* -/- Del) was generated through the CRISPR/Cas9 genomic editing system, employing gRNAs designed with the CRISPOR web tool and sourced from Integrated DNA Technologies. To generate *n1b* -/- Del, two gRNAs were co-injected with Cas9 protein at a one-cell stage embryo. gRNAs were designed with the CRISPOR web tool. The Cas9 enzyme, when complexed with the gRNAs, recognizes and cleaves specific DNA sequences, creating double-strand breaks (DSBs) at the target sites. The presence of two DSBs before and after the sequence to be deleted, and subsequent non-homologous end joining (NHEJ) repair, a defined deletion in the target gene can be generated (Fig. 3.2 A). The first gRNA targeted the same sequence in exon 1 as described for the *n1b* -/- PMSC mutant, while the second targeted a sequence downstream of the stop codon. A 205,908-base deletion, predicted to result in the almost complete loss of the *ncam1b* gene, was isolated and propagated for studies. Despite the deletion, a small mRNA of 33 bases is still translated (Fig. 3.2 C). To investigate whether a deletion occurred, PCRs with different primer combinations were performed. In the WT situation, due to the large distance of approximately 200,000 bps between primers 1f and 1r and the short extension time chosen during PCR, no amplicon would be generated (Fig. 3.2 A). In contrast, a mutated allele with the deletion exhibits only a distance of approximately 700 bps between the two primers, allowing for successful amplification. The deletion was subsequently confirmed by sequencing (data not shown). Injected siblings were grown to adulthood and tested for germline transmission of the *ncam1b* deletion using the previously established PCR strategy. Among 10 animals examined, one founder was identified carrying the deletion of *ncam1b* (data not shown). For accurate genotyping of progeny from crosses of heterozygous carriers, a second PCR was conducted, wherein one primer (2r) anneals exclusively between the two target regions (Fig. 3.2 B). This primer can only bind and generate an amplicon with primer 2f if no deletion is present. Consequently, this strategy enables

the differentiation between WT and mutated alleles. Homozygous fish were raised to adulthood and subjected to experiments. *n1b* -/- Del embryos were obtained through a cross of homozygous mutant parents.

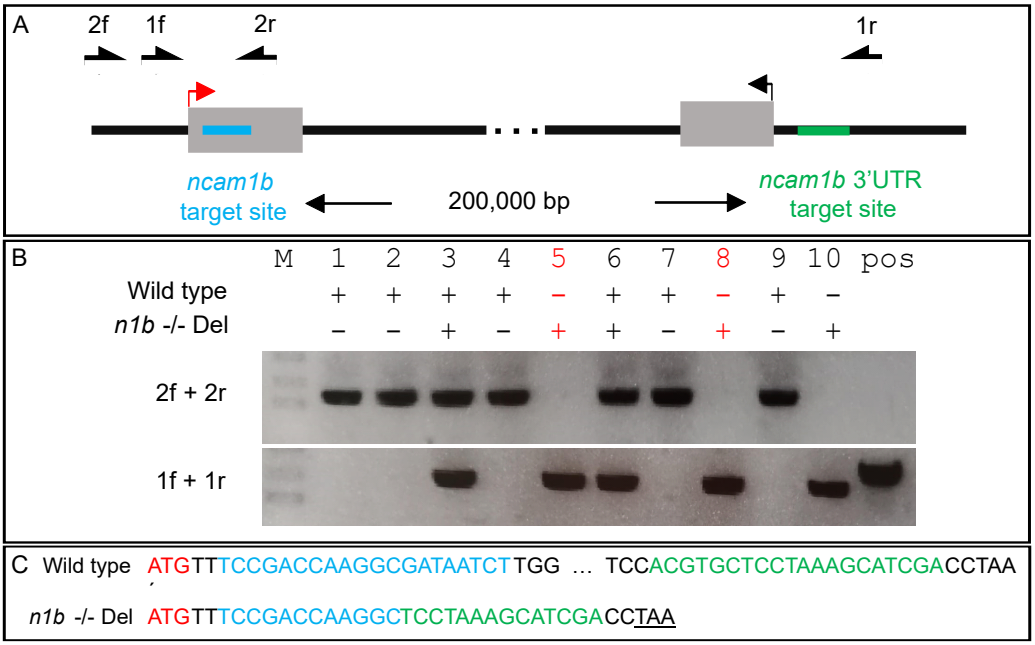

Figure 3.2: Schema of the *ncam1b* gene targeting and screening strategy. (A) Schema of the *ncam1b* gene. The gray box represents the first and the last exon, that have a distance of approximately 200,000 base pairs (bp). Red arrow: start region; black arrow: stop codon; 1f, 2f, 2r: *ncam1b*-flanking primers; 2r: primer that only binds if wild type allele is present; blue region: gRNA target site in exon 1; green region: gRNA target sites in 3' UTR region. **(B)** *n1b* -/- Del DNA sequence shows deletion with sequences of both target sites (blue and green letters) and following newly generated stop codon (underlined). **(C)** PCR represents the genotyping of adult F2 fish. Primers 1f + 1r lead to amplicons if the mutated allele is present. Primers 2f + 2r amplify if a WT allele is present. In this example, fish 5, 8 and 10 are homozygous for the *ncam1b* deletion (red).

3.2.4 Gibson assembly

The Gibson assembly technique is a widely employed, robust cloning strategy that enables the rapid and efficient joining of multiple DNA fragments into vectors via a single isothermal reaction [Gibson et al., 2009, Gibson, 2011]. In the present study, this method was used to generate a positive control construct for identifying *n1b* -/- Del mutants (Fig. 3.2 B "pos"). The critical step in Gibson assembly involves designing 20-40 bp overlapping regions between the DNA fragments designated for assembly and the vector backbone. One DNA fragment spans a few hundred base pairs around the start codon region, while the other fragment covers a few hundred base pairs around the stop codon region. These regions contain the target sites for the gRNAs used to generate *n1b* -/- Del mutants (Fig. 3.3 A). The *ncam1b* fragments were PCR-amplified from zebrafish gDNA using primers harboring the requisite overlapping sequences, while the vector backbone was amplified from the pBluescript II KS+ plasmid. The PCR amplicons were then purified and combined in specific molar ratios: both *ncam1b* amplicons: 0.05 pmol; backbone: 0.025 pmol. A Gibson Assembly® Master Mix (New England Biolabs) contains T5 exonuclease to resect the 5' ends and expose the overlapping regions, Phusion DNA polymerase to fill in the gaps and Taq DNA ligase to seal the nicks. The reaction was conducted according to

the manufacturer's instructions. The assembled construct (Fig. 3.3 B) was then transfected into electrocompetent *E. coli* cells (XL1-blue strain from Agilent Technologies) and plated on selective media to identify positive clones.

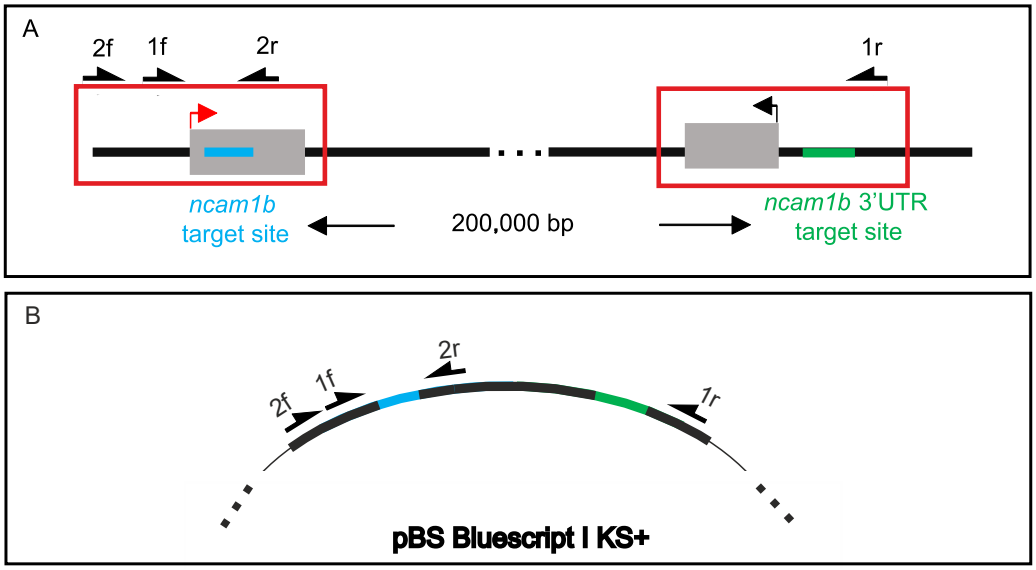

Figure 3.3: Strategy using Gibson assembly to generate a positive control for the deletion mutant. (A) Schema of the *ncam1b* genomic sequence. The blue region represents the target site in exon 1 downstream of the start codon. The green region represents the target site downstream of the stop codon. The area enclosed in red is the region that was cloned into a vector using Gibson assembly. **(B)** Assembled plasmid shows how the *ncam1b* regions are arranged in the pBluescript II KS+ and how the respective primers can be used for positive control.

Transfection by electroporation

During electroporation, electrocompetent *E. coli* cells (XL1-blue strain from Agilent Technologies) are subjected to an electrical pulse, allowing them to receive DNA. 50 µl of *E. coli* cells were mixed with 1 µl of the DNA mixture in a cuvette with a 0.2 cm gap, and electroporation was carried out at 2.5 kV. Subsequently, 1 ml of prewarmed SOC medium was added to the bacteria, following incubation at 37 °C for 20 min. After incubation on agar plates containing antibiotics, positive colonies could then be picked.

3.2.5 Genotyping

Isolation of DNA for genotyping

The DNA of embryos was isolated 24 hpf using the Hot shot method. In this process, individual embryos or pools of embryos were incubated in NaOH (20 µl per embryo) for 20 min at 95 °C. After 5 min on ice, the DNA was centrifuged at 13,000 rpm at 4 °C, and the supernatant was used for further work or stored at 4 °C. For DNA extraction from adult fish, skin swabbing was performed using a cotton swab, following Tilley et al. (2020). DNA isolation was performed using Hot shot method as well.

Sequencing

All sequencing procedures were conducted by the company Eurofins (Ebersberg, Germany). The sequencing was performed using the Sanger method.

3.2.6 Hair cell toxicity assay

Aminoglycoside antibiotics, such as neomycin, are highly toxic to mechanoreceptive hair cells [Harris et al., 2003]. 5 ml of 0.5x E2 medium was supplemented with neomycin to achieve a final concentration of 300 µM. Zebrafish larvae at 5 dpf were washed three times for 5 min each in fresh E2 medium before being transferred to the neomycin solution. After 1 h of incubation, the animals were quickly rinsed three times in new E2 medium and then maintained in E3 medium at 28.5 °C. To analyze hair cell regeneration, embryos were fixed in 4 % PFA in phosphate buffer before neomycin treatment, immediately after, and at 1 days post-treatment (dpt), 2 dpt, 3 dpt and 4 dpt. As a control, embryos were incubated with 1 % DMSO in E2 medium instead, representing the state of homeostasis.
The Delta-Notch signaling pathway plays a crucial role in regulating the coordinated differentiation of support cells into hair cells during development and regeneration through lateral inhibition [Ma et al., 2008, Matsuda and Chitnis, 2010]. It has been shown that blocking this pathway with the Notch inhibitor DAPT after hair cell damage results in increased hair cell formation [Romero-Carvajal et al., 2015]. After neomycin treatment, embryos were incubated for 1 h in E2 medium at 28.5 °C and then transferred for 48 h to a solution containing 50 µM DAPT at the same temperature. A control group was incubated in a solution of 1 % DMSO in E2 medium. Following treatment, the embryos were cooled on ice, fixed overnight in a 4 % PFA solution in phosphate buffer at 4 °C, and then immunohistochemical stained according to a standard protocol.

3.2.7 Immunohistochemistry of whole-mount embryos

Immunohistochemistry (IHC) relies on the specific binding of antibodies to their target antigens, allowing the detection of proteins. At specific time points, the embryos were fixed with 4 % PFA in phosphate buffer at 4 °C overnight. After fixation, the embryos were washed several times with 1x phosphate buffer to remove any residual PFA. Once the fixation and washing steps were complete, the embryos were ready for IHC (Table 3.27).

The incubation time for permeabilization using acetone depends on the age:

- 36 hpf: 5 min
- 48 hpf: 6 min
- older than 5 dpf: 10 min

Table 3.27: Immunohistochemistry of whole-mount embryos.

Temperature	Time	Reagent	Application
4 °C	2 min	4 % PFA in phosphate buffer	Fixation
RT	3x 5 min	1x Phosphate buffer	Washing
RT	5 sec	ddH_2O	Washing
-20 °C	depends on the age	Acetone	Permeabilization
RT	5 sec	ddH_2O	Washing
RT	3x 5 min	1x Phosphate buffer	Washing
RT	2x 5 min	Sodium borohydride	Reduction
RT	2 min	PBS	Washing
RT	30 min	PBD	Blocking
4 °C	overnight	1^{st} Antibody in PBD	Binding
RT	3x 15 min	PBD	Washing
RT	2 h	2^{nd} Antibody in PBD	Binding
RT	3x 15 min	PBD	Washing

3.2.8 Cell proliferation assay

To assess whether there is altered proliferation in the migrating primordium, zebrafish embryos were treated with bromodeoxyuridine (BrdU). This chemical analog of the nucleotide thymidine is absorbed by cells and incorporated into newly synthesized DNA as a marker during the S-phase of the cell cycle. Embryos at 36 hpf were washed in E3 medium, containing 15 % DMSO, and then incubated on ice for 20 min in E3 medium supplemented with 10 mM BrdU. After rinsing with fresh E3 medium, the embryos were incubated again for 20 min at 28.5 °C and then fixed in 4 % PFA in PBS at 4 °C overnight. To investigate proliferation during regeneration, embryos were washed in E3 medium, then incubated from 1 dpt to 2 dpt in 10 mM BrdU containing 1 % DMSO at 28.5 °C. After rinsing with fresh E3 medium, embryos were fixed in 4 % PFA in PBS at 4 °C for at least 4 h, and subsequently dehydrated in 100 % methanol at -20 °C. For long-term storage, embryos can be kept in 100 % methanol at -20 °C. Following fixation, the embryos were stained with an antibody against BrdU to visualize proliferating cells (Table 3.28).

Table 3.28: BrdU-Assay.

Temperature	Time	Reagent	Application
4 °C	overnight	4 % PFA in PBS	Fixation
-20 °C	storage	100 % MeOH	Permeabilization
RT	5 min	50 % MeOH/50 % PBS	Rehydration
RT	4x 15 min	0.5 % PBST	Washing
RT	10 min	10 µg/ml Proteinase K	Permeabilization

Table 3.28: BrdU-Assay.

Temperature	Time	Reagent	Application
RT	4x 15 min	0.5 % PBST	Washing
RT	30 min	4 % PFA in PBS	Fixation
37 °C	15 min	2 N HCl	Denaturation of BrdU-epitope
RT	15 min	0.5 % PBST	Washing
RT	1 h	PBD	Blocking
4 °C	overnight	1 st Antibody in PBD	Antibody incubation
RT	3x 15 min	PBD	Washing
RT	2 h	2 nd Antibody in PBD	Antibody incubation
RT	3x 15 min	PBD	Washing

3.2.9 Fluorescence *in situ* hybridization

in vitro transcription for preparation of probes

The *in vitro* transcription for preparation of probes for fluorescence *in situ* hybridization (FISH) was performed with a linearized plasmid with T7, following the manufacturer's instructions at 37 °C for 2 h. Probes were purified using LiCl precipitation overnight at -20 °C. After washing with 70 % ethanol, RNA was dried and dissolved in 20 µl RNase free water. To prevent the degradation of the probe by RNases, 40 units of RiboLock RNase Inhibitor were added. The integrity of the purified RNA was assessed by adding 50 % formamide and using non-denaturing agarose gel electrophoresis. Agarose gels were prepared in 1x TAE buffer containing ROTI®GelStain (Carl Roth).

Fixation and conservation of embryos

The embryos were manually dechorionated using forceps and immediately treated with 0.3 % PTU in E3 medium to prevent pigmentation. For FISH analysis, whole-mount embryos at 36 hpf were fixed with 4 % PFA in PBS at 4 °C overnight. To preserve the embryos for subsequent processing and storage, they were dehydrated in a graded methanol serie following Table 3.29 and stored at -20 °C until needed for FISH (Table 3.30 - 3.33).

Table 3.29: Methanol serie.

Temperature	Time	Reagent
RT	3x 5 min	PBST
RT	1x 5 min	25 % MeOH/75 % PBST
RT	1x 5 min	50 % MeOH/50 % PBST
RT	1x 5 min	75 % MeOH/25 % PBST
RT	1x 5 min	100 % MeOH
-20 °C	up to 6 months	100 % MeOH

FISH - Day 1

Table 3.30: Fluorescence *in situ* hybridization - Day 1.

Temperature	Time	Reagent	Application
RT	5 min	75 % MeOH/25 % PBST	Rehydration
RT	5 min	50 % MeOH/50 % PBST	Rehydration
RT	5 min	25 % MeOH/75 % PBST	Rehydration
RT	2x 5 min	100 % PBST	Rehydration
RT	30 min	4 % PFA in PBS	Fixation
RT	2x 5 min	100 % PBST	Rehydration
RT	30 min	Proteinase K (10 µg/ml)	Permeabilization
RT	2x 2 min	2 mg/ml Glycin in PBST	Stopping proteinase K
RT	30 min	4 % PFA in PBS	Fixation
RT	4x 5 min	PBST	Washing
69 °C	1h	Hyb + (fresh)	Pre hybridization
69 °C	overnight	Probes in Hyb +	Washing

Since injected embryos have very delicate tissue, the proteinase K incubation time is reduced to 10 min.

Probes in Hyb +:

- 200 ng probe in 200 µl Hyb +
- 3 min 99 °C denaturation, then cool on ice
- Heat to 69 °C, then add to embryos

FISH - Day 2

Table 3.31: Fluorescence *in situ* hybridization - Day 2.

Temperature	Time	Reagent	Application
69 °C	5 min	Hyb -	
69 °C	10 min	75 % Hyb -/25 % 2x SSCT	Washing
69 °C	10 min	50 % Hyb -/50 % 2x SSCT	Washing
69 °C	10 min	25 % Hyb -/75 % 2x SSCT	Washing
69 °C	5 min	2x SSCT	Washing
69 °C	30 min	0.2x SSCT	Washing
RT	5 min	50 % 0.2x SSCT/50 % MABT	Washing

Table 3.31: Fluorescence *in situ* hybridization - Day 2.

Temperature	Time	Reagent	Application
RT	5 min	MABT	Washing
RT	1 h	2 % Blocking solution in MABT	Blocking
4 °C	overnight	Antibody in 2 % Blocking solution in MABT	

Preparation 1 st antibody in 2 % Blocking solution in MABT:

- Wash WT embryos 4x 15 min in MABT at RT
- Anti-DIG-POD (0.05 U/ml) in 2 % Blocking Solution in MABT, RT, at least 1 h, rotating

FISH - Day 3

Table 3.32: Fluorescence *in situ* hybridization - Day 3.

Temperature	Time	Reagent	Application
RT	4x 20 min	MABT	Washing
RT	2x 5 min	PBST	Washing
RT	5 min	0.1 M Borate buffer + 0.1 % Tween 20	
RT (darkness)	30 min	90 µl Amp. diluent + 0.45 µl Cy5 (1:200)	Staining reaction
RT	3x 10 min	PBST	Stopping
RT	10 min	100 mM Glycin-HCl	Deactivation POD
RT	3x 5 min	PBST	Washing
RT	1 h	2 % Blocking solution in MABT	Blocking
4 °C	overnight	Antibody in 2 % Blocking solution in MABT	

Preparation 1 st antibody in 2 % Blocking solution in MABT:

- Wash WT embryos 4x 15 min in MABT at RT
- Anti-Fluorescein-POD (0.05 U/ml) in 2 % Blocking solution in MABT, RT, at least 1 h, rotating

FISH - Day 4

The GFP signal from *Tg(ClaudinB::lynGFP)* was diminished by the FISH procedure, so the signal is amplified again using antibody staining against GFP after the FISH procedure.

Table 3.33: Fluorescence *in situ* hybridization - Day 4.

Temperature	Time	Reagent	Application
RT	4x 20 min	MABT	Washing
RT	2x 5 min	PBST	Washing
RT	5 min	0.1 M Borate buffer + 0.1 % Tween 20	
RT (darkness)	30 min	90 µl Amp. diluent + 0.45 µl Cy3 (1:200)	Staining
RT	3x 10 min	PBST	Washing
RT	2 h	1^{st} Antibody in 2 % Blocking solution in MABT	Re-staining
RT	10 min	PBST	Washing
RT	2 h	2^{nd} Antibody in 2 % Blocking solution in MABT	
RT	10 min	PBST	Washing

Preparation 1^{st} antibody in 2 % Blocking solution in MABT

- Wash WT embryos 4x 15 min in MABT at RT
- Anti-Fluorescein-POD (0.05 U/ml) in 2 % Blocking solution in MABT, RT, at least 1 h, rotating

Evaluation and quantification of the FISH experiments

The FISH samples were imaged using an Apotome microscope and an LSM 800 confocal laser scanning microscope (both from Zeiss, Oberkochen, Germany). Images were processed and analyzed using the ZEN 2 lite software (Zeiss) and the open-source FIJI distribution of ImageJ. To visualize the entire lateral line primordium, *Tg(ClaudinB::lynGFP)* transgenic embryos were double-labeled with fluorescent probes targeting *lef1* and *fgfr1a* or *lef1* and *erm*. *lef1* is specifically expressed in the Leading Zone of the primordium [Lecaudey et al., 2008], while *fgfr1a* and *erm* mark the Trailing Zone [Aman and Piotrowski, 2008]. For each primordium imaged, the stained area was manually outlined based on the probe signals. On the one hand, the complete area was measured, and on the other hand, the longest length of this area was measured using FIJI (Fig. 3.4). To relate the length of the expression regions to the total length of the primordium, the precise start and end points of the tissue had to be clearly defined. Since heterozygous *Tg(ClaudinB::lynGFP)* parents were bred, not all of the investigated embryos exhibit a ClaudinB-driven GFP signal. In embryos that expressed ClaudinB-driven GFP, the ends of this fluorescent signal could be used to delineate the primordium boundaries. But in embryos lacking the transgene, an alternative approach was needed. To overcome these challenges, a sample of 10 embryos that showed a ClaudinB-driven GFP signal was selected for closer examination. This allowed to verify that the probes bind to the actual ends of the primordium tissue, as indicated by the GFP fluorescence. Based on this validation, the anterior and posterior ends of the primordium were validated by the ends of the fluorescence *in situ* hybridization signal.

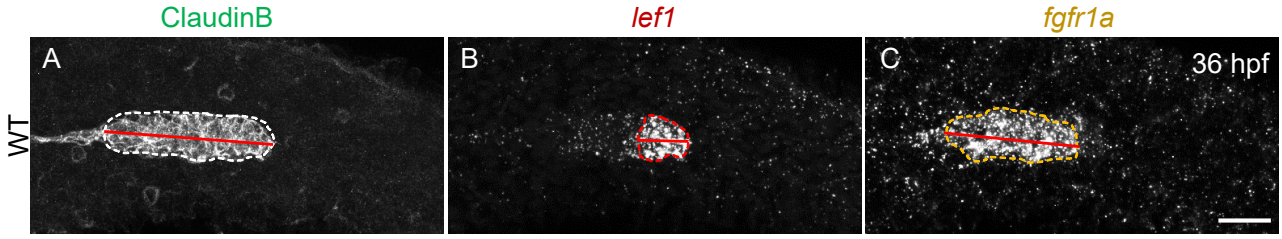

Figure 3.4: Illustration of the measurement procedure for the signal domains and its lengths in the primordium after a FISH experiment. Staining of the primordium: **(A)** GFP of *Tg(ClaudinB::lynGFP)*, fluorescence *in situ* hybridization for **(B)** *lef1* and **(C)** *fgfr1a*. **(A - C)** The areas interpreted as stained are outlined and the length of the stained regions was determined along the longest extension of the stained domain (red line).

Evaluation and quantification of Ncam1a expression in the primordium

To compare the Ncam1a expression in the primordium of WT and *ncam1b* -/- Del mutants, embryos with a *Tg(ClaudinB::lynGFP)* background were used. The use of *Tg(ClaudinB::lynGFP*) allowed for precise delineation of the primordium, ensuring that the Ncam1a signal was quantified only within this specific region of interest. By setting appropriate thresholds, the gray values corresponding to Ncam1a staining could be measured. To compare, the mutant gray value was divided by the WT gray value. This allowed to compare the mutant values relative to WT, which was set to 1. Values above 1 indicated an increase in signal in the mutant compared to WT, while values below 1 indicated a decrease in signal.

3.2.10 Molecular biological methods

Polymerase Chain Reaction

The amplification of gene segments was performed using Polymerase Chain Reaction (PCR) with different polymerases. Optimized for the polymerase and the respective primers, the following final cycle sequences were used:

- Amplification of exon 1 of *ncam1b*: HotStart Taq DNA Polymerase with antibody,
  Primer: 75 + 76
  94 °C, 3:00 min; [94 °C, 0:22 min; 52 °C, 0:22 min; 72 °C, 0:22 min] x 35 Cycles;
  72 °C, 10:00 min; 4 °C

- Amplification of 3' UTR of *ncam1b*: VeraSeq High Fidelity DNA Polymerase,
  Primer 121 + 122
  98 °C, 0:30 min; [98 °C, 0:10 min; 61 °C, 0:30 min; 72 °C, 0:20 min] x 35 Cycles;
  72 °C, 10:00 min; 4 °C

- Amplification of cDNA of *ncam1b* of WT and *n1b* -/- PMSC: Phusion Master Mix,
  Primer: 147 + 150
  98 °C, 0:30 min; [98 °C, 0:10 min; 65-50 °C (1 °C/Cycle down to 50 °C), 0:15 min; 72 °C, 1:00 min]
  98 °C, 0:30 min; [98 °C, 0:10 min; 50 °C, 0:15 min; 72 °C, 1:00 min] x 35 Cycles;
  72 °C, 5:00 min; 4 °C

- Amplification to detect deletion of exon 1 - 3' UTR in *n1b* -/- Del: HotStart Taq DNA Polymerase with antibody,
  Primer: TS728116 + 176
  94 °C, 3:00 min; [94 °C, 0:22 min; 52 °C, 0:22 min; 72 °C, 0:22 min] x 35 Cycles;
  72 °C, 10:00 min; 4 °C

- Amplification of *ncam1b* exon 1 for Gibson assembly: Q5® High-Fidelity DNA Polymerase,
  Primer: 187 + 188
  98 °C, 0:30 min; [98 °C, 0:10 min; 58 °C 0:15 min; 72 °C, 1:00 min] 5 Cycles;
  98 °C, 0:30 min; [98 °C, 0:10 min; 66 °C, 0:15 min; 72 °C, 2:00 min] 25 Cycles;
  72 °C, 5:00 min; 4 °C

- Amplification of *ncam1b* 3' UTR for Gibson assembly: Q5® High-Fidelity DNA Polymerase,
  Primer: 189 + 190
  98 °C, 0:30 min; [98 °C, 0:10 min; 72 °C 0:15 min; 72 °C, 1:00 min] 35 Cycles;
  72 °C, 2:00 min; 4 °C

- Amplification of pBS Bluescript I KS+ backbone for Gibson assembly: Q5® High-Fidelity DNA Polymerase,
  Primer: 191 + 192
  98 °C, 0:30 min; [98 °C, 0:10 min; 70 °C 0:15 min; 72 °C, 1:00 min] 5 Cycles;
  98 °C, 0:30 min; [98 °C, 0:10 min; 72 °C, 0:15 min; 72 °C, 2:00 min] 25 Cycles;
  72 °C, 2:00 min; 4 °C

Total RNA extraction

Total RNA was isolated from pools of 100 embryos (WT, *n1b* -/- PMSC, *n1b* -/- Del) for the subsequent PCR or ddPCR experiments. Embryos were transferred to 1.5 ml microcentrifuge tubes, and the medium was removed. Shock-freezing the samples in liquid nitrogen enabled long-term storage at -80 °C. To extract the RNA, 1 ml of TRIzol Reagent (Thermo Fisher Scientific, Waltham, USA) was added to each sample, and the embryos were homogenized by repeated pipetting with needles (21 G, then 26 G). The addition of 200 µl of chloroform facilitated phase separation, with the RNA partitioning into the aqueous phase. This phase was transferred to a fresh tube, and 240 µl of 100 % ethanol was added to precipitate the RNA. The RNA was then purified using MinElute columns and the RNeasy Micro Kit (Qiagen, Hilden, Germany), following the manufacturer's instructions. To eliminate any residual DNA contamination, a Turbo DNase digestion was performed in the end. Finally, the purified RNA was precipitated overnight at -20 °C by adding sodium acetate and ethanol. The precipitated RNA was resuspended in RNase-free water and stored at -80 °C until further use.

cDNA synthesis for following droplet digital PCR

For cDNA synthesis via reverse transcription of the embryonic RNA samples, 500-1000 ng of total RNA was used as a template. To enable the analysis of multiple gene transcripts via droplet digital PCR (ddPCR), random hexamer primers were utilized at a final concentration of 2.5 µM. The cDNA synthesis reaction was performed using the SuperScript IV Reverse Transcriptase (Thermo Fisher Scientific), following the manufacturer's instructions. RiboLock RNase inhibitor was included to prevent degradation of the RNA template. Following cDNA synthesis, any remaining RNA-DNA hybrids and single-stranded RNA were enzymatically digested using RNase H and RNase A. The resulting cDNA was then purified using the DNA-Clean & Concentrator Kit (Zymo, Freiburg, Germany), eluted in DNase/RNase-free water, and the concentration was determined spectrophotometrically using a NanoDrop instrument (VWR, Radnor, USA).

Droplet digital PCR

The transcription of the genes *ncam1b*, *ncam1a*, and *l1cam* (Genes of Interest, GOIs) was quantified at 36 hpf using ddPCR. Samples were collected from three biological replicates of the following conditions: WT embryos, *n1b* -/- PMSC embryos, and *n1b* -/- Del embryos. Each biological replicate consisted of a pool of 100 embryos. The gene expression of the target transcripts was normalized against the expression of housekeeping genes (HCG) (β-Actin). To determine the relative transcript amount, 1.7 - 2.5 ng of cDNA was analyzed in a ddPCR, testing technical duplicates. To identify any potential contamination by genomic DNA or other unwanted DNAs, two control reactions were included in the ddPCR analysis: a no-RT control lacking reverse transcriptase, and a no-template water control. To prepare one sample for ddPCR, the following components are pipetted into a well of a ddPCR 96-well plate while keeping the plate on ice, as described in Table 3.34.

Table 3.34: ddPCR reaction components.

ddPCR reaction components	Volume
QX200 ddPCR EvaGreen Supermix (Bio-Rad)	10 µl
Forward Primer (1 µM)	2 µl
Reverse Primer (1 µM)	2 µl
cDNA	1.7 - 2.5 ng total
DNase free water	ad 20 µl

After preparation of all samples, the reaction components were first transferred to a 96-well plate and sealed using a PCR plate heat sealer (PCR Plate Heat Seal, PX1 PCR Plate Sealer). The droplet generation was then performed using the Automated Droplet Generator (Bio-Rad, Hercules, USA). This instrument was loaded with the required consumables (Automated Droplet Generator Cartridges, Droplet Generation Oil for EvaGreen, Pipet Tips for the AutoDG System) and created an emulsion of the ddPCR reaction components. The resulting emulsion contained up to 20,000 independent droplets, allowing the subsequent PCR amplification to be divided into up to 20,000 independent reactions (Table 3.35).

Table 3.35: ddPCR program.

PCR Program	Temperature	Time	Cycles
Initiale denaturation	95 °C	5 min	1x
Denaturation	95 °C	30 sec	
Annealing	57 °C	1 min	40x
Elongation	58 °C	1 min	
Enzyme deactivation	98 °C	10 min	1x
Storage	8 °C	forever	

The digital analysis of the individual droplets was performed using the QX200 Droplet Reader and the associated QuantaSoft software (Version 1.7.4, Bio-Rad). The fluorescence intensity of the individual droplets was measured and categorized as positive or negative by applying a user-defined threshold. To calculate the relative gene expression, the ratio of GOI/HKG transcripts was determined for each sample. The ratios of the biological replicates were geometrically averaged. The ratios of the WT genotype were defined as the 100 % expression value of the respective GOI. The ratios of the *n1b* -/- Del and of the *n1b* -/- PMSC genotypes were normalized to the WT value.

4 Results

Sensory hair cells are essential for hearing and balance in humans. In contrast to fish and amphibians, hair cells in mammals are incapable of regeneration following damage, resulting in permanent hearing impairment [Davis et al., 1989, Chardin et al., 1995]. The zebrafish represents a powerful model organism to investigate not only hair cell development but also the remarkable regenerative capacity of the posterior lateral line system (pLLS) [Harris et al., 2003]. Previous studies employing morpholino-mediated knockdown approaches have highlighted the critical role of the neural cell adhesion molecule Ncam1b during the pLLS development in zebrafish [Dries et al., 2021]. Knockdown of *ncam1b* leads to severe structural abnormalities, including a reduced number of neuromast and primordium migration defects associated with impaired proliferation. Ncam1b is expressed not only during the development of the pLLS, but also in support cells and hair cells during regeneration. This observation, coupled with the developmental defects observed upon *ncam1b* knockdown, suggests that Ncam1b may play an important role in this regenerative process.

4.1 Both, *n1b* -/- PMSC and *n1b* -/- Del do not express Ncam1b

In this study, the functional role of Ncam1b during developmental and regenerative processes in pLLS was investigated using two stable, independent *ncam1b* mutant lines. The **P**re **M**ature **S**top **C**odon mutant (*n1b* -/- **PMSC**) was generated by a single gRNA co-injected with Cas9 protein. This resulted in a site-specific insertion/deletion (indel) mutation in the corresponding target site in exon 1, as evaluated by PCR and sequencing (Fig. 3.1). The newly generated stop codon in exon 1 leads to an early termination in protein biosynthesis resulting in a truncated, non-functional protein. However, to avoid alternative translational start sites and to allow faster and easier identification of carrier fish, a second *ncam1b* mutant was generated, namely the *ncam1b* **del**etion mutant (*n1b* -/- **Del**). To achieve an elimination of almost the entire open reading frame (ORF) of *ncam1b*, two CRISPR/Cas9 target sites were selected. The first site lies in close proximity downstream of the start codon and the second target sequence lies downstream of the stop codon in the 3' untranslated region (3' UTR), separated by approximately 200,000 bp from the first target site. The target site in exon 1 was chosen as the 5' target site, as no efficient target site was found upstream of the start codon. The gRNAs against exon 1 and the 3' UTR were co-injected with Cas9 protein, and the deletion event in the genomic DNA was detected by PCR (Fig. 3.2). This almost complete deletion of the gene results in a loss of gene expression and protein function.

Ncam1b expression in both mutants was studied via immunohistochemical staining at 36 hpf (Sup. S1) and 48 hpf (Fig. 4.2). In wild type (WT), Ncam1b expression was detected in the otic vesicle (Fig. 4.2 B''), in the Trailing Zone of the primordium (Fig. 4.2 H''), as well as in the deposited proneuromasts (Fig. 4.2 E''). Conversely, no antibody binding was observed in any of these or other structures in both mutant lines (Fig. 4.2 *n1b* -/- PMSC: C'', F'', I'', *n1b* -/- Del: D'', G'', J''). These results could not be confirmed in Western blots, as the Ncam1b antibody did not work reliably in that application.
As an additional control, droplet digital polymerase chain reaction (ddPCR) was performed to examine the amount of *ncam1b* mRNA in both mutants. Primers were designed to target the coding region corresponding to the Ig2 domain, a critical component for heterophilic and homophilic interactions. This design ruled out the possibility of a truncated protein escaping the stop codon and retaining essential functions. Since the *n1b* -/- PMSC mutant only has a deletion of a single base, it was hypothesized that mRNA would still be present, possibly at a lower amount, because of degradation due to nonsense-mediated mRNA decay (NMD). Indeed, the *ncam1b* mRNA level in the *n1b* -/- PMSC mutant was found to be only 39.83 % ($\pm$ 16.26, $p = 0.039$) of the WT level (Fig. 4.1, green bar). The *n1b* -/- Del mutant, lacking almost the complete coding region of *ncam1b*, exhibited no detectable *ncam1b* mRNA (2.37 %, $\pm$ 0.64, $p = 2.6 \times 10^{-8}$) (Fig. 4.1, red bar).

All experiments described below were carried out using the *n1b* -/- Del mutant, as this mutant has an almost complete loss of the coding region. Thus, there is no possibility of producing a yet truncated protein that could mask a potential phenotype. The *n1b* -/- PMSC mutant was occasionally used as an independent control mutant to validate observations and rule out off-target effects of the *n1b* -/- Del mutation.

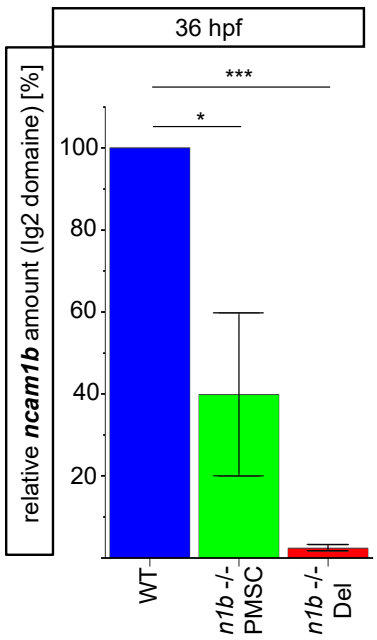

Figure 4.1: Relative mRNA expression of *ncam1b* in WT, *n1b* -/- PMSC and *n1b* -/- Del. Mean relative gene expression (normalized to the housekeeping gene β-actin) $\pm$ SEM of biological triplicates (each mean value of technical duplicates) per condition obtained by ddPCR. Pools of 100 embryos each from WT, *n1b* -/- PMSC and *n1b* -/- Del were analyzed. The *ncam1b* mRNA amount is reduced in *n1b* -/- PMSC (green bar). *ncam1b* mRNA is not detectable in *n1b* -/- Del (red bar). Two-sided *t*-test: *: $p < 0.05$, **: $p < 0.01$, ***: $p < 0.001$, n.s.: not significant.

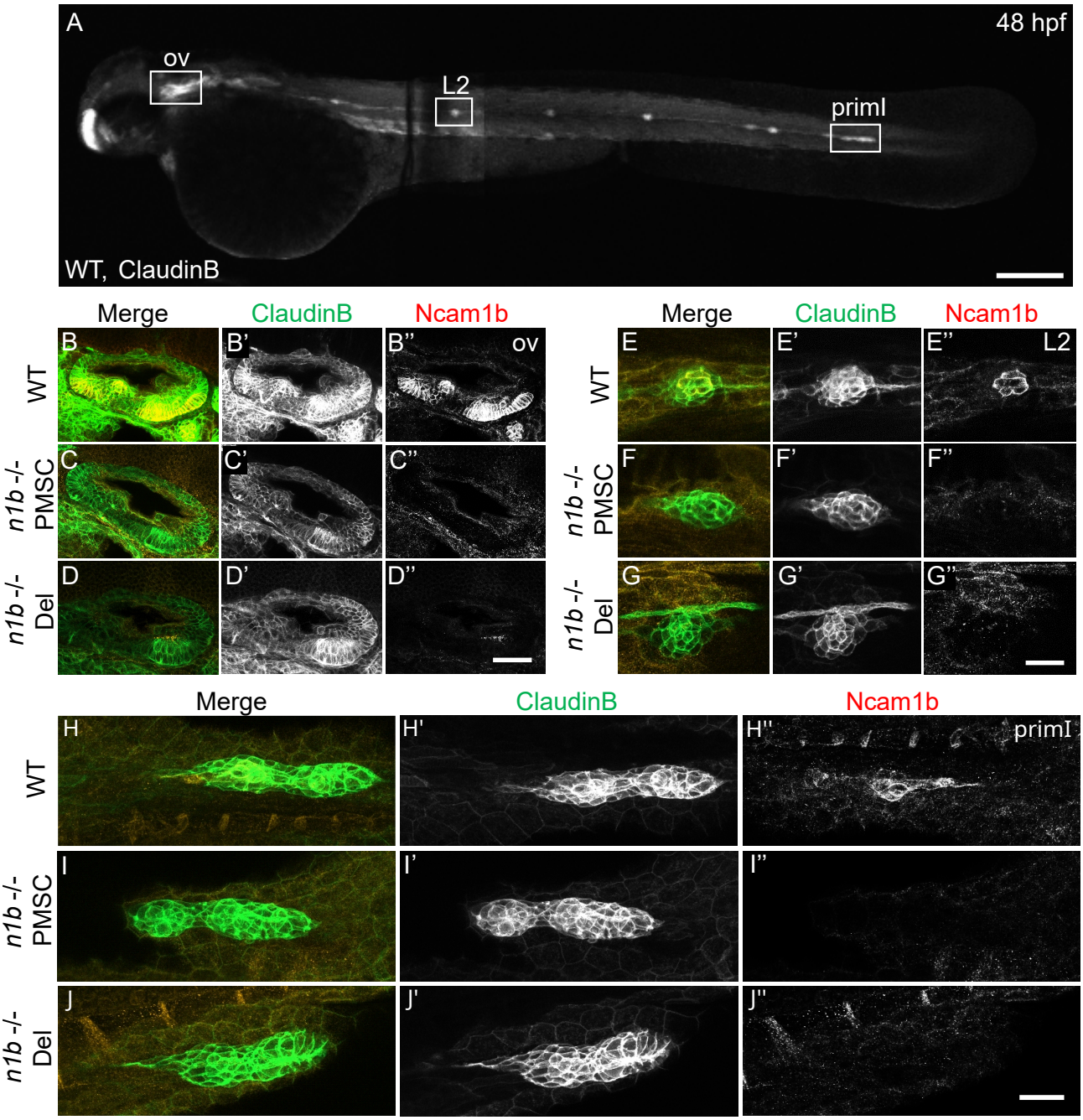

Figure 4.2: *ncam1b* mutant embryos show no expression of Ncam1b. (A) Lateral view of a 48 hpf WT *Tg(ClaudinB::lynGFP)* embryo, specifically visualizing the cells of the otic vesicle (ov), the posterior lateral line primordium (primI) and deposited proneuromasts. Otic vesicle, proneuromast L2 and primordium are highlighted. **(B - J'')** Close-up of the otic vesicle, second proneuromast (L2) and the primI respectively, showing expression of GFP (green) and Ncam1b (red) in single channel views and overlays. **(B - D'')** The WT otic vesicle shows Ncam1b antibody binding, while no staining is observed in both mutants in this region. **(E - G'')** L2, as a representative of all other proneuromasts, demonstrates that, in contrast to WT, Ncam1b expression is absent in both mutants. **(H - J'')** In primI's Trailing Zone of WT, Ncam1b antibody staining is detected, while no signal is visible in both mutants. Scale bars, Objectives: **(A)** 200 µm, 5x; **(D'')** 40 µm, 40xOil; **(G'')** 20 µm, 40xW; **(J'')** 20 µm, 40xOil.

4.2 *ncam1b* mutants phenocopy WT lateral line system development

A morpholino knockdown of *ncam1b* results in reduced proliferation leading to a smaller size and a disrupted migration of the primordium [Dries et al., 2021]. Furthermore, the primordium deposits a smaller number of proneuromasts during its migration.
Contrary to the morphant phenotype, both, *n1b* -/- PMSC and *n1b* -/- Del, displayed no defects in pLLS development (Fig. 4.3). Despite the absence of Ncam1b, the mutant primordium successfully reached the tail tip at 48 hpf (Fig. 4.3 D). In WT, the primordium traveled a distance of 1879.5 µm (± 61.96), in *n1b* -/- PMSC it reaches 1856.33 µm (± 54.31, $p = 0.83$), and in the *n1b* -/- Del mutant 1978 µm (± 20.31, $p = 0.31$). The WT primordium deposited approximately 5.25 (± 0.22) proneuromasts along its migratory journey (Fig. 4.3 F). The primordium of the *n1b* -/- PMSC and *n1b* -/- Del mutants deposited 5 or 5.33 proneuromasts, respectively (*n1b* -/- PMSC ± 0, $p = 0.44$; *n1b* -/- Del: ± 0.27, $p = 0.85$). Quantitative analysis revealed that the size of both mutant primordia was comparable to that of the WT (Fig. 4.3 E). The WT primordium measured 119.13 µm (± 5.26), the *n1b* -/- PMSC mutant primordium 115.83 µm (± 5.27, $p = 0.73$), and the *n1b* -/- Del mutant primordium 105.83 µm (± 3.34, $p = 0.16$).

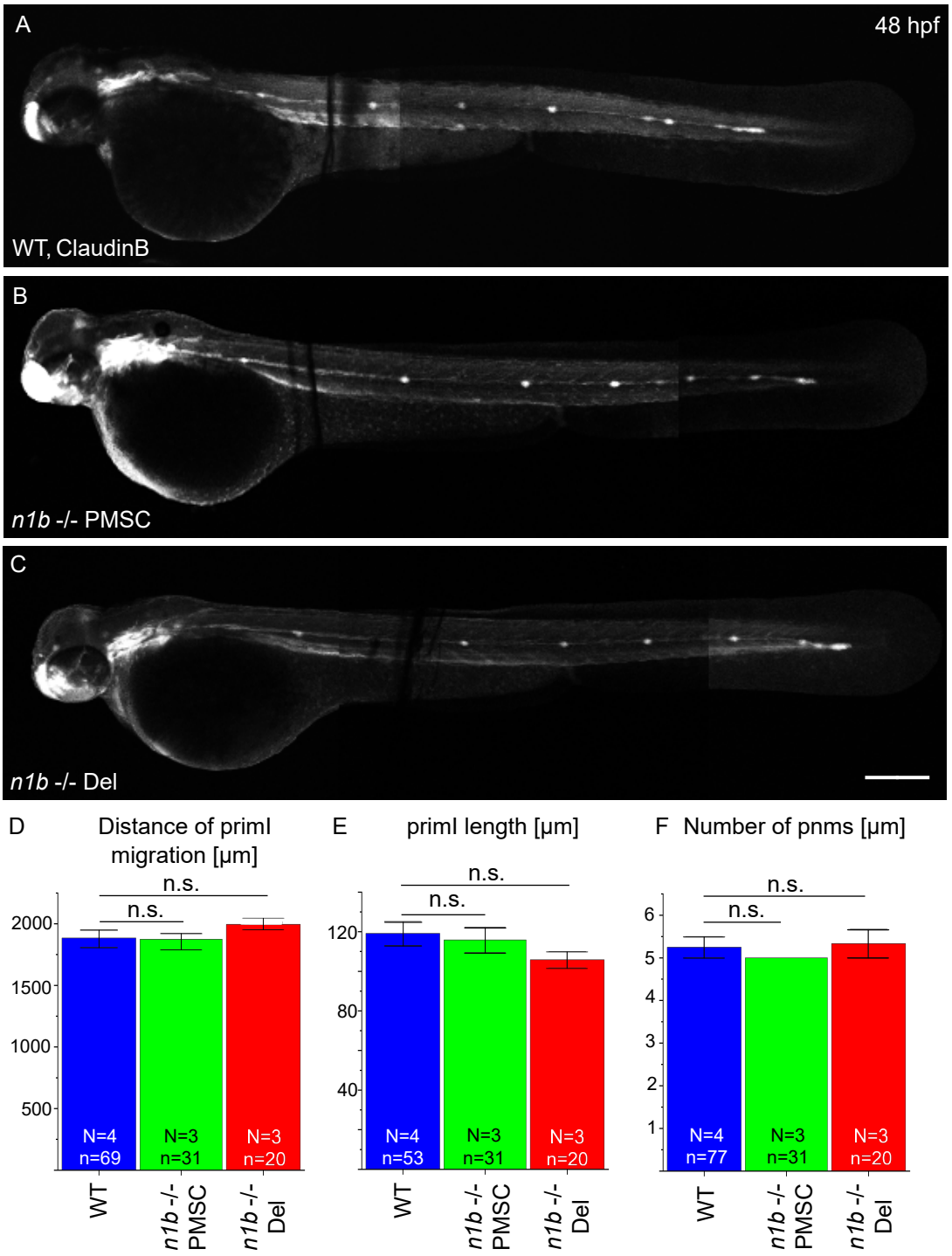

Figure 4.3: Normal development of the posterior lateral line system in *ncam1b* mutant embryos. Lateral view of 48 hpf *Tg(ClaudinB::lynGFP)* **(A)** WT, **(B)** *n1b* -/- PMSC and **(C)** *n1b* -/- Del embryos, showing normal development of the posterior lateral line system. Statistical analyses of **(D)** migration distance, **(E)** size of the primordium (primI) and **(F)** proneuromast (pnms) formation at 48 hpf show that the values for both *ncam1b* mutants do not differ from those of the WT. Two-sided *t*-test: *: $p < 0.05$, **: $p < 0.01$, ***: $p < 0.001$, n.s.: not significant. Scale bar in **(C)** 200 µm, Objective: 5x.

4.3 Ncam1a and related genes are upregulated in *ncam1b* mutants

A discrepancy between morphants and mutants often results from genetic compensation, a phenomenon in which upregulation of related genes compensates the loss of the gene of interest in mutants, thereby masking the expected phenotype [Rossi et al., 2015]. Given that *ncam1b* mutants exhibit normal pLLS development, unlike the severe defects observed in *ncam1b* morphants, it was hypothesized that other genes may be upregulated in the mutants to compensate for the loss of *ncam1b*. Zebrafish possess a paralog of *ncam1b*, namely *ncam1a*, due to a genome duplication event in the teleost lineage [Vandepoele et al., 2004]. Since *ncam1a* and *ncam1b* show overlapping expression in the pLLS, *ncam1a* was considered a potential candidate for genetic compensation. Additionally, the mRNA expression of *l1cam*, a cell adhesion molecule structurally similar to Ncam1b, was examined.

At 36 hpf, ddPCR revealed a statistically significant 3.06-fold (± 0.55, $p = 0.038$) increase in *ncam1a* mRNA expression in *n1b* -/- PMSC mutant embryos compared to WT controls (Fig. 4.4 A). Similarly, the *n1b* -/- Del mutant line exhibited a 2.94-fold (± 0.34, $p = 0.008$) significant upregulation of *ncam1a* mRNA level. Regarding *l1cam* expression, the *n1b* -/- PMSC mutants showed a statistically significant 2.34-fold (± 0.3, $p = 0.022$) increase, while the *n1b* -/- Del mutant line displayed a 2.61-fold (± 0.39, $p = 0.03$) significant upregulation of *l1cam* mRNA compared to WT embryos (Fig. 4.4 B).

The profound impact of the Ncam1b deficiency on the organism appears to elicit compensatory mechanisms that upregulate the expression of other genes. Given that the paralog *ncam1a*, with 66 % homology, is the closest gene to *ncam1b* [Mizuno et al., 2001], immunohistochemical stainings were conducted at 36 hpf to further investigate its expression in the migrating primordium (Fig. 4.4 C + D). This approach revealed a statistically significant 1.26-fold (± 0.006, $p = 0.0019$) enhanced expression of Ncam1a in the migrating primordium of the *ncam1b* mutant embryos compared to the WT controls (Fig. 4.4 E). This finding demonstrates that the increased Ncam1a expression is not only observed throughout the whole mutant embryo, as shown in whole-mount ddPCR, but is specifically enhanced in the migrating primordium. L1cam expression was not further investigated on the protein level, since no specific antibody was available.

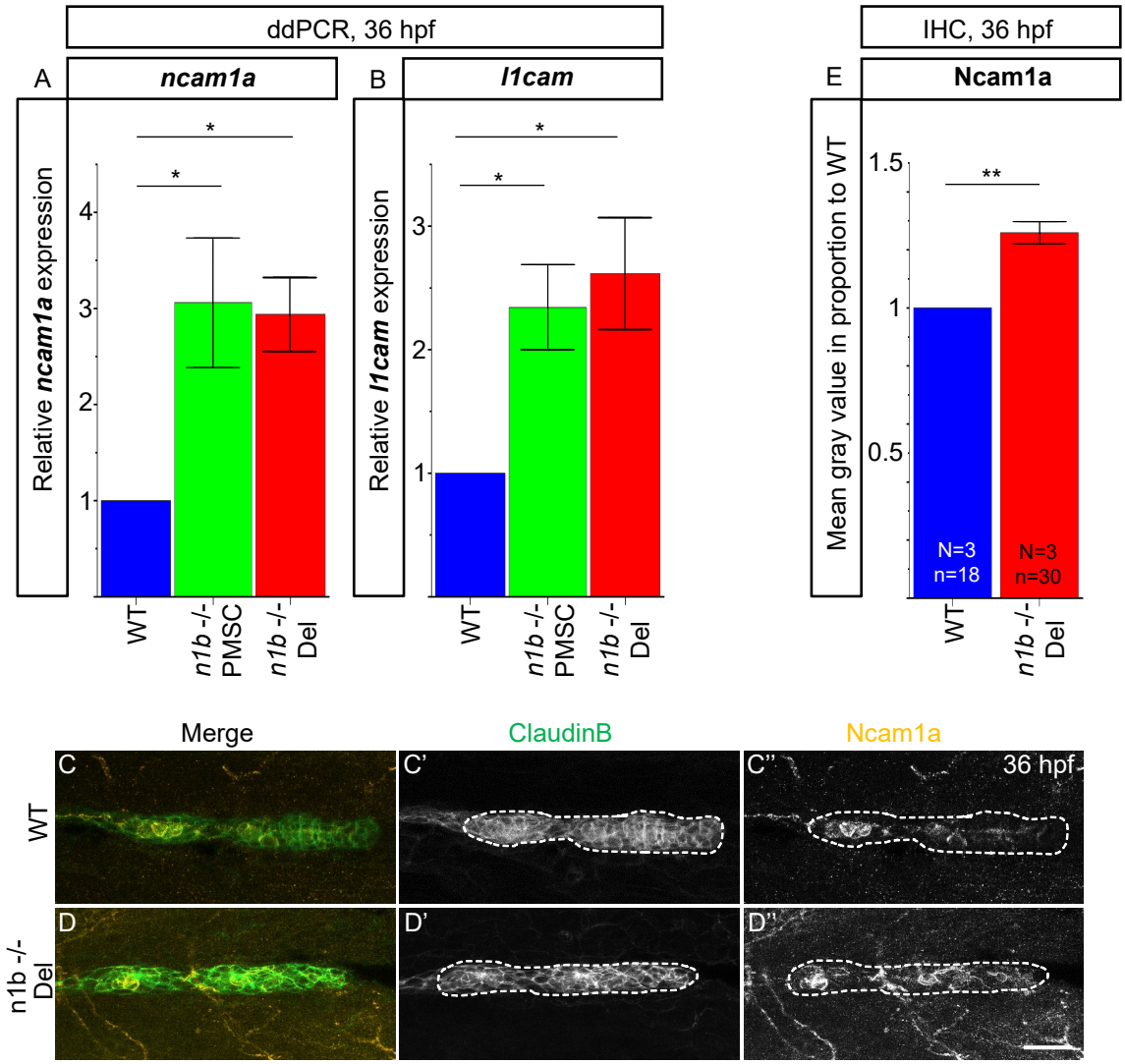

Figure 4.4: Upregulation of *ncam1a* and *l1cam* in *ncam1b* mutant embryos at 36 hpf. **(A + B)** ddPCR measurements normalized to the housekeeping gene β-actin shows significant upregulation of both, **(A)** *ncam1a* and **(B)** *l1cam* in *ncam1b* mutants. Mean gene expression levels were determined using biological triplicates, each representing the mean of technical duplicates. Separate conditions of wild type (WT), *n1b* -/- PMSC mutants, and *n1b* -/- Del mutants were analyzed, with pools of 100 embryos per condition. **(C - E)** Investigation of Ncam1a expression in the migrating primordium was conducted using immunohistochemical staining (IHC) with an antibody against Ncam1a (orange). **(C' + D')** Utilizing *Tg(ClaudinB::lynGFP)*, a threshold was set to delineate the primordium, **(C'' + D'')** enabling the measurement of Ncam1a expression specifically in this defined region. **(E)** The value of the *n1b* -/- Del mutant normalized to the WT shows a significant upregulation of Ncam1a expression. Two-sided *t*-test: *: $p < 0.05$, **: $p < 0.01$, ***: $p < 0.001$, n.s.: not significant. Scale bar in **(D'')** 20 µm, Objective: 40xW.

4.4 Morpholino-induced phenotypes persist in the absence of Ncam1b

Previous *ncam1b* knockdown approaches, such as injection of *ncam1b*-ATG or *ncam1b*-5' UTR morpholinos (MO), resulted in severe developmental phenotypes [Dries et al., 2021]. Morphant embryos exhibited reduced proliferation in a smaller primordium, disrupted migration and a decreased number of deposited proneuromasts. In contrast to the morphants, the stable *ncam1b* mutant lines, generated in the present study, revealed no overt defects in pLLS development (Fig. 4.3). Despite the complete absence of Ncam1b protein, the mutant primordium was able to successfully reach the tip of the tail at 48 hpf and deposited the same number of proneuromasts as the WT. This discrepancy between the severe phenotypes observed in *ncam1b* morphant embryos and the lack of a phenotype in the *ncam1b* mutants has raised concerns about potential off-target effects of the morpholino-mediated knockdown. To further investigate this issue, the current study employed a strategy of injecting the *ncam1b* MOs into the mutant background and analyzing the resulting phenotypes.

4.4.1 Strong effects of the *ncam1b*-ATG morpholino in *ncam1b* mutant embryos

WT and *ncam1b* mutants showed no differences in migration distance, proneuromast deposition and primordium size (Fig. 4.3). Therefore, the following statistics used the WT numbers to avoid overloading the graphs and provide a clearer overview.
The *ncam1b*-ATG morpholino (*ncam1b*-ATG MO) binds to the start codon, thereby inhibiting translation initiation. Injection of this morpholino into WT led to a pronounced phenotype, including disrupted migration, a decreased number of deposited proneuromasts and a smaller size of the primordium (Fig. 4.5 B). Injection into *n1b* -/- PMSC, and *n1b* -/- Del mutant embryos induced a very similar phenotype (Fig. 4.5 C + D). At 48 hpf, the primordium of the WT morphant shows a significantly reduced migration distance of 1414.83 µm (± 123.77, $p = 0.029$) (Fig. 4.5 E). The primordium of *n1b* -/- PMSC and *n1b* -/- Del embryos injected with the *ncam1b*-ATG MO reached distances of 1423.83 µm (± 56.47, $p = 0.73$) and 1476.125 µm (± 58.18, $p = 0.96$), respectively. Primordium lengths as well showed no statistically significant differences between *ncam1b*-ATG MO-injected WT (89 µm ± 5.39, $p = 0.02$), *n1b* -/- PMSC (85 µm ± 5.99, $p = 0.97$), and *n1b* -/- Del (89 µm ± 2.45, $p = 0.75$) embryos (Fig. 4.5 F). The number of deposited proneuromasts was slightly higher in the *n1b* -/- PMSC MO injected embryos (2.5 ± 0.41, $p = 0.57$) and *n1b* -/- Del MO injected embryos (2.5 ± 0.47, $p = 0.55$) than in WT morphants (1.67 ± 0.98), but these differences were not statistically significant (Fig. 4.5 G). In summary, the *ncam1b*-ATG MO causes the same phenotype in *ncam1b* mutants, as it does in the WT.

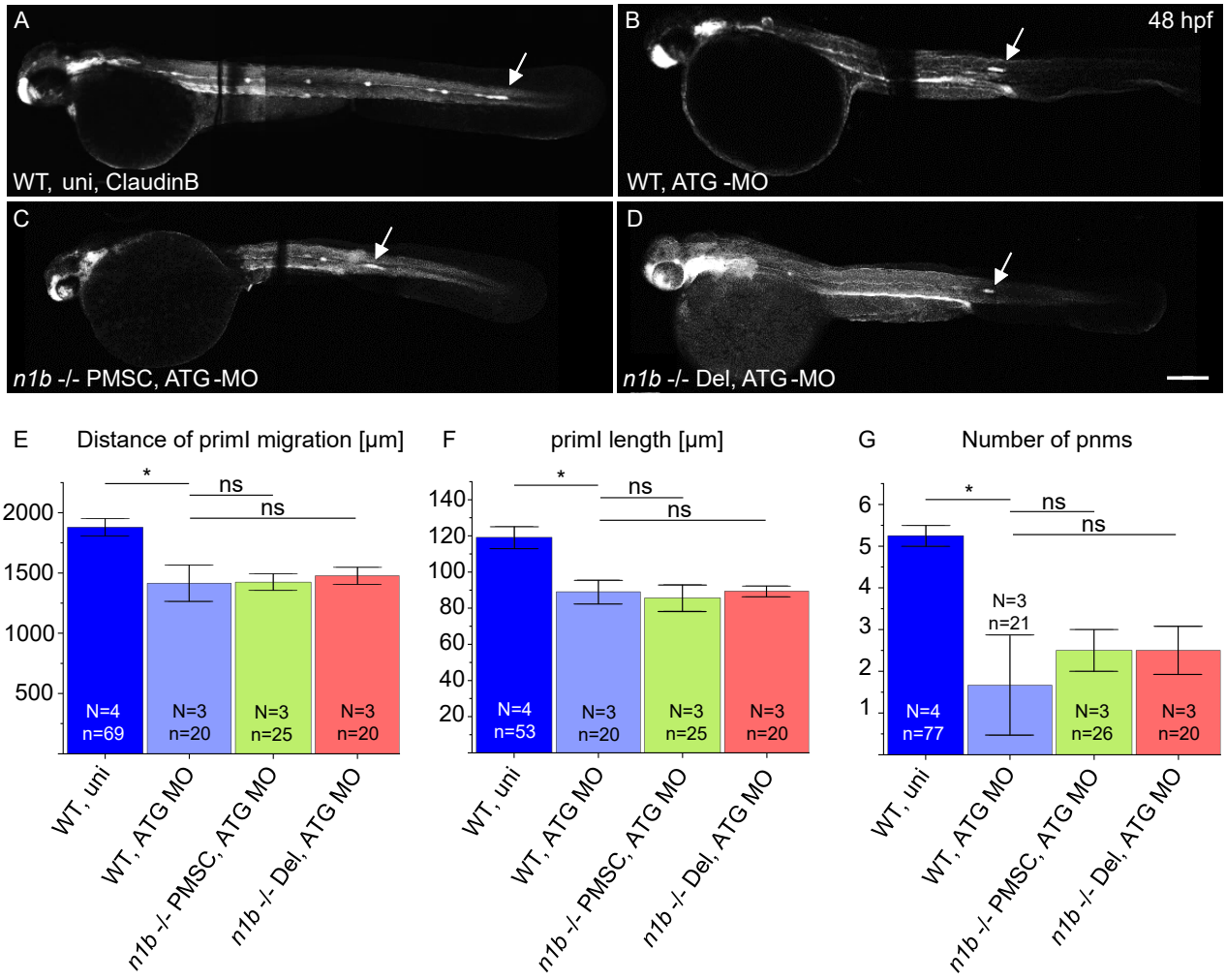

Figure 4.5: Injection of the *ncam1b*-ATG morpholino leads to a delay in the development of the lateral line organ, in both, the WT and the *ncam1b* mutants. (A - D) Whole-body images of *Tg(ClaudinB::lynGFP)* embryos show how far the primordium (primI) has migrated (white arrows) and how many proneuromasts (pnms) are deposited at 48 hpf. **(A)** In WT, primI reaches the tip of the tail and deposits 5 pnms. **(B)** *ncam1b*-ATG morpholino (ATG MO) in WT results in the primI only reaching the middle of the yolk extension and depositing one pnm. ATG MO injected in **(B)** *n1b* -/- PMSC and **(C)** *n1b* -/- Del mutants leads to primI only reaching the end of the yolk extension and depositing two pnms. **(E - G)** Statistical analyses of migration distance, primI length, and pnm formation at 48 hpf show that *ncam1b* mutants injected with ATG MO exhibit the same phenotype as WT injected with ATG MO. Two-sided *t*-test: *: $p < 0.05$, **: $p < 0.01$, ***: $p < 0.001$, n.s.: not significant. Scale bar in **(D)** 200 µm, Objective: 5x.

4.4.2 Subtle effects of the *ncam1b*-5' UTR morpholino in *ncam1b* mutant embryos

To critically evaluate the results from the *ncam1b*-ATG MO injection, the *ncam1b*-5'UTR MO, which binds upstream of the start codon in the 5' untranslated region, was injected into the *n1b* -/- Del mutants. A simplified analysis was carried out by distinguishing three distinct phenotypes (Fig. 4.6 A - C). The "WT phenotype": the primordium successfully reached the tail tip and deposited approximately 5 proneuromasts (Fig. 4.6 A). The "Moderate phenotype" is characterized by primordium reaching only as far as the yolk extension, with a maximum of 1-2 proneuromasts deposited (Fig. 4.6 B). The "Severe phenotype" showed primordium remaining stalled at the otic vesicle, if the primordium was present at all, with a complete absence of proneuromast deposition (Fig. 4.6 C). As reported before, the pLLS in WT fish and the *n1b* -/- Del mutants predominantly exhibited WT phenotype (WT: 95.89 % ± 0.6; *n1b* -/- Del: 88.75 % ± 3.37) and only a small proportion displayed the moderate phenotype (WT: 4.11 % ± 0.6; *n1b* -/- Del: 13.75 % ± 3.37) (Fig. 4.6 D). In contrast, the injection of the *ncam1b*-5' UTR MO into WT embryos led to 57.14 % (± 4.84) severe phenotype, 11.69 % (± 2.45) displayed the moderate phenotype, and only 31.17 % (± 2.98) showed an unaltered WT phenotype. Conversely, 60 % (± 6.69) of the *n1b* -/- Del mutants maintained the WT phenotype after the *ncam1b*-5' UTR MO injection, 34 % (± 6.74) exhibited moderate phenotype, and only 6 % (± 2.58) showed severe phenotype. The average distribution of phenotypes between WT embryos injected with the *ncam1b*-5' UTR MO and uninjected WT embryos showed a statistically significant difference (χ^2-test, $p = 1.39 \times 10^{-7}$) and thus confirmed the results of Dries et al. (2021). In contrast, the average distribution of phenotypes between *n1b* -/- Del mutant embryos *ncam1b*-5' UTR MO injected versus uninjected did not show a statistically significant difference (χ^2-test, $p = 0.09$). Additionally, the average distribution of phenotypes between WT embryos and *n1b* -/- Del mutant embryos injected both with the *ncam1b*-5' UTR MO showed a statistically significant difference (χ^2-test, $p = 0.0003$). In summary, the *ncam1b*-5' UTR MO did not induce a severe phenotype in *n1b* -/- Del mutants as it did after injection into the WT. This contrasts the effect of the *ncam1b*-ATG MO, which induced drastic phenotypes in both, WT and *ncam1b* mutants.

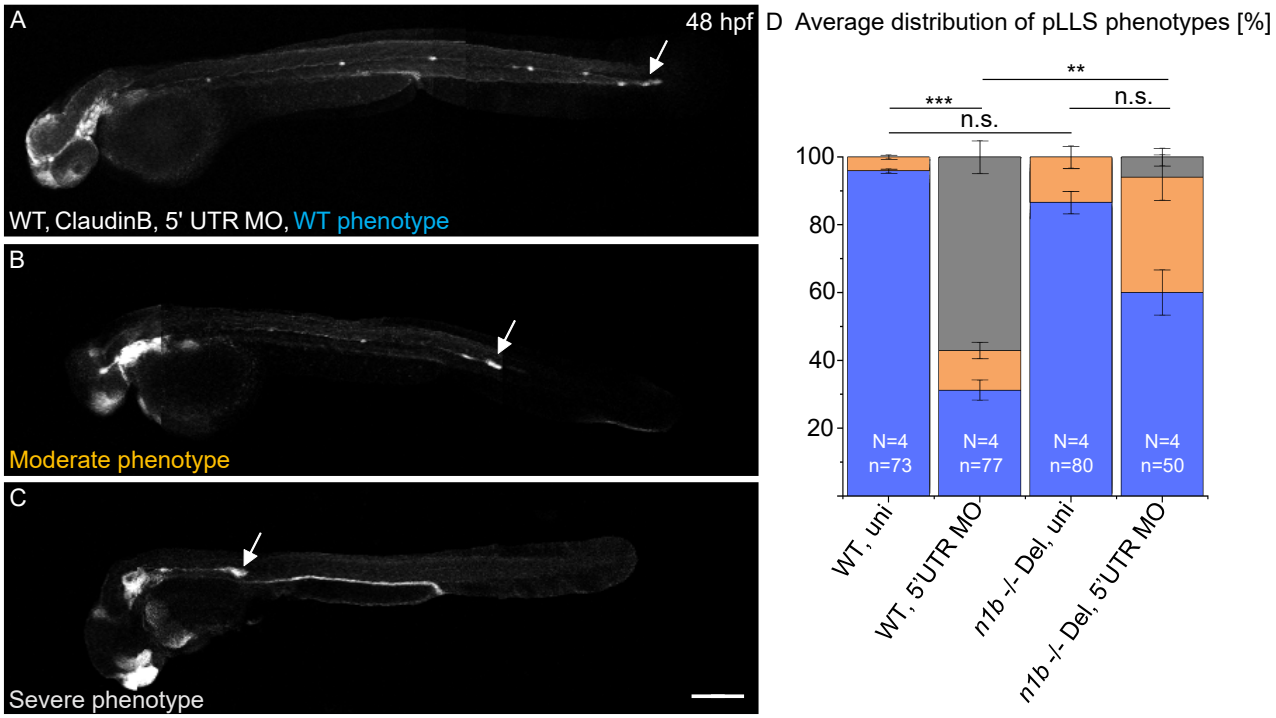

Figure 4.6: Injection of a *ncam1b*-5' UTR MO into *n1b* -/- Del embryos leads to a small, but no significant delay in lateral line system development. (A - C) A representative depiction of the three phenotypes of the posterior lateral line system (pLLS) into which the embryos (uninjected or *ncam1b*-5' UTR MO injected (5' UTR MO)) were classified at 48 hpf. **(A)** "Wild type (WT) phenotype": the primordium reaches the tip of the tail and deposits up to 5 proneuromasts. **(B)** "Moderate phenotype": the primordium reaches the end of the yolk extension and deposits 2 proneuromasts. **(C)** "Severe phenotype": the primordium is located near the otic vesicle and has not deposited any proneuromasts. **(D)** Quantification of the three phenotypes of WT and *ncam1b* -/- Del controls, as well as in injected larvae. χ^2-test *: $p < 0.05$, **: $p < 0.01$, ***: $p < 0.001$, n.s.: not significant. Scale bar in **(C)** 200 µm, Objective: 5x.

4.5 Loss of *ncam1b* disrupts the spatial patterning of *erm* and *lef1* expression in the migrating primordium

Although primordium migration seems unaffected in *ncam1b* mutants, it was investigated whether the absence of Ncam1b causes more subtle effects like differences in signaling patterns or the distribution of dividing cells within the primordium. Dries et al. (2021) found, that embryos, injected with *ncam1b*-ATG MO are characterized by reduced cell proliferation in the primordium. This is postulated to cause the shorter migration distance of a smaller primordium and the decreased number of deposited proneuromasts. The authors hypothesized that cell proliferation in the primordium is – in addition to *lef1* signaling events in the Leading Zone – triggered by *erm* expression in the Trailing Zone which is a consequence of the interaction of Ncam1b with Fgfr1a.

In order to evaluate the size of the signaling zones in *ncam1b* mutants, the transcription factor *lef1* was chosen as a marker for the Leading Zone. This zone is characterized by Wnt signaling which, via triggering Lef1 expression, leads to primordial cell proliferation [Lecaudey et al., 2008, Gamba et al., 2010, Breau et al., 2012]. The Trailing Zone is dominated by the FGF signaling pathway [Aman and Piotrowski, 2008], one of the Fgfr1a target genes being *erm*. A clear functional boundary between these signaling centers does not exist, resulting in a zone of functional overlap [Aman et al., 2011]. Double fluorescence *in situ* hybridizations (FISH) were performed to measure the area (Fig. 4.7) and the length (Sup. S2) of these expression domains in WT, *n1b* -/- Del and *ncam1b*-ATG morphants. The latter morphants were included in this study, although the *ncam1b*-ATG morpholino might cause off-target effects that induce a developmental morphological phenotype. It can be argued that this morpholino can still provide valuable insights into other developmental processes, especially when mutant controls are employed. These controls allow discerning a specific morpholino-induced phenotype from off-target effects. As judged by ***lef1*** expression, the Leading Zone is significantly enlarged by 1.96-fold (± 0.26, $p = 0.0007$) in morphants compared to controls. In mutants, the Leading Zone is enlarged by 1.25-fold (± 0.09, $p = 0.003$) relative to controls (Fig. 4.7 G). In *ncam1b* morphants, both, the area and length of the *lef1* expression domain was increased (Sup. S2 A). In *ncam1b* mutants, however, only the area of the *lef1* expression domain expanded, while its length remained unchanged. Aman et al. (2011) showed that Wnt/β-catenin signaling in the Leading Zone acts synergistically with FGF signaling to promote cell division. Fgfr1a is expressed in the Trailing Zone, and its inhibition results in a significant reduction in primordial proliferation [Aman et al., 2011]. To evaluate FGF signaling, in the current study the expression of both, *fgfr1a* and the FGF target gene *erm* were measured. No discernible differences in the ***fgfr1a*** expression region were detected between WT, *ncam1b* morphants (0.92 ± 0.1, $p = 0.56$), and *ncam1b* mutants (1.02 ± 0.1, $p = 0.86$) (Fig. 4.7 H). ***erm*** expression region is, however, significantly reduced in *ncam1b* mutants (0.54 ± 0.02, $p = 6.49 \times 10^{-8}$) and even more in *ncam1b* morphants (0.4 ± 0.02, $p = 6.92 \times 10^{-10}$) (Fig. 4.7 I). Expression of the Fgfr1a receptor does, thus, not correspond to the expression of the Fgfr1a target gene *erm* in all cases.

In summary, it could be shown by double FISH analysis, that the absence of Ncam1b disrupts the spatial patterning of *erm* and *lef1* expression in the migrating primordium, with a somewhat stronger phenotype observed in the morphants.

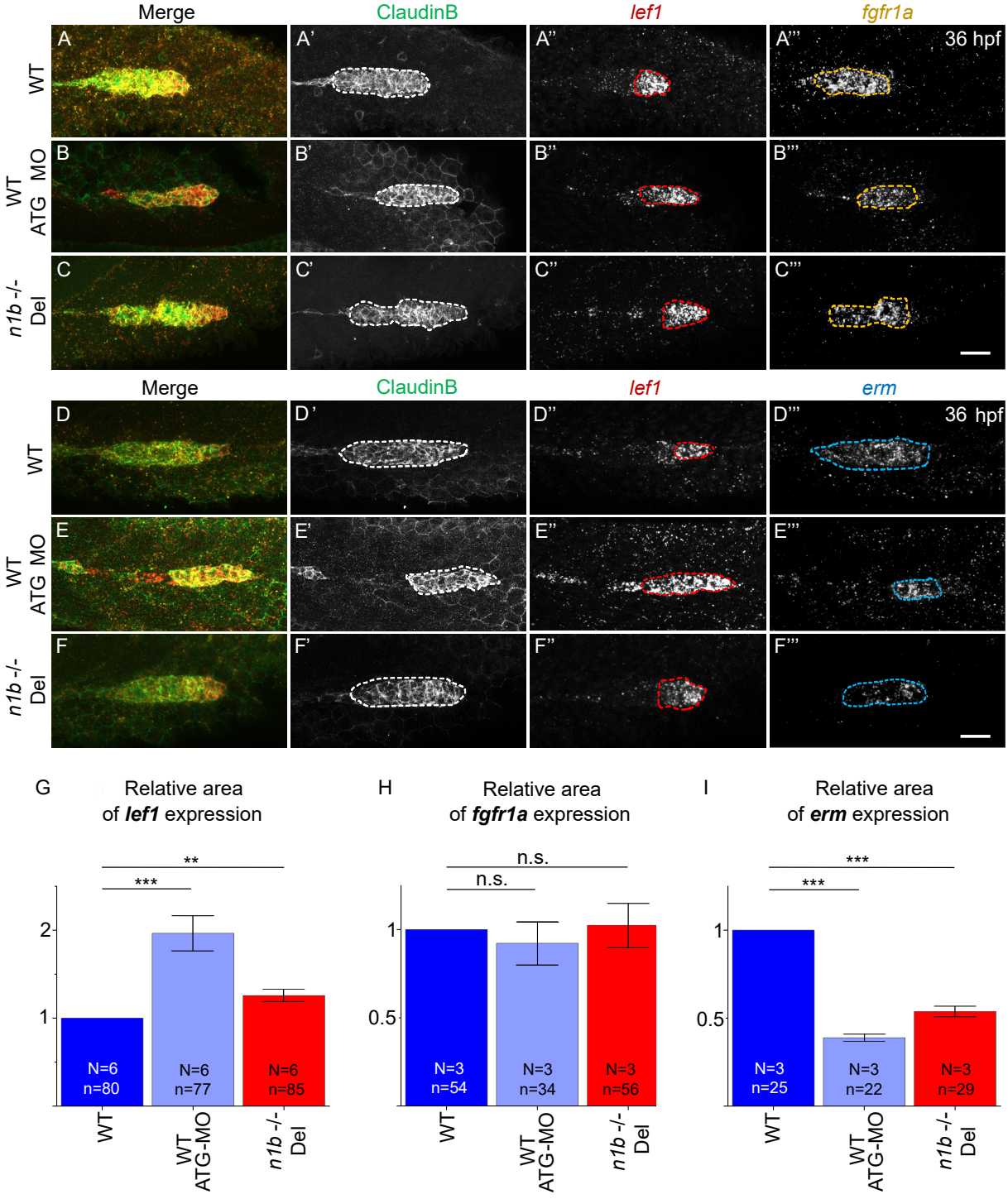

Figure 4.7: Expression domains of *lef1*, *fgfr1a*, and *erm* in the primordium in WT, *ncam1b* morphants, and *ncam1b* mutants. **(A - C''')** Double fluorescence *in situ* hybridization staining of *lef1* and *fgfr1a* in WT, *ncam1b* morphants and *ncam1b* mutants at 36 hpf. **(D - F''')** Simultaneous staining of *lef1* and *erm* in WT, *ncam1b* morphants, and *ncam1b* mutants. **(G)** *ncam1b* morphants and mutants show a significant increase in the area expressing *lef1*. **(H)** The *fgfr1a*-expressing region does not differ between WT, *ncam1b* morphants, and *ncam1b* mutants. **(I)** *ncam1b* morphants and mutants have a significantly shortened *erm*-expressing region compared to WT. Two-sided *t*-test: *: $p < 0.05$, **: $p < 0.01$, ***: $p < 0.001$, n.s.: not significant. Scale bars in **(C''')** and **(F''')** 20 µm, 40xW.

4.6 *ncam1b knockout* leads to redistribution of primordial proliferation

Erm belongs to the family of Ets transcription factors and is expressed through the active FGF signaling pathway. It is known to regulate the proliferation of serotonergic progenitors in the hypothalamus [Bosco et al., 2013], and it is also involved in the proliferation of embryonic stem cells [Akagi et al., 2015]. Dries et al. (2021) hypothesized that Ncam1b interacts with Fgfr1a in the Trailing Zone, and induces the expression of Erm as a driver of proliferation. They concluded this from the fact that not only *erm* expression but also the proliferation rate in the migrating primordium was downregulated in the *ncam1b* morphants. To assess cell division in the *ncam1b* mutant, BrdU staining was performed at 36 hpf (Fig. 4.8). Zone determination in the primordium relied on cell morphology (Fig. 4.8 C). Cells in the Leading Zone display random orientation, while those in the Trailing Zone organize into rosette-like proneuromasts, exhibiting a more structured arrangement.

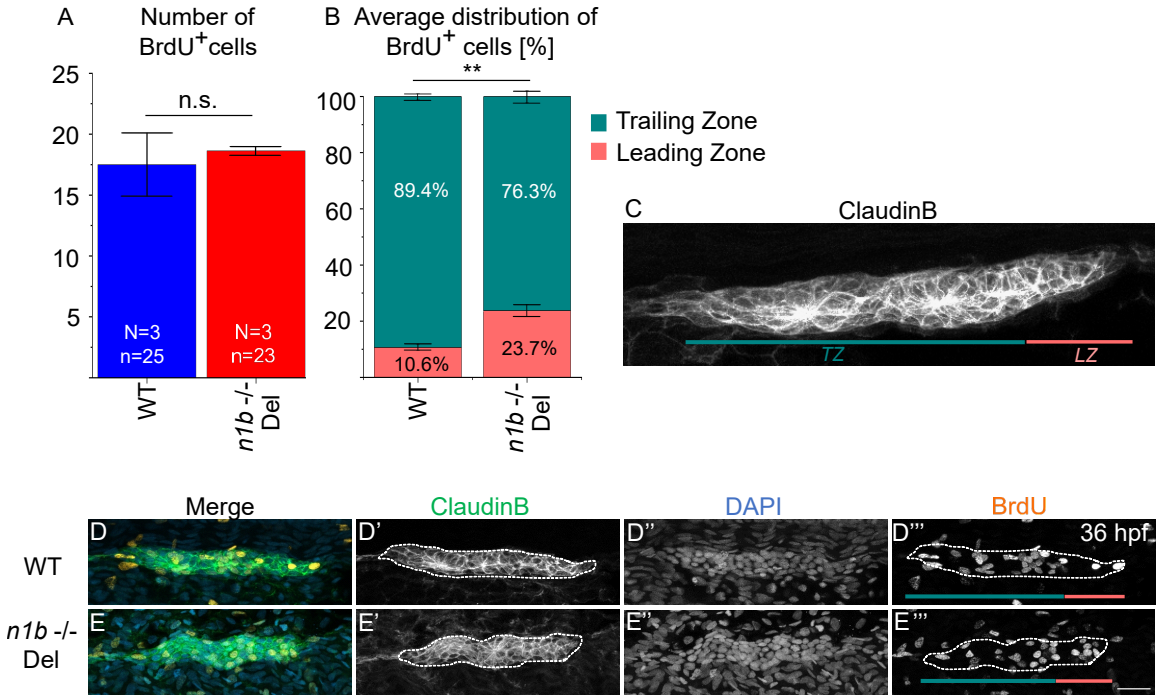

Figure 4.8: Loss of *ncam1b* leads to differences in proliferation in the primordium. **(A)** Number of BrdU-positive (BrdU$^+$) cells in the primordium of WT and *n1b* -/- Del. **(B)** Distribution of BrdU$^+$ cells in the Leading Zone (LZ) and Trailing Zone (TZ) in *ncam1b* mutant and WT. **(C)** Representation of how the primordium was divided into Leading and Trailing Zone based on the cell morphology. **(D - E)** Confocal imaging of the primordium, visualizing ClaudinB (green), DAPI and BrdU (orange), revealed that *ncam1b* mutant exhibited a distinct distribution of proliferating cells compared to WT. **(A)** Two-sided *t*-test, **(B)** χ^2-test: *: $p < 0.05$, **: $p < 0.01$, ***: $p < 0.001$, n.s.: not significant. Scale bar in **(E''')** 20 µm, Objective: 40xW.

Overall quantification of BrdU-positive (BrdU$^+$) cells in the primordium revealed no statistically significant difference between WT and *ncam1b* mutant embryos (*t*-test, $p = 0.52$) (Fig. 4.8 A). Specifically, WT embryos exhibited an average of 17.5 ($\pm$ 2.12) BrdU$^+$ cells in the primordium, while *ncam1b* mutants displayed an average of 18.63 ($\pm$ 0.32) BrdU$^+$ cells. However, upon spatial analysis, based on the morphological segmentation of the primordium into Leading and Trailing Zone, a distinct distribution of the BrdU$^+$ cells was observed (χ^2-test) (Fig. 4.8 B - E). In WT embryos, 89.4 % ($\pm$ 0.01) of the BrdU$^+$ cells were located in the Trailing Zone, while in the *ncam1b* mutants, this proportion decreased significantly to 76.3 % ($\pm$ 0.02, $p = 0.008$). Conversely, the Leading Zone of the

WT primordium contained 10.6 % (± 0.01) of the BrdU$^+$ cells, whereas, in the *ncam1b* mutants, this percentage increased significantly to 23.7 % (± 0.02, $p = 0.008$). These findings indicate that while the overall number of proliferating cells in the primordium was comparable between WT and *ncam1b* mutant embryos, the spatial distribution of the dividing cells was significantly altered in the mutants. Specifically, the *ncam1b* mutants exhibited a reduction in the number of BrdU$^+$ cells in the Trailing Zone, accompanied by an increase in the Leading Zone.

4.7 A knockout of *ncam1b* has no impact on the differentiation of hair cells during development

The neuromasts in the pLLO allow to perceive water movements and pressure changes in the environment. This is crucial for orientation, prey detection, and predator avoidance [Dykgraaf, 1933]. Disruptions in the function of the neuromasts could therefore lead to significant impairments in sensory perception and, consequently, the behavior of the zebrafish.

Previous studies have shown that Ncam1b is expressed in newly developed neuromasts as well as in cells at fully differentiated neuromasts [Dries, 2014, Dries, 2018]. This could be an indication that Ncam1b might be important not only for the differentiation of hair cells during development but also for the maintenance of the homeostatic state of the neuromast. At various time points, during development (2 dpf) as well as in the differentiated state (5 dpf, 9 dpf) the hair cells were counted, but no differences could be observed between WT and *n1b* -/- Del mutants (2 dpf: $p = 0.56$; 5 dpf: $p = 0.76$; 9 dpf: $p = 0.74$) (Fig. 4.9). At 2 dpf, still during the development of the neuromast, the WT has an average of 3.17 (± 0.36) and the *n1b* -/- Del mutant 3.5 (± 0.24, $p = 0.56$) hair cells. In the differentiated state, WT has 9.25 (± 0.65) hair cells at 5 dpf and 9.75 (± 0.38) hair cells at 9 dpf while the *ncam1b* mutant has 9.67 (± 0.95) at 5 dpf and 10 (± 0.47) hair cells at 9 dpf. The comparison between WT and *ncam1b* mutant embryos revealed no significant numerical disparities at neither 5 dpf ($p = 0.76$) nor 9 dpf ($p = 0.74$). Moreover, no conspicuous developmental distinctions were observable between the 5 dpf and 9 dpf time points (represented representatively by the WT: $p = 0.58$). This clearly shows that normal differentiation of hair cells in the neuromasts occurs in the *ncam1b* mutants.

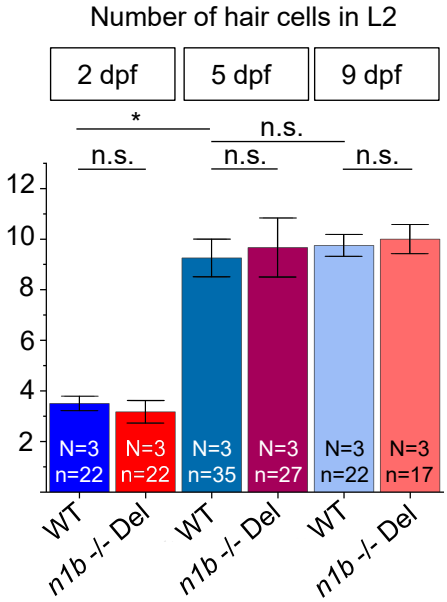

Figure 4.9: Quantification of the hair cell numbers in L2 of WT and *ncam1b* mutant at 2 dpf, 5 dpf and 9 dpf. The number of hair cells in neuromast L2 does not differ between WT (bluish bars) and *ncam1b* mutant (reddish bars) at 2 dpf, 5 dpf and 9 dpf. Furthermore, the number of hair cells does not change between 5 dpf and 9 dpf. Two-sided *t*-test: *: $p < 0.05$, **: $p < 0.01$, ***: $p < 0.001$, n.s.: not significant.

please turn to
the next page

4.8 Impaired regeneration of hair cells in the lateral line of *ncam1b* mutant larvae

Sensory hair cells can be damaged by mechanical influences, ototoxic drugs, or aging disorders [Forge and Schacht, 2000, Petit et al., 2001, Chen and Fechter, 2003, Matsui and Cotanche, 2004]. Aminoglycosides, such as neomycin, attack hair cells even at low concentrations and lead to cell death [Harris et al., 2003, Hernández et al., 2007]. The zebrafish, as well as other non-mammalian vertebrates, can quickly regenerate their hair cells by replacing them with proliferating and differentiating support cells [Corwin and Cotanche, 1988, Ryals and Rubel, 1988, Baird et al., 2000, Harris et al., 2003, Hernández et al., 2006, Taylor and Forge, 2005].
Previous work from this lab has shown that Ncam1b is not only expressed in hair cells during homeostasis but is also upregulated during regeneration after neomycin treatment [Dries, 2018]. Notably, an elevated presence of Ncam1b-expressing support cells during regeneration supports the hypothesis that Ncam1b is essential for their differentiation (reevaluated via immunohistochemical staining shown in Fig. 4.10).

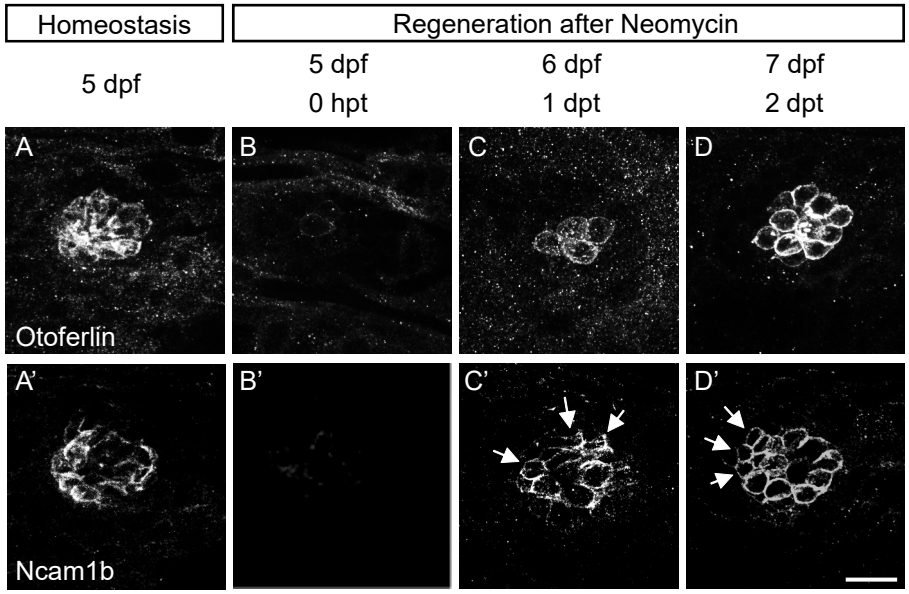

Figure 4.10: Ncam1b is upregulated during hair cell regeneration. Confocal lateral view of the second primary deposited neuromast (L2) in WT embryos during the regeneration phase. **(A - D, upper row)** Immunohistochemical staining of Otoferlin shows hair cells during homeostasis, the loss of hair cells after neomycin treatment (0 days post-treatment (0 dpt)) and their regeneration (1-2 dpt). **(A' - D', lower row)** Antibody detection of Ncam1b, which is expressed during regeneration. Ncam1b is expressed not only in hair cells but also in the surrounding support cells (white arrows). Scale bar in **(D')** 10 µm, Objective: 40xW.

A larva that develops a functional pLLO but exhibits expression of a mutated gene in neuromasts is a good candidate to test for defects in hair cell regeneration. Homozygous *ncam1b* mutants display no strong morphological abnormalities until they contain mature hair cells in neuromasts at 5 dpf (Fig. 4.9). Sensory hair cells were destroyed using neomycin and fixed at 24-hour intervals to analyze their regeneration over time. The condition of the embryos that were not treated with neomycin corresponds to homeostasis. Embryos were then immunostained with an antibody against Otoferlin (Fig. 4.11 C - H), a six-C2 domain transmembrane protein expressed in inner, outer, and vestibular hair

cells, as well as restricted regions of the brain [Roux et al., 2006]. Notably, Otoferlin is expressed in both, the progenitor cells as well as in the differentiated hair cells [Dries, 2018]. Neuromast L2 and the third terminal neuromast were quantified in this study, with DAPI used to identify the specific region. Immediately after neomycin treatment, nearly all hair cells were ablated (Fig. 4.11 D + D'). Individual cells that do not die after neomycin treatment are presumably not yet mature enough, and, thus, they are insensitive to neomycin [Santos et al., 2006]. The quantitative analysis showed that 94.72 % (± 5.3, compared to homeostasis: $p = 0.25$) of the hair cells were restored by 2 days post-treatment (dpt) in WT (Fig. 4.11 A), as already published [Song et al., 1995, Hernández et al., 2006]. In the *n1b* -/- Del mutants, only 72.89 % (± 2.28, compared to homeostasis: $p = 0.02$) of the hair cells were restored 4 dpt (Fig. 4.11 B).

To compare the regeneration rate of WT and *n1b* -/- Del mutants, the percentages of regenerated hair cells were assessed. To that end, the number of regenerated hair cells was divided by the number of hair cells during homeostasis (Fig. 4.11 I + J). Interestingly, the number of regenerating hair cells does not differ between WT and mutants at 1 dpt (WT: 53.86 % ± 4.75; *n1b* -/- Del: 45.52 % ± 1.66, $p = 0.14$). At 2 dpt, however, the slower regeneration in the *ncam1b* mutant became significant, with just 59.2 % (± 4.57, $p = 0.005$) regenerated at 2 dpt, 64.39 % (± 3.34, $p = 0.0009$) at 3 dpt, and 72.98 % (± 2.28, $p = 0.002$) at 4 dpt. The results of this study highlight that Ncam1b plays an important role in the regeneration of sensory hair cells. Without Ncam1b, there is a significant delay in the restoration of hair cells. Whether there is a limit to the regeneration of hair cells in the *ncam1b* mutant, or if they eventually reach the normal number of hair cells, was not investigated in this study. Since the second neuromast L2, representative of an older neuromast, and the third terminal neuromast, representative of a young neuromast, did not show major differences in regeneration, the following experiments focused on L2.

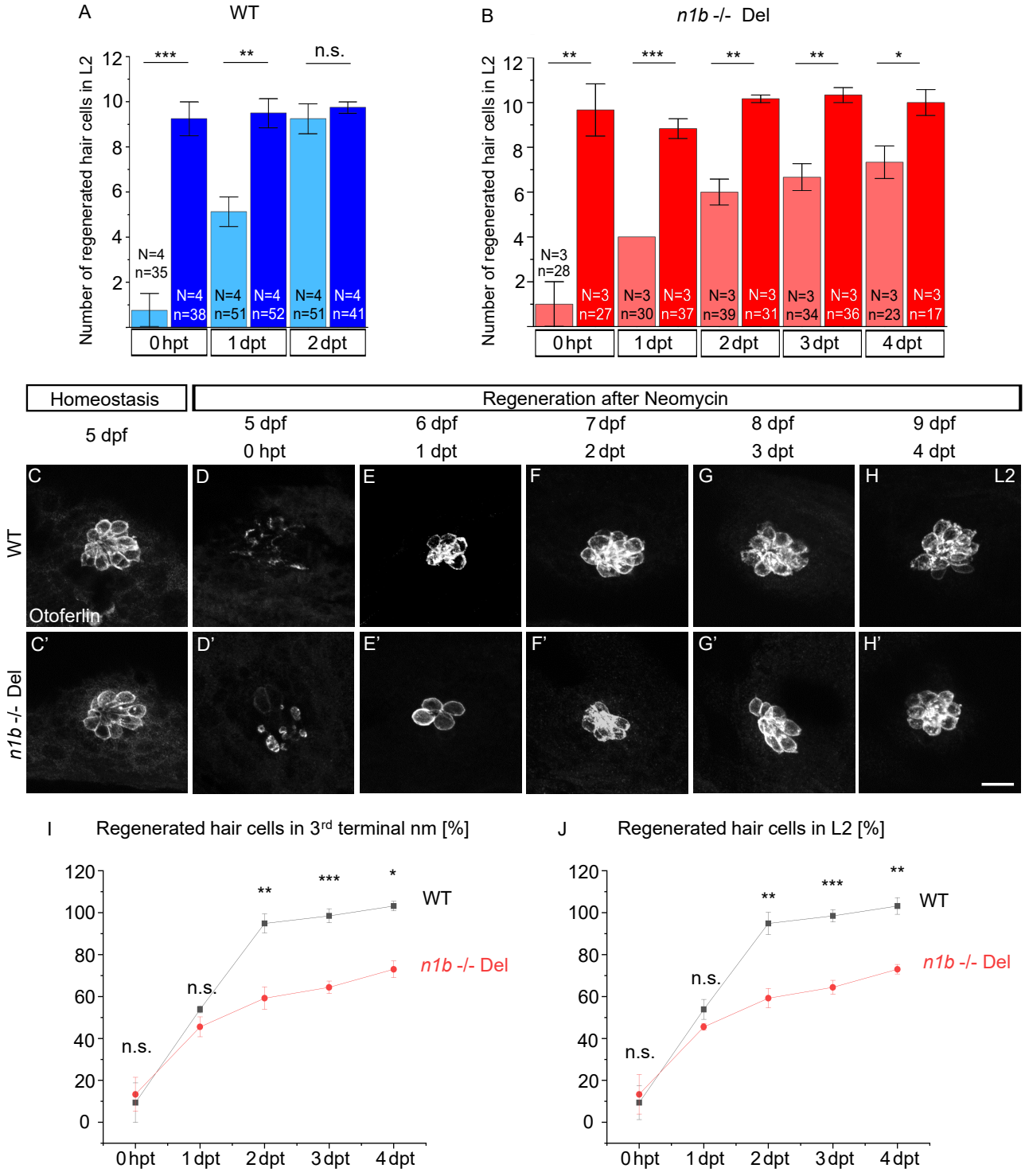

Figure 4.11: *ncam1b* loss of function leads to decreased regeneration of hair cells in zebrafish embryos. (A + B) Quantification of the regenerated hair cells in L2 after neomycin treatment in WT and *n1b* -/- Del mutant. To investigate how long WT and *n1b* -/- Del take to fully regenerate neuromasts after neomycin treatment, the Otoferlin-positive cells of neomycin-treated embryos (light blue for WT and light red for *n1b* -/- Del) and untreated embryos (dark blue for WT and dark red for *n1b* -/- Del) were counted and compared. **(A)** In WT, the hair cells are fully regenerated after two days. **(B)** In the *ncam1b* mutant, the hair cells are not fully regenerated after four days. **(C - H)** Confocal image analysis of hair cell regeneration in L2 in WT and *ncam1b* mutant embryos after neomycin treatment. **(I + J)** The percentages of regenerated hair cells (assessed by dividing the number of regenerated hair cells by the number of hair cells in homeostasis at the same time point) were compared between WT and *ncam1b* mutant at different time points after neomycin treatment. Exemplary, the 3^{rd} terminal neuromast and L2 were investigated. Two-sided *t*-test: *: $p < 0.05$, **: $p < 0.01$, ***: $p < 0.001$, n.s.: not significant. Scale bar in **(H')** 10 µm, Objective: 40xW.

4.9 Ncam1a is not upregulated in neuromasts during regeneration of hair cells in *ncam1b* mutants

The *n1b* -/- Del mutant showed impaired regeneration of hair cells after ablation by neomycin treatment. In contrast to WT larvae, which have already restored 94.86 % of the hair cells after two days, the *ncam1b* mutant has still regenerated only 72.89 % of the hair cells after four days (Fig. 4.11). Nevertheless, the lack of *ncam1b* does not seem to completely prevent regeneration, as some hair cells do regenerate. In previous studies, it was already shown that Ncam1b is expressed in WT hair cells during **homeostasis** and its expression even increases up to 8 dpf [Dries, 2018]. Ncam1a, in contrast, is no longer required in the differentiated neuromast, as evidenced by the lack of any detectable signal during immunohistochemistry. During **regeneration**, the expression of Ncam1b is strongly increased, with not only the regenerating hair cells, but also the surrounding support cells strongly expressing Ncam1b. In contrast, there is no upregulation of Ncam1a during regeneration [Dries, 2018]. Previous experiments of the current study have shown an upregulation of the *ncam1a* paralog and other genes during the development of the lateral line organ in *ncam1b* mutants (Fig. 4.4). This suggests genetic compensation, allowing for the normal development of pLLO despite the knockout of *ncam1b*.

To assess whether Ncam1a is upregulated in *ncam1b* mutants during the regeneration process of hair cells as well, immunohistochemical staining was conducted at 1 dpt and 2 dpt. Consistent with Dries (2018), no Ncam1a expression was detected in the neuromasts of WT at both time points (Fig. 4.12 A''' + C'''). Interestingly, the *ncam1b* mutants also exhibited no detectable Ncam1a expression in the neuromasts at 1 dpt and 2 dpt (Fig. 4.12 B''' + D'''). This suggests that the partial regeneration of hair cells in *ncam1b* mutants is not attributable to genetic compensation through Ncam1a.

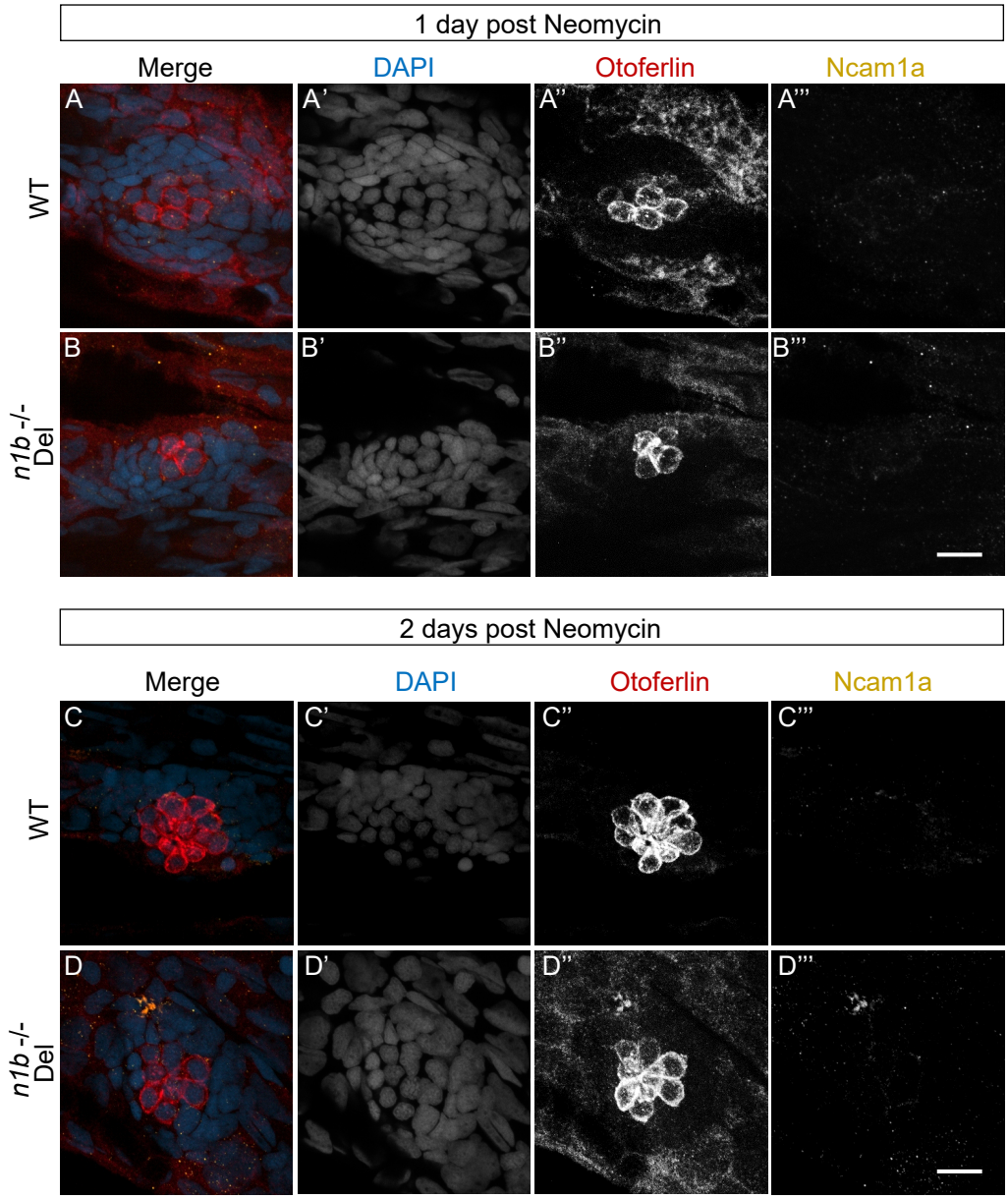

Figure 4.12: No Ncam1a upregulation in neuromasts during regeneration of hair cells, neither in WT nor in *ncam1b* mutant. Ncam1a is not expressed in WT and in *ncam1b* mutant neuromasts during hair cell regeneration at neither **(B''')** 1 day nor **(D''')** 2 days post neomycin treatment. As a positive control for the Ncam1a antibody, specific expression regions of Ncam1a, such as the motor neurons, were examined (Data not shown). Two-sided *t*-test: *: $p < 0.05$, **: $p < 0.01$, ***: $p < 0.001$, n.s.: not significant. Scale bars, Objectives: **(B''')** and **(D''')** 10 µm, 40xW.

4.10 Increased number of proliferating Sox2$^+$ support cells during regeneration of hair cells in *ncam1b* mutants

Hair cells are regenerated from support cells dividing and then differentiating into hair cells [Mackenzie and Raible, 2012, Wibowo et al., 2011]. Thus, the slower hair cell regeneration in *n1b* -/- Del mutants may result from defects in proliferation or from defects in their differentiation. To test whether support cells are capable of dividing during the regeneration process, the number of these cells was compared between the *ncam1b* mutant and WT at 2 dpt with neomycin. For this, *n1b* -/- PMSC and *n1b* -/- Del mutants, as well as WT embryos, treated with neomycin were fixed at 2 dpt and immunohistochemically stained for Sox2 (Fig. 4.13 A - C), a well-established marker for support cells in the lateral line neuromasts [Hernández et al., 2007]. In the inner ear, Sox2 is initially expressed in both, the progenitor cells of hair cells and support cells [Kiernan et al., 2005, Neves et al., 2007]. After hair cells differentiate, Sox2 is downregulated from these cells but remains expressed in the support cells. To quantify and compare the number of support cells, Sox2$^+$ cells in the mutants were counted at 2 dpt and expressed as a ratio relative to WT (Fig. 4.13 D). The *n1b* -/- PMSC mutant has 44.79 % ($\pm$ 9.24, $p = 0.017$) and the *n1b* -/- Del mutant has 47.58 % ($\pm$ 12.00 $p = 0.03$) more Sox2$^+$ cells than WT. In absolute numbers, the WT has an average of 28.83 ($\pm$ 3.55) Sox2$^+$ cells at 2 dpt. The *n1b* -/- PMSC mutant has an average of 40.5 ($\pm$ 3.89) and the *n1b* -/- Del mutant has 41.33 ($\pm$ 2.45) Sox2$^+$ cells. Despite the increased number of support cells, it was presumed that proliferation proceeded normally in the mutants and was not the underlying cause for the impaired hair cell regeneration. To confirm this, a BrdU assay was performed (Fig. 4.13 E - G). BrdU$^+$ support cells were counted, and the mutant cell count was expressed as a ratio to WT (Fig. 4.13 H). *n1b* -/- Del mutants showed 23.08 % ($\pm$ 7.08, $p = 0.02$) more BrdU$^+$ support cells than WT. This relates to absolute numbers of 7.17 ($\pm$ 0.31) BrdU$^+$ support cells in WT, and 9.5 ($\pm$ 0.62) BrdU$^+$ support cells in *n1b* -/- Del mutants. An increased number of proliferating support cells in the *n1b* -/- Del mutant, in parallel to a reduced number of hair cells, suggests that Ncam1b does not influence the proliferation of support cells, but rather the differentiation of those cells into hair cells.

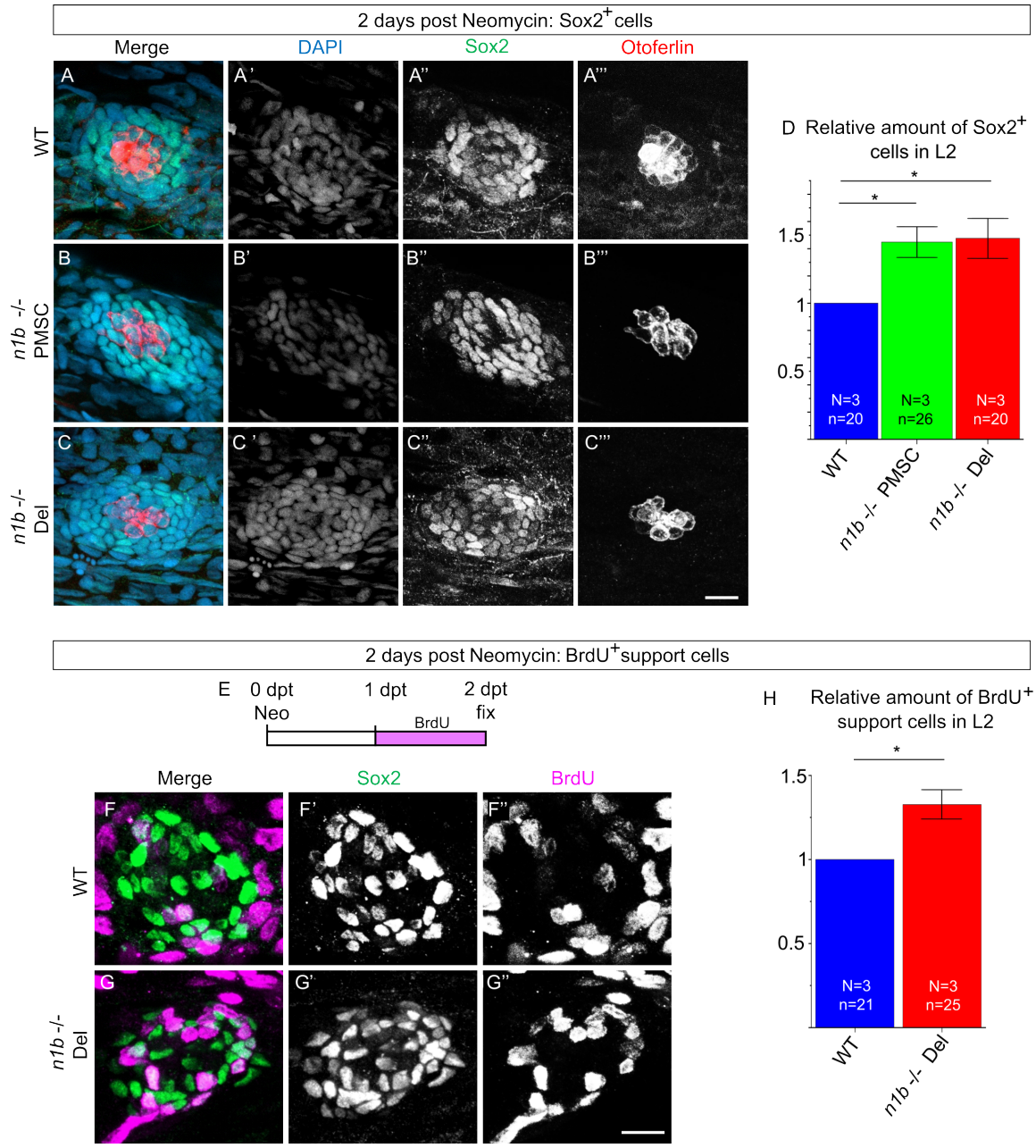

Figure 4.13: *ncam1b* mutants have more proliferating Sox2 expressing cells during regeneration. **(A - C)** Neuromast L2 of WT and both, *n1b* -/- PMSC and *n1b* -/- Del mutant embryos, were stained with an antibody against Sox2 (green), Otoferlin (red) and DAPI. **(D)** Relative number of Sox2$^+$ cells per neuromast (assessed by dividing the number of Sox2$^+$ cells in *ncam1b* mutant by the number of Sox2$^+$ cells in WT). Quantification shows that *ncam1b* mutants have more Sox2$^+$ cells in neuromasts 2 days post neomycin treatment than the WT. **(E)** Embryos treated with neomycin were incubated 1 dpt - 2 dpt with the BrdU, and then fixed with PFA. Then, immunohistochemical staining against Otoferlin and BrdU was performed to investigate the number of proliferating support cells. **(F - G)** Neuromast L2 of WT and *n1b* -/- Del mutant embryos were stained with an antibody against Sox2 (green) and BrdU (magenta). **(H)** Quantification of the number of BrdU$^+$ support cells (Sox2$^+$) shows that *n1b* -/- Del mutants have more BrdU$^+$ support cells in neuromasts 2 days post neomycin treatment. The relative number of BrdU$^+$ support cells per neuromast (assessed by dividing the number of positive cells of *ncam1b* mutant by the number of positive cells of WT). Quantification shows that *ncam1b* mutants have more proliferating support cells in neuromasts 2 days post neomycin treatment compared to WT. Two-sided *t*-test: *: $p < 0.05$, **: $p < 0.01$, ***: $p < 0.001$, n.s.: not significant. Scale bar in **(C'')** and **(G'')** 10 µm, Objective: 40xW.

4.11 Inhibition of Notch signaling rescues the decreased number of hair cells in *ncam1b* mutants after neomycin-induced damage

The increased number of proliferating Sox2$^+$ support cells together with a decreased number of hair cells observed during regeneration in *ncam1b* mutant embryos, indicate that Ncam1b may impair support cell differentiation during hair cell regeneration. As Notch-mediated lateral inhibition has previously been shown to maintain the balance of support and hair cells during hair cell regeneration in the lateral line system [Jiang et al., 2014, Romero-Carvajal et al., 2015] it was tested, whether Notch signaling is affected in *n1b* -/- Del mutant neuromasts. To that end, *ncam1b* mutants and WT embryos were treated with the Notch γ-secretase inhibitor DAPT immediately following neomycin-induced hair cell damage (Fig. 4.14 A - C). Larvae were fixed 2 dpt, as at this time point during regeneration the number of hair cells in *ncam1b* mutants significantly differs from the WT. As anticipated, WT embryos treated with DAPT after neomycin treatment exhibited an increased number of hair cells (22.17 ± 3.19) compared to DMSO-treated control WT embryos (9.25 ± 2.29, $p = 0.0002$)(Fig. 4.14 D, blue bars). In the *ncam1b* mutant as well, an increased number of sensory hair cells can be observed after the DAPT treatment (21.125 ± 4.38, $p = 0.00021$), compared to DMSO-treated control mutant embryos (6 ± 1.41, $p = 0.00021$) (Fig. 4.14 D, red bars). After DAPT treatment, mutants show a comparable increase in the number of hair cells as WT embryos ($p = 0.6$).

The rescue of the delayed hair cell regeneration phenotype in *ncam1b* mutants upon inhibition of Notch signaling with DAPT provides strong evidence that dysregulation of the Notch pathway is a major cause of this defect. If misregulation of another pathway was responsible for the phenotype, inhibiting Notch would not have been able to restore normal regeneration. Dysregulation of the Notch pathway in *n1b* -/- Del mutants may lead to the accumulation of proliferating support cells and a reduction in hair cell differentiation during the regenerative process.

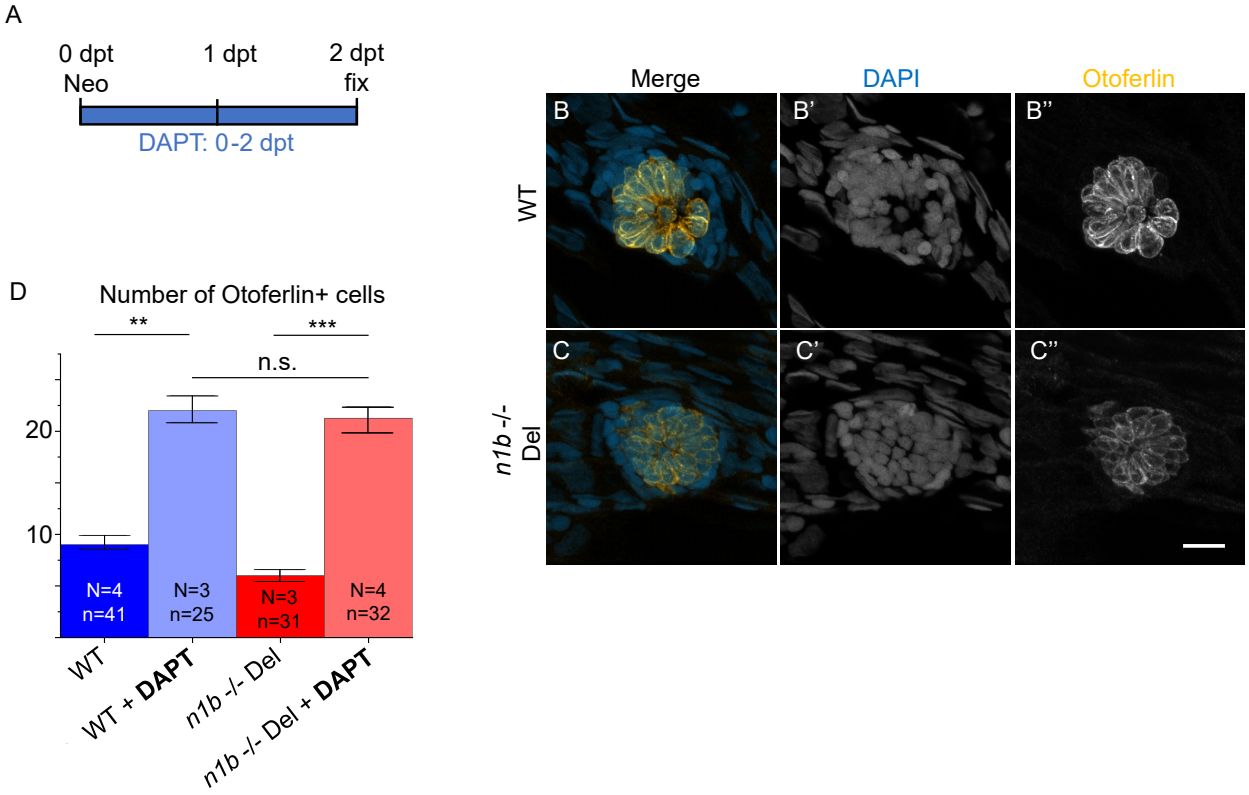

Figure 4.14: Rescue of impaired hair cell regeneration in *ncam1b* mutants by inhibition of Notch signaling. (A) 7 dpf embryos of both *n1b* -/- Del mutants were treated with neomycin (Neo) for 1 hour and then incubated with the Notch inhibitor DAPT for two days. Controls were incubated in 1 % DMSO in E2 without DAPT. Subsequently, immunohistochemical staining for Otoferlin was conducted to quantify the number of hair cells. **(B - C)** Confocal images of hair cells stained with Otoferlin (orange) in WT embryos and *ncam1b* mutants treated with DAPT. **(D)** Quantification of hair cells shows a dramatic increase of hair cells in both, WT and *ncam1b* mutant. Two-sided *t*-test: *: $p < 0.05$, **: $p < 0.01$, ***: $p < 0.001$, n.s.: not significant. Scale bar in **(C'')** 10 µm, Objective: 40xW.

5 Discussion

Hearing and balance, two vital senses, rely on the intricate function of hair cells. While adult mammals cannot regenerate these specialized cells upon damage, leading to permanent auditory impairment, the zebrafish possesses a remarkable ability to replenish hair cells in their posterior lateral line system (pLLS) [Harris et al., 2003, Taylor and Forge, 2005]. This unique regenerative process has established zebrafish as a powerful model organism for investigating not only hair cell development but also the mechanisms underlying driving cellular renewal. Previous research in this lab has shed a first light on the critical role played by the neural cell adhesion molecule Ncam1b during pLLS development in zebrafish. Morpholino-mediated knockdown of *ncam1b* results in severe structural abnormalities, including a reduced number of neuromasts and impaired migration of the primordium, a consequence of compromised cellular proliferation [Dries et al., 2021].
The present study aimed to further elucidate the functional significance of Ncam1b by employing the CRISPR/Cas9 technology to generate two independent *ncam1b* mutants. Surprisingly, the *ncam1b* mutants exhibited normal development of the pLLS and its hair cells. However, upon closer examination of the migrating primordium, differences in signaling and the distribution of proliferating cells were observed. Additionally, it was demonstrated that not only in the whole-mount embryo but also specifically in the migrating primordium, the paralog Ncam1a is upregulated, suggesting compensatory mechanisms. Other genes, such as *l1cam*, were also upregulated. Despite the seemingly normal development of hair cells in *ncam1b* mutants, the absence of Ncam1b has a significant impact during hair cell regeneration. Here, Ncam1a does not appear to function as a genetic compensator. Hair cells regenerate more slowly in *ncam1b* mutants, likely due to an accumulation of proliferating support cells and impaired differentiation into hair cells. This slower regeneration of *ncam1b* mutants can be rescued by the Notch inhibitor DAPT.

5.1 Ncam1b mutant zebrafish do not recapitulate the morpholino-induced phenotype

The knockdown of *ncam1b* in zebrafish embryos has been shown to lead to a strongly altered development of the pLLS [Dries et al., 2021]. The significantly smaller primordium exhibits slowed migration, which can even result in a U-turn of the primordium. Additionally, the deposition of neuromasts is restricted in *ncam1b* morphants. It was hypothesized that this phenotype is due to the lack of interaction between Ncam1b and Fgfr1a, resulting in reduced FGF signaling and consequently decreased cell proliferation in the primordium. To provide a genetically defined platform for further analysis of *ncam1b* function a **P**re **M**ature **S**top **C**odon mutant (*n1b* -/- PMSC) with an early stop codon in exon 1 (Fig. 3.1) and a **del**etion mutant (*n1b* -/- Del) lacking almost the entire coding sequence of *ncam1b* were generated (Fig. 3.2). Surprisingly, in contrast to *ncam1b* morphants, analysis of the stable *ncam1b* mutants reveal normal development of pLLS (Fig. 4.3). The primordium, with a normal length, migrates to the tail tip until 48 hpf and deposits 5 proneuromasts during this process. Several recent studies have highlighted significant discrepancies between the phenotypes observed in morpholino knockdown experiments and genetic mutants in zebrafish. Kok et al. (2015) performed a reverse genetic screening targeting 20 genes that had previously been reported to exhibit morpholino-induced phenotypes. 50 % of the knockout lines they generated failed to reproduce the morphant phenotypes. Furthermore, when they compared 98 published morphant phenotypes to the corresponding knockout phenotypes in the

Sanger Zebrafish Mutation Project [Kettleborough et al., 2013], 80 % of the morphant phenotypes were not observed in the genetic mutants. This discrepancy is not limited to a few isolated cases. Several other studies have also reported a failure to observe morphant phenotypes in zebrafish mutants. Examples include the genes *tcf7*, *wnt1*, *pak4*, *megamind*, *ift88* and *flt4* [Nagayoshi et al., 2008 vs. Aman et al., 2011; Amoyel et al., 2005 vs. Gerety and Wilkinson, 2011; Law and Sargent, 2013 vs . Law and Sargent, 2014; McIntyre et al., 2012 vs. Borovina and Ciruna, 2013; Covassin et al., 2006 vs. Kok et al., 2015]. Similar observations have been reported in other model organisms, such as *Arabidopsis* and *Drosophila* [Yamamoto et al., 2014, Gao et al., 2015], suggesting that this is a broader issue in the field of functional genomics. The reasons for those discrepancies are not entirely clear, but several potential explanations have been proposed. These include the unexpected escape from frameshift mutations, the presence of gene compensation mechanisms, and the possibility of off-target effects associated with morpholino use. The case of the *ncam1b* morphant and mutant phenotypes in zebrafish lateral line development serve as a further example illustrating potential discrepancies that can arise between morpholino-induced and genetic knockout phenotypes. The reasons for this discrepancy will be further discussed in the following sections.

5.1.1 Ncam1b protein is absent in *n1b* -/- PMSC and *n1b* -/- Del mutant zebrafish

Both, the *n1b* -/- PMSC and *n1b* -/- Del mutants fail to express the Ncam1b protein, as demonstrated by immunostaining (Fig. 4.2). Further investigation revealed that the ***n1b* -/- PMSC** mutant exhibits a reduced amount of *ncam1b* mRNA, suggesting the occurrence of nonsense-mediated mRNA decay (Fig. 4.1). cDNA sequencing demonstrated no evidence of alternative splicing in the *n1b* -/- PMSC mutant that could have resulted in a functional transcript (Fig. 3.1). The ***n1b* -/- Del** mutant showed no detectable *ncam1b* mRNA in the ddPCR analysis, indicating the absence of *ncam1b* mRNA expression. In summary, these results confirm that both the *n1b* -/- PMSC and *n1b* -/- Del mutant lines are true mutants without Ncam1b protein expression.

5.1.2 Genetic compensation in *ncam1b* mutants

Genetic robustness is the remarkable ability of living organisms to maintain their viability and fitness despite genetic variations or mutations. One key mechanism underlying this robustness is the phenomenon of genetic compensation [Rossi et al., 2015]. When a gene is knocked out and a premature stop codon occurs, the mRNA is degraded due to nonsense-mediated mRNA decay (NMD) to prevent the translation of defective transcripts [El-Brolosy et al., 2019]. This triggers compensatory mechanisms like upregulation of paralogous genes, genes with sequence similarity, or other components of the affected biological pathways [Lykke-Andersen and Jensen, 2015, El-Brolosy et al., 2019].
The current study shows that ***n1b* -/- PMSC** mutant exhibits a reduced amount of *ncam1b* mRNA, suggesting mRNA degradation and the possible occurrence of NMD (Fig. 4.1). This is underpinned by ddPCR measurements which demonstrate the upregulation of other genes, namely *ncam1a* and *l1cam*, shown here at 36 hpf (Fig. 4.4). In the ***n1b* -/- Del** mutant, although almost the entire coding sequence is deleted, a short 33 bp transcript remains until the new stop codon (Fig. 3.2 C). Several lines of evidence suggest that this truncated mRNA is targeted by NMD: Firstly, NMD is typically triggered when a stop codon occurs more than 50 - 55 nucleotides upstream of the final exon-exon junction [Nagy and Maquat, 1998]. Even though the *n1b* -/- Del mutant lacks most of the coding region, the remaining

33 bps likely position the new stop codon in an NMD-sensitive context. So, even though a large portion of the *ncam1b* coding sequence is deleted, the short remaining transcript with the new stop codon is still suspected to undergo NMD. Secondly, upregulation of other genes like *ncam1a* and *l1cam* was observed in this mutant (Fig. 4.4). This compensatory gene expression is a hallmark of NMD activation in response to a premature termination codon. The compensatory upregulation of other genes supports this hypothesis, even if the NMD response could not be directly demonstrated by ddPCR in this particular mutant. Similar phenomena of genetic compensation have been observed in other zebrafish mutants, such as the *nid1a* -/- mutant, where *nid1b* and *nid2a* were mobilized to compensate for the loss-of-function of *nid1a* [Zhu et al., 2017]. Additionally, a broader study by El-Brolosy and colleagues (2019) found that in several homozygous zebrafish mutants, including *hbegfa*, *vcla*, *hif1ab*, *vegfaa egfl7* and *alcama*, the corresponding family member genes are upregulated [El-Brolosy et al., 2019].
The fact that Ncam1a, as a paralog of Ncam1b, is specifically upregulated in the migrating primordium indicates that it could be a key player in this compensatory mechanism. Ncam1a and Ncam1b are duplicated paralogs that arose from a second round of genome duplication in the teleost fish lineage. They share 66 % homology in their amino acid sequences, with the main differences being in the intracellular region [Mizuno et al., 2001]. This high degree of sequence similarity suggests that Ncam1a and Ncam1b likely have overlapping functions. Additionally, Ncam1a and Ncam1b have some overlapping expressions, with Ncam1a being more broadly expressed in the primordium [Dries, 2014]. Furthermore, previous studies have shown that Ncam1a can bind to Fgfr1a, albeit in a weaker mode compared to Ncam1b [Lange, 2019, Dries, 2018, Dries et al., 2021]. This suggests that Ncam1a may be able to partially compensate Ncam1b in regulating FGF signaling and cell proliferation in the primordium. Whether indeed the upregulation of *ncam1a* in the *ncam1b* mutants compensates for the loss of *ncam1b* could be evaluated by a *ncam1a* knockdown in the mutant or by generating double mutants. Another possibility to avoid NMD and the subsequent genetic compensation response would be to delete either the promoter region or the entire gene locus of *ncam1b* [El-Brolosy et al., 2019]. L1cam emerges as a second promising candidate to investigate potential compensatory roles in *ncam1b* mutant zebrafish during developmental processes. As a member of the immunoglobulin superfamily, L1cam shares significant functional overlap with Ncam1b in mediating axon guidance, neurite outgrowth, and neural development [Maness and Schachner, 2006]. This functional similarity suggests that L1cam may be capable of compensating for the loss of Ncam1b. However, L1cam was not further investigated due to the lack of a suitable antibody. The upregulation of *l1cam* in *ncam1b* mutants indicates that the genetic compensation involves multiple components, highlighting the complexity of this adaptive response.

5.1.3 Questioning the dispensability of Ncam1b

When analyzing the effects of a genetic knockout, it is crucial to consider the potential impact of genetic compensation mechanisms. The lack of an obvious phenotype in a knockout model does not necessarily mean the protein is unimportant or dispensable. This observation may indicate the organism's remarkable ability to adapt and maintain its viability and fitness despite genetic changes. Genetic compensation is a key survival strategy used by organisms to offset the loss of a gene [Peng, 2019]. When a gene is knocked out, the organism can activate compensatory pathways, often involving the increased expression of related genes or parallel biological processes. However, this compensatory response may come at a significant energy cost to the organism [Plech et al., 2017]. By activating

alternative mechanisms to compensate for gene loss, the organism may need to reallocate resources from other important processes, which can be more energy-demanding than directly utilizing the gene product. Despite the increased energy demands, the organism frequently considers this compensatory mechanism a worthwhile investment to maintain its overall fitness and functionality. Experiments in yeast have provided insights into the energetic implications of genetic compensation [Giaever et al., 2002]. These studies have shown that an increased tolerance to mutations correlates with a high expression of genes responsible for energy metabolism. This suggests that the negative effects of mutations can be buffered if enough energy is available. Similarly, in the case of the *ncam1b* mutant zebrafish, the increased expression of compensatory genes like *ncam1a* and *l1cam* may require additional energy resources to maintain lateral line development. Furthermore, studies in yeast have revealed that less than 20 % of genes are considered "essential", while a much larger number of mutations shows a measurable effect on relative fitness [Giaever et al., 2002]. Similar genetic results have also been obtained in mice. In a study by the Sanger Institute Mouse Genetics Project, in which 500 knockout mouse lines were generated, only about 42 % of the genes were found to be essential for the viability of the animals [White et al., 2013].
In conclusion, the apparent lack of an overt phenotype in *ncam1b* mutant zebrafish should not be misconstrued as evidence that Ncam1b is dispensable, as genetic compensation mechanisms may be masking its functional importance by upregulating related genes like *ncam1a* and *l1cam* at a significant energetic cost to the organism.

5.1.4 Critical evaluation of potential off-target effects in *ncam1b* morphants

The discrepancy between the developmental phenotypes observed in the *ncam1b* mutant and morphant zebrafish lines raises questions about the potential for off-target effects associated with morpholino knockdown experiments. Morpholinos are widely used to transiently suppress gene expression, but they have been shown to sometimes produce phenotypes that are not recapitulated in genetic mutants, suggesting the possibility of off-target effects [Kok et al., 2015]. Injection of the *ncam1b*-ATG morpholino into the *ncam1b* mutants resulted in a severe phenotype, similar to the initial knockdown experiments in wild type (WT) embryos. This suggests that the *ncam1b*-ATG morpholino may induce pronounced off-target effects that are independent of the *ncam1b* genotype. In contrast, the *ncam1b*-5'UTR morpholino, which targets a region close by had a more variable, milder impact on the mutant embryos, potentially due to weaker off-target interactions. Nevertheless, Langhauser et al. (2012) and Dries et al. (2021) presented strong evidence for the specificity of the *ncam1b*-ATG morpholino knockdown, such as the rescue of the migration and neuromast deposition defects by co-injecting *ncam1b* mRNA, and the fact that the *ncam1b*-5'UTR morpholino phenocopied the *ncam1b*-ATG morpholino. Ncam1b protein expression was drastically reduced following morpholino injection [Dries et al., 2021], but Ncam1a protein expression was unaltered [Langhauser et al., 2012]. The reduced primordium size is not due to increased apoptosis, as co-injection of a *p53* morpholino does not rescue the phenotype and Western blots show that the *ncam1b*-ATG morpholino does not affect the expression of the apoptosis marker *p53*. Several studies have demonstrated that morphant phenotypes, despite successful control experiments, can result from the off-target effects of morpholinos. A well-documented case of such an off-target effect is the impact on the *megamind* lincRNA, which led to brain and eye defects [Ulitsky et al., 2011]. The morphant phenotype could be rescued by mRNA injection. Nevertheless, injecting the morpholino

into the mutant still led to this phenotype [Kok et al., 2015]. Kok et al. (2015) demonstrated that five of their twelve studied morphant phenotypes, which failed to be observed in mutants, were rescued in previous studies by co-injecting mRNA. mRNA rescue of a morphant phenotype may thus not always be a reliable proof of the morpholino specificity as the mRNA may also interfere nonspecifically [Kok et al., 2015].
In summary, this experiment suggests that both, the *ncam1b*-ATG and 5'UTR morpholinos may induce off-target effects on both, the migration distance and size of the primordium as well as on the deposition of proneuromasts in the zebrafish. However, this does not necessarily mean that other phenotypes observed with the *ncam1b*-ATG and 5' UTR morpholinos are off-target effects as well. The discrepancy between the *ncam1b* morphant and mutant phenotypes highlights the growing challenge in zebrafish research, where morpholino-induced effects may not always accurately reflect the role of a gene, due to potential off-target effects. The mutant phenotype, however, must also be critically examined, as genetic compensation can mask the absence of the gene.

The latter morphants were included in this study, although the *ncam1b*-ATG morpholino might cause off-target effects that induce a developmental morphology phenotype. This morpholino can still provide valuable insights into other developmental processes, especially when mutant controls are performed. These controls allow discerning a specific morpholino-induced phenotype from off-target effects.

5.2 Ncam1b regulates the balance between Wnt and FGF signaling in the lateral line primordium

In WT embryos, Wnt signaling is active in the Leading Zone of the primordium, driving proliferation through the expression of Lef1 [Gamba et al., 2010]. In contrast, the FGF signaling pathway dominates in the Trailing Zone, regulating proliferation via Erm [Aman and Piotrowski, 2008, Lecaudey et al., 2008]. In *ncam1b* morphants, no *erm* expression can be observed in the Trailing Zone by *in situ* hybridization-mediated (ISH) NBT/BCIP staining [Dries et al., 2021]. This suggests that Ncam1b plays an important role in activating *erm* expression, likely through its interaction with Fgfr1a.
In the present study, a double fluorescence *in situ* hybridization (FISH) was used to compare the two signaling centers Wnt and FGF in *ncam1b* morphants and mutants with those of WT. To characterize the Wnt pathway, embryos were stained with a *lef1* probe, and to characterize the FGF pathway with a *fgfr1a* or an *erm* probe. Expression area size (Fig. 4.7) and length (Sup. S2) were measured and compared. In contrast to Dries et al. (2021), where the authors were only able to detect *erm* expression in 18 % of *ncam1b* morphant embryos using ISH, the present study found that 100 % of embryos showed an *erm* probe signal after FISH analysis. This suggests that FISH is significantly more sensitive than ISH for detecting genes that are not expressed at high levels like *erm* in *ncam1b* morphants. This is likely due to the use of fluorescent probes and signal amplification.
In the current study, *ncam1b* morphants showed a drastically reduced ***erm***-expressing area in the primordium (Fig. 4.7 I). This corroborates the findings of Dries et al. (2021). In *ncam1b* mutants, the *erm* expression domain was also reduced, although not to the same extent as in the morphants. This suggests, that the loss of *ncam1b* leads to a downregulation of the proliferation marker *erm*, indicative of a downregulation of FGF signaling. The difference in the reduction of *erm* between the mutant and the morphant could be due to a compensatory mechanism in the mutant, allowing *erm* expression to be

at least partially maintained. The ***fgfr1a*** expression area, however, did not differ significantly between WT, *ncam1b* morphants, and *ncam1b* mutants, indicating that the expression of *fgfr1a* is not directly regulated by Ncam1b (Fig. 4.7 H). This is consistent with the findings of Dries et al. (2021), who did not find differences in *fgfr1a* expression in *ncam1b* morphants. *ncam1b* morphants and mutants showed enlarged ***lef1*** expression in the primordium. The *lef1* expression domain was substantially increased in *ncam1b* morphants than in the mutant primordium. In addition to measuring the size of the expression areas of *fgfr1a*, *lef1*, and *erm*, the lengths of these expression domains were also quantified (Sup. S2). The analysis revealed that while the area of *lef1* expression increased in the *ncam1b* mutants, its length did not. The increase in area without a corresponding change in length for *lef1* suggests localized primordium thickening in the Leading Zone of *ncam1b* mutants.

The activity of the FGF and Wnt signaling pathways occurs in an antagonistically acting feedback loop [Aman and Piotrowski, 2008]. FGF signaling induces the expression of the Wnt inhibitor Dkk 1, while Wnt signaling drives the expression of the FGF inhibitor Sef. In the absence of Ncam1b, the reduced FGF signaling leads to lower expression of the FGF target gene *erm*. Since both *erm* and *dkk1* are targets of signaling pathways triggered by activation of Fgfr1a, it can be speculated that *dkk1* might be downregulated in the absence of Ncam1b similar to *erm*. Reduced *dkk1* expression in the Trailing Zone would lead to less inhibition of Wnt signaling in the Leading Zone, allowing it to expand. Whether *erm* is indeed triggered by Ncam1b-mediated FGF signaling remains to be determined. The present study suggests that the loss of Ncam1b disrupts the normal antagonistic feedback loop between the FGF and Wnt signaling pathways in the primordium. This shift in the balance between these two key signaling cascades ultimately alters the expression patterns of the proliferation markers *erm* (FGF-dependent) and *lef1* (Wnt-dependent) in *ncam1b* mutants. The degree of this shift may be more pronounced in the *ncam1b* morphants compared to the mutants, potentially due to the presence of compensatory mechanisms that develop in the mutants. This suggests the *ncam1b* mutants may employ ways to better maintain the FGF-Wnt signaling equilibrium compared to the acute knockdown in the morphants.

5.3 Loss of *ncam1b* disrupts the spatial distribution of proliferating cells in the lateral line primordium

Lef1 and Erm play important roles in regulating cell proliferation within the primordium of zebrafish. Changes in their expression may, thus, lead to alterations in the spatial distribution of proliferating cells within the primordium. Dries et al. (2021) investigated proliferation in *ncam1b* morphants solely by counting the total number of $BrdU^+$ cells in the primordium. They found a reduced number of proliferating cells despite an enlarged *lef1*-expressing region in the Leading Zone. From this, they concluded that a mere expansion of the *lef1* expression is not sufficient to promote proliferation and that additional factors must be present.

The present study on *ncam1b* mutants analyzes proliferation in the primordium by not only counting the total number of proliferating cells but also determining their spatial distribution within the Leading Zone and the Trailing Zone (Fig. 4.8). In WT embryos, the majority of proliferating cells (around 90 %) are localized in the Trailing Zone. While the total number of cells does not differ between the WT and *ncam1b* mutants, their distribution is altered: mutants contain double as many proliferating cells in the Leading Zone as the WT (23.7 % vs. 10.6 %). These changes correlate with differences in

the expression regions of the key proliferation regulators *lef1* and *erm*. In *ncam1b* mutants, the *erm* expression area is reduced (Fig. 4.7), which is consistent with the decreased proliferation in the Trailing Zone. Simultaneously, a significantly enlarged *lef1* expression area is observed, suggesting an expansion of the Wnt signaling pathway in the Leading Zone, which in turn causes an increase in the number of proliferating cells. This suggests that the loss of *ncam1b* leads to a shift in the balance between Wnt and FGF signaling pathways, which influences the spatial distribution of proliferating cells in the primordium. Dries et al. (2021) found proliferation to be much stronger affected in *ncam1b* morphants than reported herein for *ncam1b* mutants. Especially they report a drastic reduction of cell proliferation despite an increased *lef1* expression in the Trailing Zone. McGraw et al. (2011) discussed, that, besides the well-documented Wnt target gene *lef1*, other, yet unknown factors mediate proliferation in the Leading Zone [McGraw et al., 2011]. It may be speculated, that these factors are affected by the *ncam1b* morpholino knockdown while their function is maintained by genetic compensation in the *ncam1b* mutant. The present study, thus, underscores that the regulation of proliferation in the primordium is too complex to be attributed to just the spatial distribution of *lef1*-expressing cells.
In summary, these findings show that Ncam1b plays an important role in the spatial coordination of proliferation in the primordium by maintaining the balance between Wnt and FGF signaling pathways. A loss of *ncam1b* leads to a shift in this balance, which affects the distribution of proliferating cells, but not overall proliferation, likely through compensatory mechanisms.

5.4 Model of Ncam1b regulation of FGF and Wnt signaling pathways and proliferation in the migrating primordium

Previous research in our lab has provided initial insights into the crucial role of Ncam1b during the development of the pLLS in zebrafish. Morpholino-mediated knockdown of *ncam1b* results in a severe developmental phenotype, including a reduced number of proneuromasts and impaired primordium migration, which are consequences of disrupted cellular proliferation. In contrast, no overall developmental phenotype was observed in the present work, which is likely due to genetic compensation by paralogous genes such as *ncam1a* and *l1cam*. Therefore, the study focused more closely on the migrating primordium and its proliferation.

The summary of the results regarding the function of Ncam1b in regulating FGF and Wnt signaling pathways, and the resulting proliferation within the primordium, is depicted in Fig. 5.1: (A) In wild type embryos, *fgfr1a* and the FGF target gene *erm* are expressed in the Trailing Zone (anterior two-thirds) of the primordium, while the Wnt target gene *lef1* is expressed in the Leading Zone (posterior third). Ncam1b interacts with Fgfr1a (yellow box), activating *erm* expression and regulating proliferation in the Trailing Zone. FGF signaling leads to the expression of Dkk1, a Wnt inhibitor, while Wnt signaling in the Leading Zone promotes local proliferation through *lef1* expression. Additionally, unknown factors also appear to be necessary for proliferation (indicated by question marks). The FGF inhibitor Sef is also expressed due to Wnt signaling. (B) In *ncam1b* morphants, the *erm* expression domain, representing the FGF signaling, is significantly reduced, indicating downregulation of this pathway. The absence of interaction with Fgfr1a in *ncam1b*-ATG morphants leads to reduced *erm* expression and decreased proliferation (black thunderbolt). Similarly, the reduced FGF signaling may also result in decreased inhibition of Wnt signaling by Dkk1, allowing Wnt signaling and thus *lef1* to expand in the Leading Zone. Despite increased *lef1* expression, no proliferation is observed in morphants (red thunderbolt). (C) In *ncam1b* mutants, Ncam1a is upregulated and can interact with Fgfr1a, though less effectively than Ncam1b. FGF signaling in the Trailing Zone is reduced but not as weak as in morphants, resulting in a less severe reduction in *erm* expression and proliferation. The *lef1* expression domain (reflecting Wnt signaling) is enlarged in mutants, leading to increased proliferation in the Leading Zone. The spatial distribution of proliferating cells was altered in ncam1b mutants: there were twice as many proliferating cells in the Leading Zone compared to the wild type. Nevertheless, the overall proliferation rate in mutants remained unchanged, unlike the significant reduction seen in (B) morphants.

In summary, this study reveals that Ncam1b is essential for the spatial regulation of cell proliferation in the primordium by preserving the equilibrium between Wnt and FGF signaling pathways. When *ncam1b* is lost, this balance is disrupted, leading to changes in the distribution of proliferating cells. However, the overall proliferation rate in mutants can still be maintained through compensatory mechanisms.

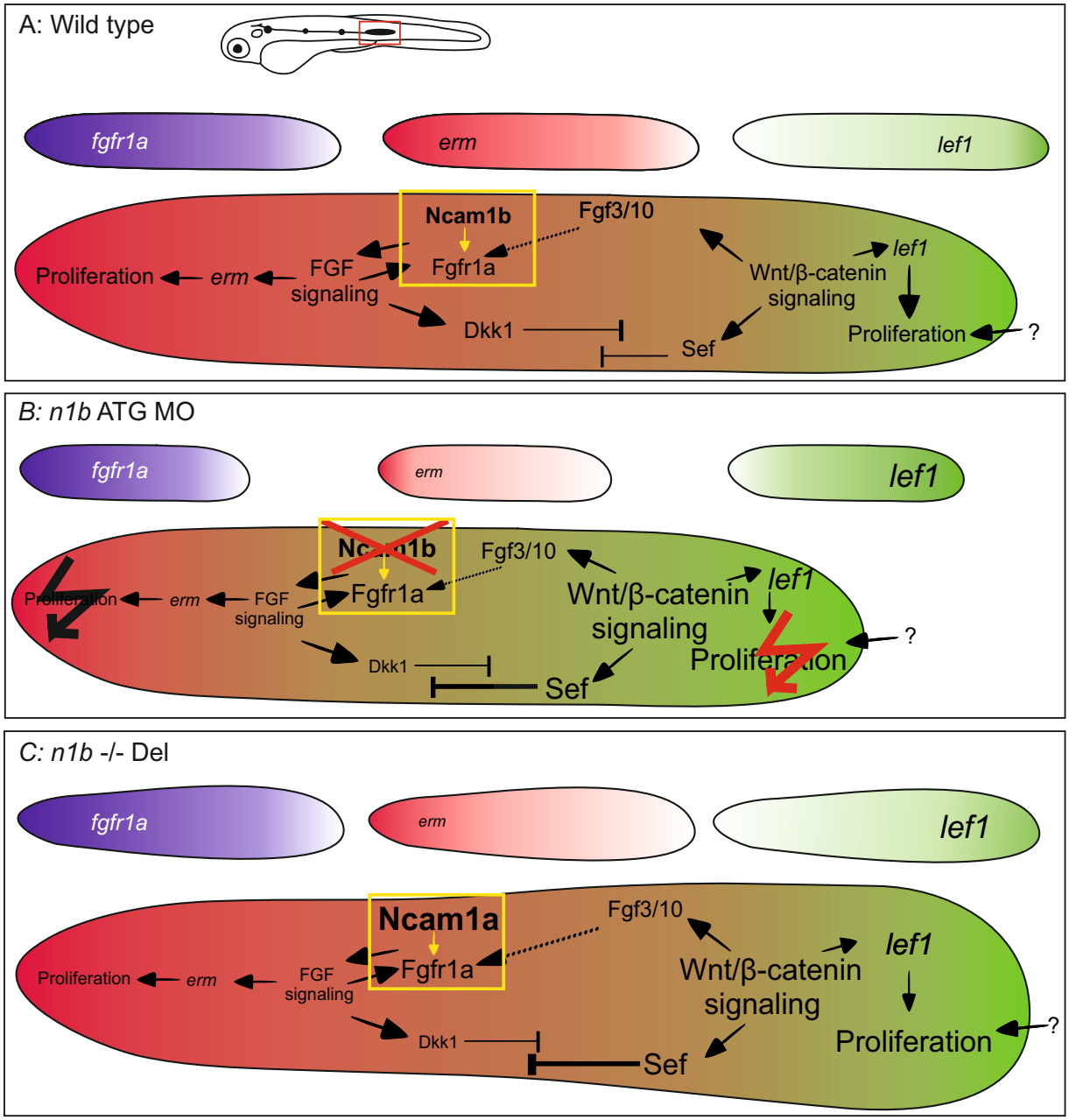

Figure 5.1: Model of signaling in the migrating primordium in WT, *ncam1b* morphant, and *ncam1b* mutant. Rostral is left, caudal is right. Small primordia depict *fgfr1a* (purple), *erm* (red), and *lef1* (green) expression distributions. The large primordium represents overall complex signaling. *erm* and *lef1* expression regions are color-coded.

5.5 *ncam1b* knockout does not influence hair cell development

The neuromasts in the lateral line allow the fish to perceive water movements and pressure changes in its surroundings [Dykgraaf, 1933]. This is crucial for its orientation, prey search, and predator avoidance. The neuromasts contain sensory hair cells that transduce mechanical stimuli into electrical signals. These signals are then transmitted via nerve fibers to the zebrafish brain [Metcalfe et al., 1985, Pujol-Martí and López-Schier, 2013]. Disruptions in the development or function of the neuromasts could therefore lead to significant impairments in sensory perception and behavior. Previous studies have shown that Ncam1b is expressed in both, newly developed proneuromasts, as well as in differentiated neuromasts [Dries, 2014, Dries, 2018]. This suggests that Ncam1b may play an important role not only in hair cell differentiation during the development but also in maintaining the homeostatic state of the neuromasts. The present work shows that the complete loss of *ncam1b* in mutants has no impact on the number of hair cells in the neuromast, neither during development nor in the differentiated state (Fig. 4.9). While Ncam1b is expressed in neuromast structures, the findings suggest that the absence of Ncam1b does not prevent the normal differentiation of hair cells within these structures.

5.6 Ncam1b has a crucial role during the regeneration of lateral line hair cells

Zebrafish are able to efficiently regenerate their neuromast hair cells after damage by ototoxic substances like neomycin [Harris et al., 2003]. While in humans and other mammals, injured sensory cells have only limited capacity for replacement, zebrafish are capable of fully compensating for the loss of these cells [Harris et al., 2003]. Prior studies from this lab have demonstrated that Ncam1b is not only expressed in hair cells under normal homeostatic conditions but its expression is also upregulated during the process of regeneration following neomycin-induced hair cell damage [Dries, 2018]. The increased expression of Ncam1b in support cells during the regeneration leads to the hypothesis that Ncam1b may play an essential role in their differentiation into new hair cells.

The present study shows that the complete loss of *ncam1b* causes a significant impairment of hair cell regeneration (Fig. 4.11). While WT larvae were able to regenerate 95 % of their hair cells within two days after neomycin treatment, see also Harris et al. (2003), *ncam1b* mutants showed a much slower regeneration process. It took the mutants four days to regenerate only 73 % of the hair cells, a statistically significant difference from the WT. These observations strongly suggest that Ncam1b plays a crucial role in the regeneration of neuromast hair cells. Interestingly, a complete loss of *ncam1b* does not affect the normal development and differentiation of the neuromast hair cells. In the mutants, the number of hair cells was unchanged compared to WT, both during development and in the mature neuromasts (Fig. 4.9). This underscores that Ncam1b is specifically required for the regenerative capacity of hair cells, but can be compensated for when knocked out during their initial development and differentiation. Similar to the *ncam1b* mutant, in the *phoenix* mutation, support cells are not able to regenerate, in this case due to misregulated proliferation [Behra et al., 2009]. The *phoenix* mutation does, however, not seem to interfere with the support cells' initial development and maturation. This suggests that the genetic programs controlling support cell proliferation during regeneration are distinct from those governing their original formation and differentiation. Regeneration is, thus, not simply a replay of development, but rather a distinct process with its specific molecular underpinnings.

5.7 Delayed but not absent hair cell regeneration: Indications of alternative regenerative capacities

Rapid and efficient regeneration of hair cells is crucial for the zebrafish, as it allows them to quickly restore their sensory perception and associated behaviors. It is demonstrated here, that Ncam1b has a crucial role in regulating hair cell regeneration after neomycin-induced damage (Fig. 4.11). While WT larvae were able to regenerate 95 % of the hair cells within just two days after damage, the *ncam1b* mutants had only replaced 73 % within four days. This suggests that the absence of *ncam1b* does not entirely prevent hair cell regeneration. Consequently, other mechanisms must exist that can at least partially compensate for the function of Ncam1b during the regeneration process.

The observation that initial hair cell regeneration (until 1 dpt) occurs at the same rate in *ncam1b* mutants and WT larvae, suggests that the early mechanisms driving regeneration are Ncam1b-independent. At later stages, Ncam1b becomes indispensable for efficient regeneration. This temporal separation of Ncam1b dependency indicates that hair cell regeneration proceeds through distinct molecular phases. In addition, the delayed rather than completely absent regeneration in *ncam1b* mutants implies that other factors continue to drive the regenerative process. Potential candidates regulating the initial Ncam1b-independent phase, as well as potentially acting in parallel to Ncam1b's functions during later stages, could include other cell adhesion molecules, morphogens, transcription factors or epigenetic regulators.

Previous studies have shown that in some cases, paralogous genes can act in a compensatory manner to offset the loss of a gene during regeneration, as seen for example for Sox2 and Sox3 [Undurraga et al., 2019]. In the context of the pLLS, this study shows that in *ncam1b* mutants, the paralog *ncam1a*, as well as other genes, are upregulated during the development of the neuromast structures. Ncam1a can, however, not be detected neither in the mature WT neuromasts (see also Dries, 2018) nor in *ncam1b* mutant larvae following neomycin treatment (Fig. 4.12). This suggests that the potential regeneration observed in these mutants is not due to direct compensation by the Ncam1a paralog. The existence of other, yet unidentified proteins must be speculated to account for some degree of hair cell regeneration in the absence of Ncam1b. Potential candidates might include other cell adhesion molecules of the immunoglobulin superfamily, such as ICAM1, VCAM1, L1cam or cadherins. *l1cam* might be regarded as a possible candidate as it was shown in this study to be upregulated during the development of the pLLS. L1cam has been shown to have the potential to promote regeneration processes in the nervous system, such as after spinal cord injuries [Becker et al., 2004]. Given the functional similarities between Ncam1b and L1cam, L1cam could compensate for the loss of Ncam1b during hair cell regeneration in the lateral line.

Overall, regeneration is a multi-step process governed by distinct temporally-regulated molecular programs. The absence of Ncam1b leads to impaired regeneration. Regeneration, however, is still possible, either through genetic compensation or parallel mechanisms occurring simultaneously, or a combination of both.

5.8 The absence of Ncam1b leads to accumulation of proliferating support cells during regeneration

Cell proliferation presents an important first step in providing the required cell numbers for tissue repair [Namdaran et al., 2012]. Subsequently, these proliferated cells must undergo correct differentiation into the cell types needed to restore the full functionality of the regenerated tissue. This interplay of proliferation and differentiation is essential during the regeneration of sensory hair cells in zebrafish [Stone and Cotanche, 2007]. In the present study, the cause for impaired hair cell regeneration in *ncam1b* mutants was investigated. It is shown that the loss of *ncam1b* leads to an accumulation of proliferating support cells (Fig. 4.13). The support cells proliferate, but cannot differentiate into hair cells, leading to a reduced number of regenerated hair cells (Fig. 4.11). It can be concluded that Ncam1b promotes the differentiation of support cells rather than their proliferation.

5.9 Dysregulated Notch signaling potentially causes impaired hair cell regeneration in *ncam1b* mutants

Key signaling pathways, like Notch, Wnt/β-Catenin, FGF and Bmp, that are involved in hair cell development are also crucial for the process of hair cell regeneration [Steiner et al., 2014, Jiang et al., 2014, Baek et al., 2022]. The Notch signaling pathway appears to play an important role in regulating hair cell regeneration by balancing the ratio between hair cells and support cells. Notch signaling specifies support cells by inhibiting the proneural gene *atoh1a*, which is required for the acquisition of a neurogenic cell fate [Matsuda and Chitnis, 2010, Driver et al., 2013, Kozlovskaja-Gumbrienė et al., 2017]. Alterations in Notch signaling have been found to significantly impact hair cell regeneration. Overexpression of the intracellular domain of Notch, which constitutively activates the pathway, inhibits hair cell regeneration [Wibowo et al., 2011]. Conversely, blocking Notch signaling using pharmacological inhibitors, such as DAPT, promotes an increase in hair cell numbers during the regeneration process [Ma et al., 2008, Wibowo et al., 2011]. The current work shows that a lack of Ncam1b leads to an accumulation of proliferating support cells, which do not differentiate into hair cells. Blocking Notch signaling with DAPT rescued the reduced number of regenerated hair cells in the *ncam1b* mutants (Fig. 4.14). As Notch signaling is known to balance the ratio of hair cells and support cells, increased Notch activity in *ncam1b* mutants could explain the accumulation of proliferating support cells. This would imply that Ncam1b normally inhibits Notch signaling in this context. One potential candidate mediating the dysregulated Notch signaling in *ncam1b* mutants could be the Notch 3 receptor, which shows expression in the support cells of the neuromasts.

5.9.1 Fgfr1a as an intermediate candidate for the crosstalk between Ncam1b and Notch

It is known that neural cell adhesion molecules such as F3/contactin and NB-3 can interact with Notch receptors as alternative ligands, promoting the development of oligodendrocytes [Hu et al., 2006]. In the context of Ncam1b, however, no direct interactions with Notch are known. It can therefore be assumed, that Ncam1b indirectly regulates Notch signaling through an intermediate candidate. Based on the evidence that Ncam1b can directly interact with Fgfr1a [Francavilla et al., 2009, Dries et al., 2021] and Fgfr1a can interact with the Notch signaling pathway [Kozlovskaja-Gumbrienė et al., 2017, Lush et al., 2019], it is worth considering Fgfr1a as a potential candidate mediating crosstalk between

Ncam1b and Notch signaling in the context of hair cell regeneration. Research by Lee et al. (2016) demonstrated that inhibiting Fgfr1a signaling, either with the chemical inhibitor SU5402 or by using a dominant-negative heat shock line results in impaired hair cell regeneration [Lee et al., 2016]. In contrast, *fgf3* -/- mutants show an increased number of hair cells during development and regeneration. Since inhibition of the Fgfr1a receptor and knockout of one of its ligands, namely *fgf3*, lead to completely different phenotypes, it implies that other additional ligands of Fgfr1a that are responsible for hair cell regeneration. The findings that both, *ncam1b* mutant (shown in this work) and Fgfr1a inhibition (demonstrated by Lee et al., 2016) lead to impaired hair cell regeneration strongly suggest that Ncam1b and Fgfr1a function in the same pathway regulating this process. This lends further support to the hypothesis that Fgfr1a could mediate the crosstalk between Ncam1b and Notch signaling during hair cell regeneration.

5.9.2 Context-dependent interactions between Fgfr1a and Notch signaling

The relationship between FGF signaling and Notch signaling has been investigated in different contexts, yielding seemingly contradictory findings. Kozlovskaja-Gumbrienė et al. (2017) found that during neuromast **development**, FGF signaling acts upstream of Notch and is required for its activation, as inhibition of the Fgfr1a by SU5402 led to downregulation of Notch target genes [Kozlovskaja-Gumbrienė et al., 2017]. In contrast, Lush et al. (2019) observed that during neuromast **homeostasis**, the expression of Notch target genes is independent of *fgf3*-induced FGF signaling, suggesting a potential uncoupling of these pathways in this context [Lush et al., 2019]. These studies highlight the context-dependent nature of the crosstalk between Fgfr1a and Notch signaling. While they appear contradictory, these studies reflect the complexity and dynamic interactions of these pathways in different biological processes. In the context of hair cell **regeneration**, the relationship between FGF signaling and Notch signaling remains unclear. However, the previously discussed interaction between Ncam1b and Fgfr1a, coupled with the suspected upregulation of Notch signaling in *ncam1b* mutants, suggests Fgfr1a is a promising candidate to be evaluated as a potential mediator between Ncam1b and Notch in further studies.

5.9.3 Potential negative feedback loop between Ncam1b and Notch signaling

Notably, Dries (2018) showed that inhibition of Notch signaling leads to upregulation of Ncam1b, indicating an inhibitory effect of Notch on Ncam1b. Together with the observations described in this study, suggesting that Ncam1b may have an inhibitory effect on Notch, this points to the existence of an inhibitory feedback loop between Ncam1b and Notch signaling.

5.10 Model of Ncam1b function in regulating hair cell regeneration

While Ncam1b is expressed in neuromasts during lateral line development, neuromast formation and hair cell differentiation during this phase are not affected by complete *ncam1b* knockout. Ncam1b becomes, however, indispensable for efficient regeneration after hair cell damage. The role of Ncam1b in coordinating the proliferation of support cells and their subsequent differentiation into new hair cells during regeneration, as deduced from the results presented in the current study, is delineated in the following model (Fig. 5.2). (A) In wild type zebrafish, Ncam1b is expressed in differentiated hair cells and a subset of support cells within the neuromasts of the lateral line organ. (B) Hair cells are lost after damage. (C) These support cells then proliferate and begin to express Ncam1b. (D + E) In wild type, the progenitor cells can properly differentiate into new hair cells, restoring the neuromast structure and function. (A' - C') In *ncam1b* mutants, support cell proliferation still occurs normally in response to hair cell damage. (D' - E') The proliferating progenitor support cells, however, fail to differentiate properly into new hair cells due to dysregulated Notch signaling. This leads to an accumulation of undifferentiated progenitor cells and impaired regeneration of hair cells. Notably, while the absence of Ncam1b significantly impairs hair cell regeneration, the observation that regeneration is not completely abolished, implies the involvement of additional factors or compensatory mechanisms involved in cell differentiation beyond Ncam1b. (F) The defect in support cell differentiation appears to stem from dysregulated Notch signaling in the absence of Ncam1b. Increased Notch activity inhibits hair cell differentiation by preventing proneural gene expression. (G) Ncam1b may regulate Notch signaling indirectly via its interaction with the Fgfr1a receptor, which can modulate Notch activity. (H) Moreover, an inhibitory feedback loop may exist between Ncam1b and Notch, as Notch inhibition leads to Ncam1b upregulation [Dries, 2018] and Ncam1b knockout may lead to Notch increasing (current study). In summary, this model suggests that Ncam1b plays a crucial role in promoting the differentiation of proliferating support cells into hair cells during regeneration by inhibiting Notch signaling, potentially through crosstalk with the Fgfr1a pathway.

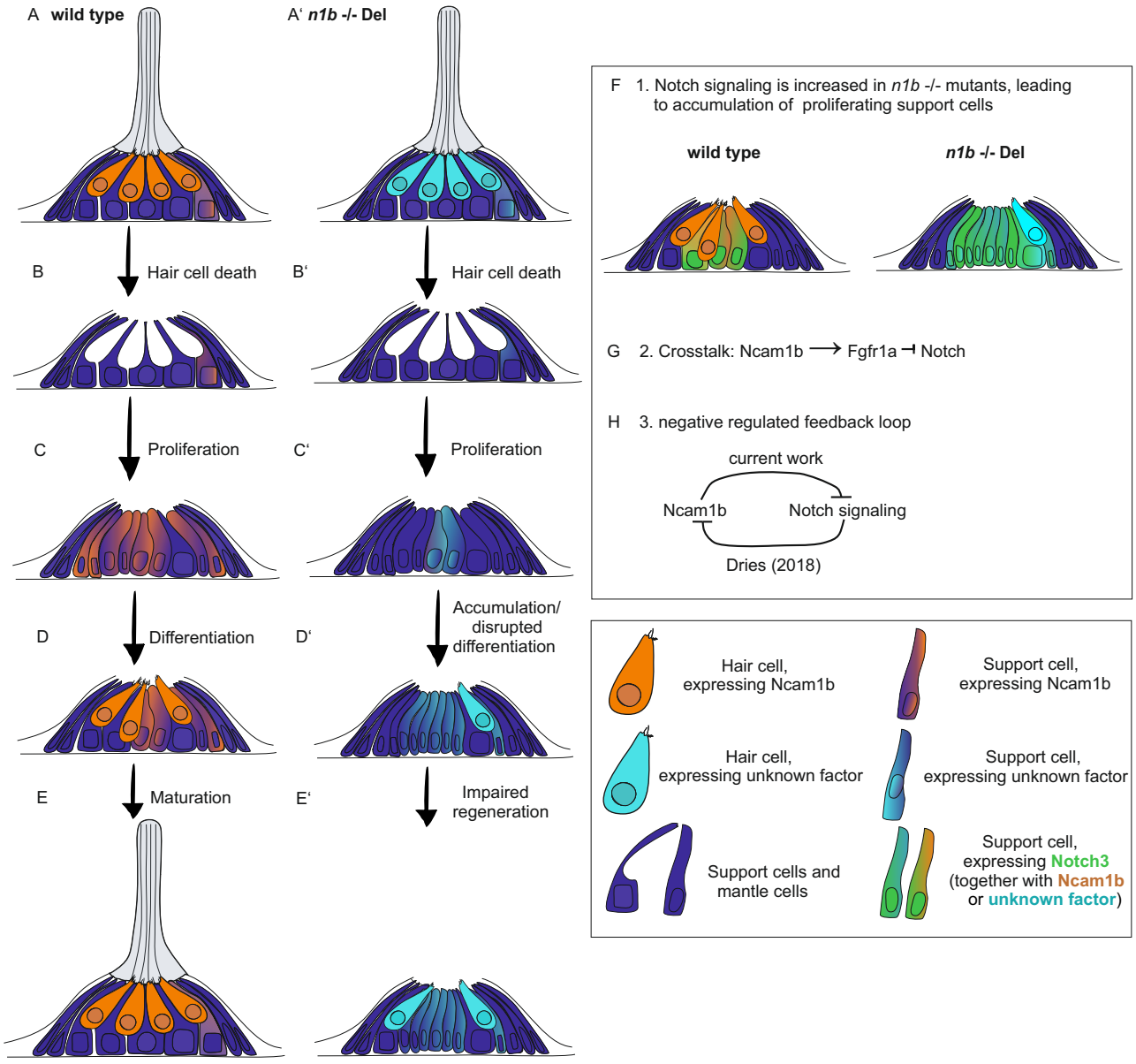

Figure 5.2: Model for the function of Ncam1b during differentiation and regeneration of hair cells. (A - E) Regeneration of hair cells in wild type. **(A' - E')** Impaired regeneration in Ncam1b mutants due to proliferating support cells that cannot differentiate into hair cells. **(F - H)** Three-step hypothesis to explain the impaired regeneration in *ncam1b* mutants.

6 Outlook

The present study provides novel insights into the role of the neural cell adhesion molecule Ncam1b during the development and regeneration of the lateral line organ in the zebrafish.
Firstly, Ncam1b coordinates the balance between the Wnt and FGF signaling pathways in the migrating primordium and it is crucial for the proper spatial distribution of proliferating cells. Its absence in mutants, however, does not visibly impact the development of the lateral line organ. Similar findings have been reported for other genes, suggesting potential compensatory mechanisms. Further investigations should, thus, focus on the upregulation of *ncam1a* or related genes in the mutants, which could mask a possibly stronger phenotype. To that end, the generation of double mutants could be undertaken. To gain further insights, future studies could investigate whether deleting the promoter region or the entire gene locus of *ncam1b* can intensify the mutant phenotype, thus circumventing nonsense-mediated mRNA decay.
Secondly, Ncam1b plays a crucial role in the regeneration of hair cells following neomycin damage. The study demonstrates that Ncam1b regulates the balance between support cell proliferation and differentiation. To understand this function in more detail, long-term studies could elucidate whether the loss of *ncam1b* merely delays regeneration or if complete regeneration is not possible in the mutant. An intriguing observation is that the impaired regeneration of hair cells in *ncam1b* mutants can be rescued by Notch inhibition. This suggests that Ncam1b regulates the balance between proliferation and differentiation via participating in Notch signaling. Investigating these interactions and their consequences will be the focus of ongoing studies. These will aim at, among others, the spatiotemporal expression of Notch target genes like *deltaD* and *notch1b/3* in regenerating neuromasts in wild type and *ncam1b* mutants. Pharmacological inhibition or activation of Fgfr1a and Notch receptors will help to understand the interplay between the Fgfr1a and Notch pathways. To further substantiate the proposed negative feedback between the Notch pathway and Ncam1b regulation, examining the *ncam1b* expression levels in *notch 3* mutant zebrafish would offer corroborating insights.
Thinking beyond the lateral line system, one could imagine a function of Ncam1b in neuronal regeneration in the adult zebrafish brain. Based on initial findings of Ncam1 expression in the brains of zebrafish [Marx, 2002] and mice [Shen et al., 1999, Nacher et al., 2002, Bonfanti, 2006] it is tempting to (i) study the expression of Ncam1 paralogs in the adult brain in more detail and (ii) compare the regenerative capacity of wild type and *ncam1b* mutant neurons.

7 Supplementary Data

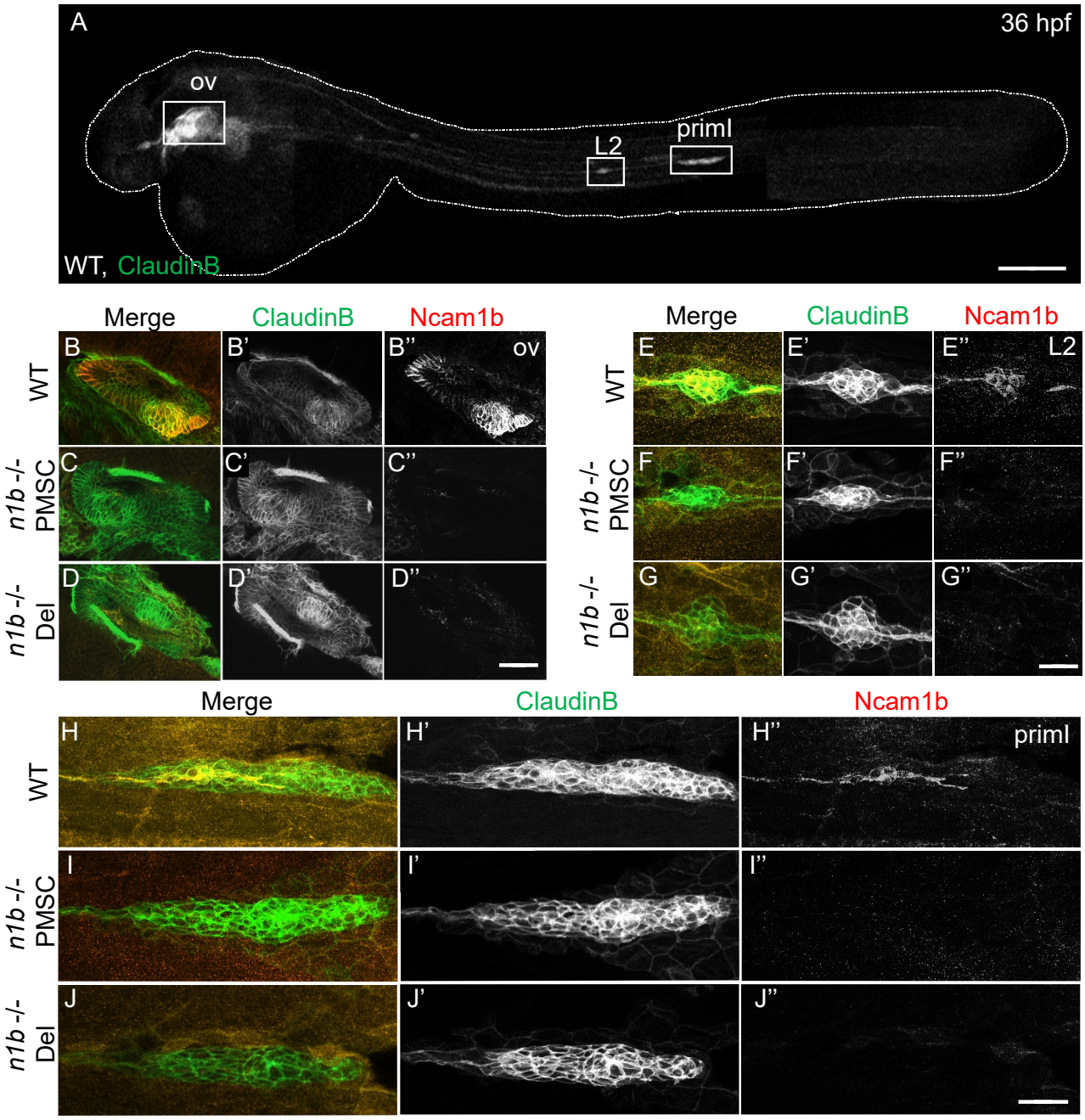

Figure S1: *ncam1b* mutant embryos show no expression of Ncam1b at 36 hpf. **(A)** Lateral view of a 36 hpf WT *Tg(ClaudinB::lynGFP)* embryo, showing the region from the otic vesicle (OV), the proneuromast L2 and the primordium (primI). **(B-J'')** A close-up of the otic vesicle (ov), second proneuromats (L2) and primI respectively, showing expression of GFP (green) and Ncam1b (red) in single channel views and overlays. **(B-D'')** WT otic vesicle shows Ncam1b antibody binding, while no staining is observed in both mutants at this region. **(E-G'')** L2, which is intended to be representative of all other proneuromasts, demonstrates that in contrast to WT, Ncam1b expression is absent in both mutants. **(H-J'')** In the primI's Trailing Zone of WT, Ncam1b antibody staining is detected, while no signal is present in both mutants. Scale bar in **A** 200 µm, Objective: 5x. Scale bars, Objectives: **(A)** 200 µm, 5x; **(D'')** 40 µm, 40xOil; **(G'')** 20 µm, 40xW; **(J'')** 20 µm, 40xOil.

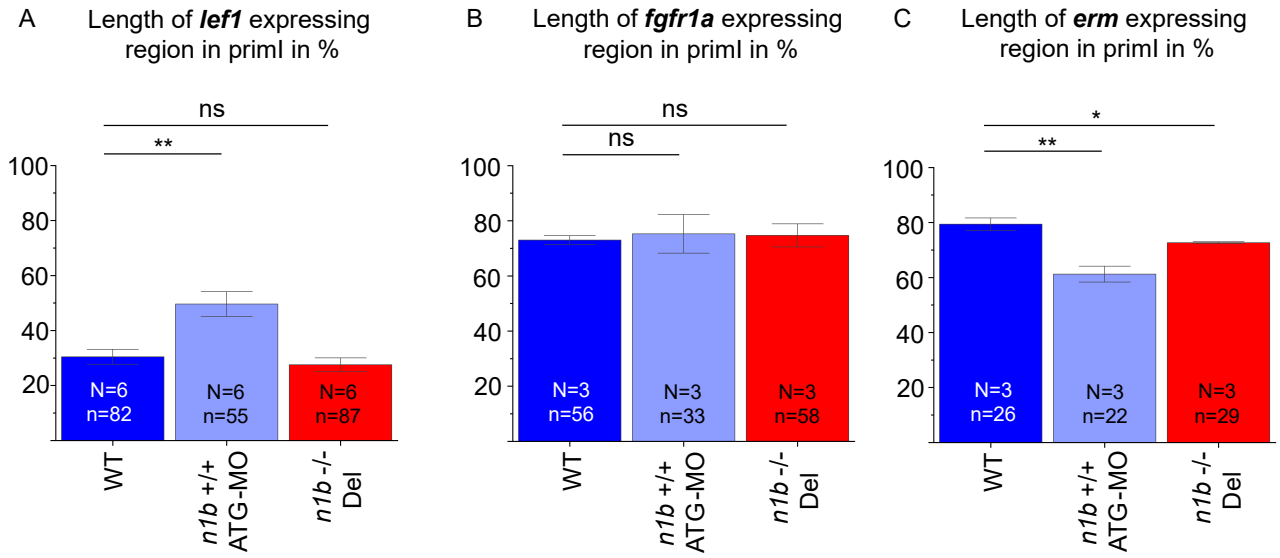

Figure S2: Expression domain length of *lef1*, *fgfr1a*, and *erm* in the primordium at 36 hpf in WT, *ncam1b* morphants, and *ncam1b* mutants. **(A)** *ncam1b* morphants show a significant increase in the length of *lef1* expression. **(B)** The length of the *fgfr1a*-expressing region does not differ between WT, *ncam1b* morphants, and *ncam1b* mutants. **(C)** *ncam1b* morphants and mutants have a significantly shortened *erm*-expressing area length compared to WT. Two-sided $t-test$: *: $p < 0.05$, **: $p < 0.01$, ***: $p < 0.001$, n.s.: not significant.

8 References

Akagi, T., Kuure, S., Uranishi, K., Koide, H., Costantini, F., and Yokota, T. (2015). ETS-related transcription factors ETV4 and ETV5 are involved in proliferation and induction of differentiation-associated genes in embryonic stem (ES) cells. *The Journal of biological chemistry*, 290:22460–22473.

Aman, A., Nguyen, M., and Piotrowski, T. (2011). Wnt/β-catenin dependent cell proliferation underlies segmented lateral line morphogenesis. *Developmental biology*, 349:470–482.

Aman, A. and Piotrowski, T. (2008). Wnt/β-catenin and Fgf signaling control collective cell migration by restricting chemokine receptor expression. *Developmental cell*, 15:749–761.

Baek, S., Tran, N. T., Diaz, D. C., Tsai, Y. Y., Acedo, J. N., Lush, M. E., and Piotrowski, T. (2022). Single-cell transcriptome analysis reveals three sequential phases of gene expression during zebrafish sensory hair cell regeneration. *Developmental Cell*, 57:799–819.e6.

Baird, R. A., Burton, M. D., Fashena, D. S., and Naeger, R. A. (2000). Hair cell recovery in mitotically blocked cultures of the bullfrog saccule. *Proceedings of the National Academy of Sciences of the United States of America*, 97:11722–11729.

Balak, K. J., Corwin, J. T., and Jones, J. E. (1990). Regenerated hair cells can originate from supporting cell progeny: evidence from phototoxicity and laser ablation experiments in the lateral line system. *The Journal of neuroscience : the official journal of the Society for Neuroscience*, 10:2502–2512.

Becker, C. G., Lieberoth, B. C., Morellini, F., Feldner, J., Becker, T., and Schachner, M. (2004). L1.1 Is Involved in Spinal Cord Regeneration in Adult Zebrafish. *Journal of Neuroscience*, 24:7837–7842.

Behra, M., Bradsher, J., Sougrat, R., Gallardo, V., Allende, M. L., and Burgess, S. M. (2009). Phoenix Is Required for Mechanosensory Hair Cell Regeneration in the Zebrafish Lateral Line. *PLoS Genetics*, 5.

Bielefeld, E. C., Tanaka, C., di Chen, G., and Henderson, D. (2010). Age-related hearing loss: is it a preventable condition? *Hearing research*, 264:98–107.

Bleckmann, H. (2008). Peripheral and central processing of lateral line information. *Journal of Comparative Physiology A: Neuroethology, Sensory, Neural, and Behavioral Physiology*, 194:145–158.

Bonfanti, L. (2006). PSA-NCAM in mammalian structural plasticity and neurogenesis. *Progress in Neurobiology*, 80:129–164.

Bosco, A., Bureau, C., Affaticati, P., Gaspar, P., Bally-Cuif, L., and Lillesaar, C. (2013). Development of hypothalamic serotoninergic neurons requires Fgf signalling via the ETS-domain transcription factor Etv5b. *Development (Cambridge, England)*, 140:372–384.

Breau, M. A., Wilson, D., Wilkinson, D. G., and Xu, Q. (2012). Chemokine and Fgf signalling act as opposing guidance cues in formation of the lateral line primordium. *Development (Cambridge)*, 139:2246–2253.

Burns, J. C. and Corwin, J. T. (2013). A historical to present-day account of efforts to answer the question: "What puts the brakes on mammalian hair cell regeneration?". *Hearing Research*, 297:52–67.

Chardin, S., Romand, R., Staecker, H., Lefebvre, P., Malgrange, B., Moonen, G., and Water, T. R. V. D. (1995). Regeneration and mammalian auditory hair cells. *Science*, 267:707–711.

Chen, G. D. and Fechter, L. D. (2003). The relationship between noise-induced hearing loss and hair cell loss in rats. *Hearing Research*, 177:81–90.

Chitnis, A. B., Nogare, D. D., and Matsuda, M. (2012). Building the posterior lateral line system in zebrafish. *Developmental Neurobiology*, 72:234–255.

Colak-Champollion, T., Lan, L., Jadhav, A. R., Yamaguchi, N., Venkiteswaran, G., Patel, H., Cammer, M., Meier-Schellersheim, M., and Knaut, H. (2019). Cadherin-Mediated Cell Coupling Coordinates Chemokine Sensing across Collectively Migrating Cells. *Current Biology*, 29:2570–2579.e7.

Concordet, J. P. and Haeussler, M. (2018). CRISPOR: intuitive guide selection for CRISPR/Cas9 genome editing experiments and screens. *Nucleic Acids Research*, 46:W242–W245.

Coombs, S. and Montgomery, J. C. (1999). The Enigmatic Lateral Line System. *Comparative Hearing: Fish and Amphibians*, pages 319–362.

Corwin, J. T. (1981). Postembryonic production and aging in inner ear hair cells in sharks. *The Journal of comparative neurology*, 201:541–553.

Corwin, J. T. (1985). Perpetual production of hair cells and maturational changes in hair cell ultrastructure accompany postembryonic growth in an amphibian ear. *Proceedings of the National Academy of Sciences of the United States of America*, 82:3911–3915.

Corwin, J. T. and Cotanche, D. A. (1988). Regeneration of sensory hair cells after acoustic trauma. *Science (New York, N.Y.)*, 240:1772–1774.

Corwin, J. T. and Warchol, M. E. (1991). Auditory hair cells: structure, function, development, and regeneration. *Annual review of neuroscience*, 14:301–333.

Cotanche, D. A. (1987). Regeneration of hair cell stereociliary bundles in the chick cochlea following severe acoustic trauma. *Hearing research*, 30:181–195.

Covault, J. and Sanes, J. R. (1985). Neural cell adhesion molecule (N-CAM) accumulates in denervated and paralyzed skeletal muscles. *Proceedings of the National Academy of Sciences of the United States of America*, 82:4544–4548.

Cruz, I. A., Kappedal, R., Mackenzie, S. M., Hailey, D. W., Hoffman, T. L., Schilling, T. F., and Raible, D. W. (2015). Robust regeneration of adult zebrafish lateral line hair cells reflects continued precursor pool maintenance. *Developmental biology*, 402:229–238.

Cruz, R. M., Lambert, P. R., and Rubel, E. W. (1987). Light microscopic evidence of hair cell regeneration after gentamicin toxicity in chick cochlea. *Archives of otolaryngology - head and neck surgery*, 113:1058–1062.

Cunningham, B. A., Hemperly, J. J., Murray, B. A., Prediger, E. A., Brackenbury, R., and Edelman, G. M. (1987). Neural cell adhesion molecule: structure, immunoglobulin-like domains, cell surface modulation, and alternative RNA splicing. *Science (New York, N.Y.)*, 236:799–806.

Dambly-Chaudière, C., Cubedo, N., and Ghysen, A. (2007). Control of cell migration in the development of the posterior lateral line: antagonistic interactions between the chemokine receptors CXCR4 and CXCR7/RDC1. *BMC developmental biology*, 7.

David, N. B., Sapède, D., Saint-Etienne, L., Thisse, C., Thisse, B., Dambly-Chaudière, C., Rosa, F. M., and Ghysen, A. (2002). Molecular basis of cell migration in the fish lateral line: Role of the chemokine receptor CXCR4 and of its ligand, SDF1. *Proceedings of the National Academy of Sciences of the United States of America*, 99:16297.

Davis, R. I., Ahroon, W. A., and Hamernik, R. P. (1989). The relation among hearing loss, sensory cell loss and tuning characteristics in the chinchilla. *Hearing research*, 41:1–14.

Dries, R. (2014). *Neuronale Zelladhäsionsmoleküle und ihre Glycanmodifikationen in der Entwicklung des Seitenlinienorgans von Danio rerio*. Master Thesis, KIT - Karlsruhe Institute of Technology.

Dries, R. (2018). *Neuronale Zelladhäsionsmoleküle im Zebrafisch: Divergente Funktionen und Wechselwirkungen während der Entwicklung und Regeneration des posterioren Seitenlinienorgans*. Dissertation, KIT - Karlsruhe Institute of Technology.

Dries, R., Lange, A., Heiny, S., Berghaus, K. I., Bastmeyer, M., and Bentrop, J. (2021). Cell Proliferation and Collective Cell Migration During Zebrafish Lateral Line System Development Are Regulated by Ncam/Fgf-Receptor Interactions. *Frontiers in cell and developmental biology*, 8.

Driver, E. C., Sillers, L., Coate, T. M., Rose, M. F., and Kelley, M. W. (2013). The Atoh1-lineage gives rise to hair cells and supporting cells within the mammalian cochlea. *Developmental biology*, 376:86–98.

Dykgraaf, S. (1933). Untersuchungen über die Funktion der Seitenorgane an Fischen. *Zeitschrift für Vergleichende Physiologie*, 20:162–214.

Dykgraaf, S. (1963). The functioning and significance of the lateral-line organs. *Biological Reviews*, 38:51–105.

El-Brolosy, M. A., Kontarakis, Z., Rossi, A., Kuenne, C., Günther, S., Fukuda, N., Kikhi, K., Boezio, G. L., Takacs, C. M., Lai, S. L., Fukuda, R., Gerri, C., Giraldez, A. J., and Stainier, D. Y. (2019). Genetic compensation triggered by mutant mRNA degradation. *Nature 2019 568:7751*, 568:193–197.

Esterberg, R., Hailey, D. W., Coffin, A. B., Raible, D. W., and Rubel, E. W. (2013). Disruption of intracellular calcium regulation is integral to aminoglycoside-induced hair cell death. *The Journal of neuroscience : the official journal of the Society for Neuroscience*, 33:7513–7525.

Esterberg, R., Hailey, D. W., Rubel, E. W., and Raible, D. W. (2014). ER-mitochondrial calcium flow underlies vulnerability of mechanosensory hair cells to damage. *The Journal of neuroscience : the official journal of the Society for Neuroscience*, 34:9703–9719.

Faucherre, A., Pujol-Martí, J., Kawakami, K., and López-Schier, H. (2009). Afferent neurons of the zebrafish lateral line are strict selectors of hair-cell orientation. *PloS one*, 4:e4477.

Fields, R. D. and Itoh, K. (1996). Neural cell adhesion molecules in activity-dependent development and synaptic plasticity. *Trends in Neurosciences*, 19:473–480.

Forge, A. and Schacht, J. (2000). Aminoglycoside antibiotics. *Audiology and neuro-otology*, 5:3–22.

Francavilla, C., Cattaneo, P., Berezin, V., Bock, E., Ami, D., Marco, A. D., Christofori, G., and Cavallaro, U. (2009). The binding of NCAM to FGFR1 induces a specific cellular response mediated by receptor trafficking. *The Journal of Cell Biology*, 187:1101.

Gamba, L., Cubedo, N., Lutfalla, G., Ghysen, A., and Dambly-Chaudiere, C. (2010). lef1 Controls Patterning and Proliferation in the Posterior Lateral Line System of Zebrafish. *Developmental Dynamics*, 239:3163–3171.

Gao, Y., Zhang, Y., Zhang, D., Dai, X., Estelle, M., and Zhao, Y. (2015). Auxin binding protein 1 (ABP1) is not required for either auxin signaling or Arabidopsis development. *Proceedings of the National Academy of Sciences of the United States of America*, 112:2275–2280.

Gascon, E., Vutskits, L., and Kiss, J. Z. (2007). Polysialic acid–neural cell adhesion molecule in brain plasticity: From synapses to integration of new neurons. *Brain Research Reviews*, 56:101–118.

Gennarini, G., Rougon, G., Deagostini-Bazin, H., Hirn, M., and Goridis, C. (1984). Studies on the transmembrane disposition of the neural cell adhesion molecule N-CAM. A monoclonal antibody recognizing a cytoplasmic domain and evidence for the presence of phosphoserine residues. *European journal of biochemistry*, 142:57–64.

Ghysen, A. and Dambly-Chaudière, C. (2007). The lateral line microcosmos. *Genes & development*, 21:2118–2130.

Giaever, G., Chu, A. M., Ni, L., and et. al. (2002). Functional profiling of the Saccharomyces cerevisiae genome. *Nature 2002 418:6896*, 418:387–391.

Gibson, D. G. (2011). Enzymatic assembly of overlapping DNA fragments. *Methods in enzymology*, 498:349–361.

Gibson, D. G., Young, L., Chuang, R. Y., Venter, J. C., Hutchison, C. A., and Smith, H. O. (2009). Enzymatic assembly of DNA molecules up to several hundred kilobases. *Nature methods*, 6:343–345.

Gilmour, D. T., Maischein, H. M., and Nüsslein-Volhard, C. (2002). Migration and function of a glial subtype in the vertebrate peripheral nervous system. *Neuron*, 34:577–588.

Gompel, N., Cubedo, N., Thisse, C., Thisse, B., Dambly-Chaudière, C., and Ghysen, A. (2001). Pattern formation in the lateral line of zebrafish. *Mechanisms of Development*, 105:69–77.

Gower, H. J., Barton, C. H., Elsom, V. L., Thompson, J., Moore, S. E., Dickson, G., and Walsh, F. S. (1988). Alternative splicing generates a secreted form of N-CAM in muscle and brain. *Cell*, 55:955–964.

Grant, K. A., Raible, D. W., and Piotrowski, T. (2005). Regulation of latent sensory hair cell precursors by glia in the zebrafish lateral line. *Neuron*, 45:69–80.

Haas, P. and Gilmour, D. (2006). Chemokine signaling mediates self-organizing tissue migration in the zebrafish lateral line. *Developmental cell*, 10:673–680.

Harris, J. A., Cheng, A. G., Cunningham, L. L., MacDonald, G., Raible, D. W., and Rubel, E. W. (2003). Neomycin-Induced Hair Cell Death and Rapid Regeneration in the Lateral Line of Zebrafish (Danio rerio). *JARO: Journal of the Association for Research in Otolaryngology*, 4:219.

He, H. T., Barbet, J., Chaix, J. C., and Goridis, C. (1986). Phosphatidylinositol is involved in the membrane attachment of NCAM-120, the smallest component of the neural cell adhesion molecule. *The EMBO journal*, 5:2489–2494.

Heiny, S. (2013). *Untersuchungen zur Funktion des neuronalen Zelladhaesionsmolekuels NCAM waehrend der Entwicklung des Seitenlinienorgans in Danio rerio.* Master of Science, KIT - Karlsruher Institut für Technologie.

Hemperly, J. J., Murray, B. A., Edelman, G. M., and Cunningham, B. A. (1986). Sequence of a cDNA clone encoding the polysialic acid-rich and cytoplasmic domains of the neural cell adhesion molecule N-CAM. *Proceedings of the National Academy of Sciences of the United States of America*, 83:3037–3041.

Hernández, P. P., Moreno, V., Olivari, F. A., and Allende, M. L. (2006). Sub-lethal concentrations of waterborne copper are toxic to lateral line neuromasts in zebrafish (Danio rerio). *Hearing Research*, 213:1–10.

Hernández, P. P., Olivari, F. A., Sarrazin, A. F., Sandoval, P. C., and Allende, M. L. (2007). Regeneration in zebrafish lateral line neuromasts: Expression of the neural progenitor cell marker Sox2 and proliferation-dependent and -independent mechanisms of hair cell renewal. *Developmental Neurobiology*, 67:637–654.

Hinsby, A. M., Lundfald, L., Ditlevsen, D. K., Korshunova, I., Juhl, L., Meakin, S. O., Berezin, V., and Bock, E. (2004). ShcA regulates neurite outgrowth stimulated by neural cell adhesion molecule but not by fibroblast growth factor 2: evidence for a distinct fibroblast growth factor receptor response to neural cell adhesion molecule activation. *Journal of Neurochemistry*, 91:694–703.

Hudspeth, A. J. (1989). How the ear's works work. *Nature*, 341:397–404.

Jacques, B. E., Montgomery, W. H., Uribe, P. M., Yatteau, A., Asuncion, J. D., Resendiz, G., Matsui, J. I., and Dabdoub, A. (2014). The role of Wnt/β-catenin signaling in proliferation and regeneration of the developing basilar papilla and lateral line. *Developmental Neurobiology*, 74:438–456.

Jiang, L., Romero-Carvajal, A., Haug, J. S., Seidel, C. W., and Piotrowski, T. (2014). Gene-expression analysis of hair cell regeneration in the zebrafish lateral line. *Proceedings of the National Academy of Sciences of the United States of America*, 111.

Jørgensen, O. S. and Bock, E. (1974). Brain specific synaptosomal membrane proteins demonstrated by crossed immunoelectrophoresis. *Journal of neurochemistry*, 23:879–880.

Kazmierczak, P., Sakaguchi, H., Tokita, J., Wilson-Kubalek, E. M., Milligan, R. A., Müller, U., and Kachar, B. (2007). Cadherin 23 and protocadherin 15 interact to form tip-link filaments in sensory hair cells. *Nature 2007 449:7158*, 449:87–91.

Kerstetter, A. E., Azodi, E., Marrs, J. A., and Liu, Q. (2004). Cadherin-2 function in the cranial ganglia and lateral line system of developing zebrafish. *Developmental dynamics : an official publication of the American Association of Anatomists*, 230:137–143.

Kettleborough, R. N., Busch-Nentwich, E. M., Harvey, S. A., Dooley, C. M., Bruijn, E. D., Eeden, F. V., Sealy, I., White, R. J., Herd, C., Nijman, I. J., Fényes, F., Mehroke, S., Scahill, C., Gibbons, R., Wali, N., Carruthers, S., Hall, A., Yen, J., Cuppen, E., and Stemple, D. L. (2013). A systematic genome-wide analysis of zebrafish protein-coding gene function. *Nature*, 496:494–497.

Kidd, A. R. and Bao, J. (2012). Recent advances in the study of age-related hearing loss: a mini-review. *Gerontology*, 58:490–496.

Kiernan, A. E., Pelling, A. L., Leung, K. K., Tang, A. S., Bell, D. M., Tease, C., Lovell-Badge, R., Steel, K. P., and Cheah, K. S. (2005). Sox2 is required for sensory organ development in the mammalian inner ear. *Nature*, 434:1031–1035.

Kimmel, C. B., Ballard, W. W., Kimmel, S. R., Ullmann, B., and Schilling, T. F. (1995). Stages of embryonic development of the zebrafish. *Developmental dynamics : an official publication of the American Association of Anatomists*, 203:253–310.

Kiselyov, V. V., Soroka, V., Berezin, V., and Bock, E. (2005). Structural biology of NCAM homophilic binding and activation of FGFR. *Journal of neurochemistry*, 94:1169–1179.

Kok, F. O., Shin, M., Ni, C. W., Gupta, A., Grosse, A. S., vanImpel, A., Kirchmaier, B. C., Peterson-Maduro, J., Kourkoulis, G., Male, I., DeSantis, D. F., Sheppard-Tindell, S., Ebarasi, L., Betsholtz, C., Schulte-Merker, S., Wolfe, S. A., and Lawson, N. D. (2015). Reverse genetic screening reveals poor correlation between morpholino-induced and mutant phenotypes in zebrafish. *Developmental cell*, 32:97–108.

Kozlovskaja-Gumbrienė, A., Yi, R., Alexander, R., Aman, A., Jiskra, R., Nagelberg, D., Knaut, H., McClain, M., and Piotrowski, T. (2017). Proliferation-independent regulation of organ size by Fgf/Notch signaling. *eLife*, 6.

Lange, A. (2019). *Investigations of the interaction of Fgf receptor Fgfr1a and neural cell adhesion molecule Ncam1 during development of the zebrafish posterior lateral line system.* Master Thesis, KIT - Karlsruhe Institute of Technology.

Langhauser, M., Ustinova, J., Rivera-Milla, E., Ivannikov, D., Seidl, C., Slomka, C., Finne, J., Yoshihara, Y., Bastmeyer, M., and Bentrop, J. (2012). Ncam1a and Ncam1b: two carriers of polysialic acid with different functions in the developing zebrafish nervous system. *Glycobiology*, 22:196–209.

Lecaudey, V., Cakan-Akdogan, G., Norton, W. H., and Gilmour, D. (2008). Dynamic Fgf signaling couples morphogenesis and migration in the zebrafish lateral line primordium. *Development (Cambridge, England)*, 135:2695–2705.

Ledent, V. (2002). Postembryonic development of the posterior lateral line in zebrafish. *Development (Cambridge, England)*, 129:597–604.

Lee, S. G., Huang, M., Obholzer, N. D., Sun, S., Li, W., Petrillo, M., Dai, P., Zhou, Y., Cotanche, D. A., Megason, S. G., Li, H., and Chen, Z. Y. (2016). Myc and Fgf Are Required for Zebrafish Neuromast Hair Cell Regeneration. *PLoS ONE*, 11.

Linbo, T. L., Stehr, C. M., Incardona, J. P., and Scholz, N. L. (2006). Dissolved copper triggers cell death in the peripheral mechanosensory system of larval fish. *Environmental toxicology and chemistry*, 25:597–603.

Lush, M. E., Diaz, D. C., Koenecke, N., Baek, S., Boldt, H., Peter, M. K. S., Gaitan-Escudero, T., Romero-Carvajal, A., Busch-Nentwich, E. M., Perera, A. G., Hall, K. E., Peak, A., Haug, J. S., and Piotrowski, T. (2019). scRNA-Seq reveals distinct stem cell populations that drive hair cell regeneration after loss of Fgf and Notch signaling. *eLife*, 8.

Lykke-Andersen, S. and Jensen, T. H. (2015). Nonsense-mediated mRNA decay: an intricate machinery that shapes transcriptomes. *Nature Reviews Molecular Cell Biology 2015 16:11*, 16:665–677.

López-Schier, H. and Hudspeth, A. J. (2006). A two-step mechanism underlies the planar polarization of regenerating sensory hair cells. *Proceedings of the National Academy of Sciences of the United States of America*, 103:18615–18620.

Ma, E. Y., Rubel, E. W., and Raible, D. W. (2008). Notch Signaling Regulates the Extent of Hair Cell Regeneration in the Zebrafish Lateral Line. *Journal of Neuroscience*, 28:2261–2273.

Mackenzie, S. M. and Raible, D. W. (2012). Proliferative Regeneration of Zebrafish Lateral Line Hair Cells after Different Ototoxic Insults. *PLoS ONE*, 7.

Maness, P. F. and Schachner, M. (2006). Neural recognition molecules of the immunoglobulin superfamily: signaling transducers of axon guidance and neuronal migration. *Nature Neuroscience 2007 10:1*, 10:19–26.

Marx, M. (2002). *Synthese, Expressionsmuster und Funktion von Polysialinsäure (PSA) während der Entwicklung des Nervensystems im Zebrafisch*. Dissertation, KIT - Karlsruhe Institute of Technology.

Matsuda, M. and Chitnis, A. B. (2010). Atoh1a expression must be restricted by Notch signaling for effective morphogenesis of the posterior lateral line primordium in zebrafish. *Development*, 137:3477–3487.

Matsui, J. I. and Cotanche, D. A. (2004). Sensory hair cell death and regeneration: two halves of the same equation. *Current opinion in otolaryngology and head and neck surgery*, 12:418–425.

McGraw, H. F., Drerup, C. M., Culbertson, M. D., Linbo, T., Raible, D. W., and Nechiporuk, A. V. (2011). Lef1 is required for progenitor cell identity in the zebrafish lateral line primordium. *Development*, 138:3921–3930.

Metcalfe, W. K., Kimmel, C. B., and Schabtach, E. (1985). Anatomy of the posterior lateral line system in young larvae of the zebrafish. *The Journal of comparative neurology*, 233:377–389.

Mizuno, T., Kawasaki, M., Nakahira, M., Kagamiyama, H., Kikuchi, Y., Okamoto, H., Mori, K., and Yoshihara, Y. (2001). Molecular diversity in zebrafish NCAM family: three members with different VASE usage and distinct localization. *Molecular and cellular neurosciences*, 18:119–130.

Montgomery, J., Carton, G., Voigt, R., Baker, C., and Diebel, C. (2000). Sensory processing of water currents by fishes. *Philosophical Transactions of the Royal Society of London. Series B: Biological Sciences*, 355:1325–1327.

Montgomery, J. C., Baker, C. F., and Carton, A. G. (1997). The lateral line can mediate rheotaxis in fish. *Nature 1997 389:6654*, 389:960–963.

Murakami, S. L., Cunningham, L. L., Werner, L. A., Bauer, E., Pujol, R., Raible, D. W., and Rubel, E. W. (2003). Developmental differences in susceptibility to neomycin-induced hair cell death in the lateral line neuromasts of zebrafish (Danio rerio). *Hearing Research*, 186:47–56.

Murray, B. A., Hemperly, J. J., Prediger, E. A., Edelman, G. M., and Cunningham, B. A. (1986). Alternatively spliced mRNAs code for different polypeptide chains of the chicken neural cell adhesion molecule (N-CAM). *Journal of Cell Biology*, 102:189–193.

Nacher, J., Alonso-Llosa, G., Rosell, D., and McEwen, B. (2002). PSA-NCAM expression in the piriform cortex of the adult rat. Modulation by NMDA receptor antagonist administration. *Brain Research*, 927:111–121.

Nagiel, A., Andor-Ardó, D., and Hudspeth, A. J. (2008). Specificity of afferent synapses onto plane-polarized hair cells in the posterior lateral line of the zebrafish. *The Journal of neuroscience : the official journal of the Society for Neuroscience*, 28:8442–8453.

Nagy, E. and Maquat, L. E. (1998). A rule for termination-codon position within intron-containing genes: When nonsense affects RNA abundance. *Trends in Biochemical Sciences*, 23:198–199.

Namdaran, P., Reinhart, K. E., Owens, K. N., Raible, D. W., and Rubel, E. W. (2012). Identification of Modulators of Hair Cell Regeneration in the Zebrafish Lateral Line. *The Journal of Neuroscience*, 32:3516.

Nechiporuk, A. and Raible, D. W. (2008). FGF-dependent mechanosensory organ patterning in zebrafish. *Science*, 320:1774–1777.

Neves, J., Kamaid, A., Alsina, B., and Giraldez, F. (2007). Differential expression of Sox2 and Sox3 in neuronal and sensory progenitors of the developing inner ear of the chick. *Journal of Comparative Neurology*, 503:487–500.

Nicolson, T. (2005). The genetics of hearing and balance in zebrafish. *Annual review of genetics*, 39:9–22.

Nikaido, M., Acedo, J. N., Hatta, K., and Piotrowski, T. (2017). Retinoic acid is required and Fgf, Wnt, and Bmp signaling inhibit posterior lateral line placode induction in zebrafish. *Developmental biology*, 431:215–225.

Nuñez, V. A., Sarrazin, A. F., Cubedo, N., Allende, M. L., Dambly-Chaudière, C., and Ghysen, A. (2009). Postembryonic development of the posterior lateral line in the zebrafish. *Evolution and development*, 11:391–404.

Oishi, N. and Schacht, J. (2011). Emerging treatments for noise-induced hearing loss. *Expert opinion on emerging drugs*, 16:235–245.

Owens, K. N., Cunningham, D. E., Macdonald, G., Rubel, E. W., Raible, D. W., and Pujol, R. (2007). Ultrastructural analysis of aminoglycoside-induced hair cell death in the zebrafish lateral line reveals an early mitochondrial response. *Journal of Comparative Neurology*, 502:522–543.

Peng, J. (2019). Gene redundancy and gene compensation: An updated view. *Journal of Genetics and Genomics*, 46:329–333.

Petit, C., Levilliers, J., and Hardelin, J. P. (2001). Molecular genetics of hearing loss. *Annual review of genetics*, 35:589–646.

Plech, M., Tomala, K., Tutaj, H., Piwcewicz, D. E., de Visser, J. A. G., and Korona, R. (2017). Power provides protection: Genetic robustness in yeast depends on the capacity to generate energy. *PLOS Genetics*, 13:e1006768.

Pujol-Martí, J. and López-Schier, H. (2013). Developmental and architectural principles of the lateral-line neural map. *Frontiers in neural circuits*, 7.

Raible, D. W. and Kruse, G. J. (2000). Organization of the Lateral Line System in Embryonic Zebrafish. *J. Comp. Neurol*, 421:189–198.

Raman, D., Sobolik-Delmaire, T., and Richmond, A. (2011). Chemokines in health and disease. *Experimental cell research*, 317:575.

Romero-Carvajal, A., Acedo, J. N., Jiang, L., Kozlovskaja-Gumbriene, A., Alexander, R., Li, H., and Piotrowski, T. (2015). Regeneration of Sensory Hair Cells Requires Localized Interactions between the Notch and Wnt Pathways. *Developmental cell*, 34:267–282.

Rossi, A., Kontarakis, Z., Gerri, C., Nolte, H., Hölper, S., Krüger, M., and Stainier, D. Y. (2015). Genetic compensation induced by deleterious mutations but not gene knockdowns. *Nature*, 524:230–233.

Roux, I., Safieddine, S., Nouvian, R., Grati, M., Simmler, M. C., Bahloul, A., Perfettini, I., Gall, M. L., Rostaing, P., Hamard, G., Triller, A., Avan, P., Moser, T., and Petit, C. (2006). Otoferlin, defective in a human deafness form, is essential for exocytosis at the auditory ribbon synapse. *Cell*, 127:277–289.

Rubel, E. W., Furrer, S. A., and Stone, J. S. (2013). A brief history of hair cell regeneration research and speculations on the future. *Hearing research*, 297:42–51.

Rutishauser, U. (1996). Polysialic acid in the vertebrate nervous system: a promoter of plasticity in cell-cell interactions. *Trends in Neurosciences*, 19:422–427.

Rutishauser, U. (2008). Polysialic acid in the plasticity of the developing and adult vertebrate nervous system. *Nature Reviews Neuroscience 2007 9:1*, 9:26–35.

Rutishauser, U., Hoffman, S., and Edelman, G. M. (1982). Binding properties of a cell adhesion molecule from neural tissue. *Proceedings of the National Academy of Sciences of the United States of America*, 79:685–689.

Ryals, B. M. and Rubel, E. W. (1988). Hair cell regeneration after acoustic trauma in adult Coturnix quail. *Science (New York, N.Y.)*, 240:1774–1776.

Santos, F., MacDonald, G., Rubel, E. W., and Raible, D. W. (2006). Lateral line hair cell maturation is a determinant of aminoglycoside susceptibility in zebrafish (Danio rerio). *Hearing Research*, 213:25–33.

Sapède, D., Gompel, N., Dambly-Chaudière, C., and Ghysen, A. (2002). Cell migration in the postembryonic development of the fish lateral line. *Development (Cambridge, England)*, 129:605–615.

Schindelin, J., Arganda-Carreras, I., Frise, E., Kaynig, V., Longair, M., Pietzsch, T., Preibisch, S., Rueden, C., Saalfeld, S., Schmid, B., Tinevez, J. Y., White, D. J., Hartenstein, V., Eliceiri, K., Tomancak, P., and Cardona, A. (2012). Fiji: an open-source platform for biological-image analysis. *Nature methods*, 9:676–682.

Seidman, M. D., Ahmad, N., and Bai, U. (2002). Molecular mechanisms of age-related hearing loss. *Ageing Research Reviews*, 1:331–343.

Shen, H., Glass, J. D., Seki, T., and Watanabe, M. (1999). Ultrastructural Analysis of Polysialylated Neural Cell Adhesion Molecule in the Suprachiasmatic Nuclei of the Adult Mouse. *Anat Rec*, 256:448–457.

Smith, G. M., Jacobberger, J. W., and Miller, R. H. (1993). Modulation of adhesion molecule expression on rat cortical astrocytes during maturation. *Journal of neurochemistry*, 60:1453–1466.

Song, J., Yan, H. Y., and Popper, A. N. (1995). Damage and recovery of hair cells in fish canal (but not superficial) neuromasts after gentamicin exposure. *Hearing Research*, 91:63–71.

Soroka, V., Kolkova, K., Kastrup, J. S., Diederichs, K., Breed, J., Kiselyov, V. V., Poulsen, F. M., Larsen, I. K., Welte, W., Berezin, V., Bock, E., and Kasper, C. (2003). Structure and interactions of NCAM Ig1-2-3 suggest a novel zipper mechanism for homophilic adhesion. *Structure*, 11:1291–1301.

Steiner, A. B., Kim, T., Cabot, V., and Hudspeth, A. J. (2014). Dynamic gene expression by putative hair-cell progenitors during regeneration in the zebrafish lateral line. *Proceedings of the National Academy of Sciences of the United States of America*, 111.

Stone, J. S. and Cotanche, D. A. (2007). Hair cell regeneration in the avian auditory epithelium. *The International journal of developmental biology*, 51:633–647.

Taylor, R. R. and Forge, A. (2005). Hair cell regeneration in sensory epithelia from the inner ear of a urodele amphibian. *The Journal of comparative neurology*, 484:105–120.

Thompson, J., Dickson, G., Moore, S. E., Gower, H. J., Putt, W., Kenimer, J. G., Barton, C. H., and Walsh, F. S. (1989). Alternative splicing of the neural cell adhesion molecule gene generates variant extracellular domain structure in skeletal muscle and brain. *Genes & development*, 3:348–357.

Tilley, C. A., Gutierrez, H. C., Sebire, M., Obasaju, O., Reichmann, F., Katsiadaki, I., Barber, I., and Norton, W. H. (2020). Skin swabbing is a refined technique to collect DNA from model fish species. *Scientific Reports 2020 10:1*, 10:1–17.

Ulitsky, I., Shkumatava, A., Jan, C. H., Sive, H., and Bartel, D. P. (2011). Conserved Function of lincRNAs in Vertebrate Embryonic Development despite Rapid Sequence Evolution. *Cell*, 147:1537–1550.

Undurraga, C. A., Gou, Y., Sandoval, P. C., Nuñez, V. A., Allende, M. L., Riley, B. B., Hernández, P. P., and Sarrazin, A. F. (2019). Sox2 and Sox3 are essential for development and regeneration of the zebrafish lateral line. *bioRxiv*, page 856088.

Valentin, G., Haas, P., and Gilmour, D. (2007). The Chemokine SDF1a Coordinates Tissue Migration through the Spatially Restricted Activation of Cxcr7 and Cxcr4b. *Current Biology*, 17:1026–1031.

Vandepoele, K., Vos, W. D., Taylor, J. S., Meyer, A., and Peer, Y. V. D. (2004). Major events in the genome evolution of vertebrates: paranome age and size differ considerably between ray-finned fishes and land vertebrates. *Proceedings of the National Academy of Sciences of the United States of America*, 101:1638–1643.

VeneroGalanternik, M., Kramer, K. L., and Piotrowski, T. (2015). Heparan Sulfate Proteoglycans Regulate Fgf Signaling and Cell Polarity during Collective Cell Migration. *Cell Reports*, 10:414–428.

White, J. K., Gerdin, A. K., Karp, N. A., Ryder, E., Buljan, M., Bussell, J. N., Salisbury, J., Clare, S., Ingham, N. J., Podrini, C., and et. al. (2013). Genome-wide generation and systematic phenotyping of knockout mice reveals new roles for many genes. *Cell*, 154:452.

Whitfield, T. T. (2002). Zebrafish as a model for hearing and deafness. *Journal of Neurobiology*, 53:157–171.

Wibowo, I., Pinto-Teixeira, F., Satou, C., Higashijima, S. I., and López-Schier, H. (2011). Compartmentalized Notch signaling sustains epithelial mirror symmetry. *Development (Cambridge, England)*, 138:1143–1152.

Williams, E. J., Furness, J., Walsh, F. S., and Doherty, P. (1994a). Activation of the FGF receptor underlies neurite outgrowth stimulated by L1, N-CAM, and N-cadherin. *Neuron*, 13:583–594.

Williams, E. J., Walsh, F. S., and Doherty, P. (1994b). The production of arachidonic acid can account for calcium channel activation in the second messenger pathway underlying neurite outgrowth stimulated by NCAM, N-cadherin, and L1. *Journal of neurochemistry*, 62:1231–1234.

Williams, J. A. and Holder, N. (2000). Cell turnover in neuromasts of zebrafish larvae. *Hearing Research*, 143:171–181.

Yamamoto, S., Jaiswal, M., Charng, W. L., Gambin, T., Karaca, E., Mirzaa, G., Wiszniewski, W., Sandoval, H., and et. al. (2014). A drosophila genetic resource of mutants to study mechanisms underlying human genetic diseases. *Cell*, 159:200–214.

Yorgason, J. G., Fayad, J. N., and Kalinec, F. (2006). Understanding drug ototoxicity: molecular insights for prevention and clinical management. *Expert opinion on drug safety*, 5:383–399.

Zhu, P., Ma, Z., Guo, L., Zhang, W., Zhang, Q., Zhao, T., Jiang, K., Peng, J., and Chen, J. (2017). Short body length phenotype is compensated by the upregulation of nidogen family members in a deleterious nid1a mutation of zebrafish. *Journal of genetics and genomics = Yi chuan xue bao*, 44:553–556.

9 Appendix

9.1 List of Figures

9.2 List of Tables

10 Abbreviations

Amp. diluent	Amplification diluent
bp	Base pair
BSA	Bovine serum albumin
BrdU	Bromodeoxyuridine
cDNA	Complementary DNA
CRISPR-Cas	Clustered, regularly interspaced short palindromic repeats - CRISPR associated systems
crRNA	CRISPR RNA
Cxcl	Cxc ligand
Cxcr	Cxc receptor
ddPCR	Droplet Digital PCR
DEPC	Diethyl pyrocarbonate
Dkk	Dickkopf
DMSO	Dimethyl sulfoxide
dpf	Days post fertilization
DSB	Double-strand break
E2/3	Embryo medium 2/3
Erm	Ets-related molecule (= Etv5)
Fgf	Fibroblast growth factor
FISH	Fluorescence *in situ* hybridization
FN-domain	Fibronectin type III domain
GOI	Genes of Interest
gDNA	Genomic DNA
GFP	Green fluorescent protein
HCG	Housekeeping genes
HSZs	Haarsinneszellen
hpf	Hours post fertilization
hpt	Hours post-treatment
IHC	Immunohistochemistry
Ig-domain	Immunoglobulin domain
ISH	*in situ* hybridization
pnm	Proneuromast
primI	Posterior lateral line primordium
L1/L2/L3	First/second/third neuromast deposited by primI
Lef1	Lymphoid enhancer-binding factor 1
MO	Morpholino
mRNA	Messenger ribonucleic acid
NBT/BCIP	Nitro blue tetrazolium chloride/5-Bromo-4-chloro-3-indolyl phosphate
n1b -/- Del	*ncam1b* deletion mutant
n1b -/- PMSC	*ncam1b* premature stop codon mutant

NCAM1	Neural Cell Adhesion Molecule 1
NMD	Nonsense-mediated mRNA decay
ORF	Open reading frame
PBS	Phosphate buffered saline
PFA	Paraformaldehyde
primI	Primary posterior lateral line primordium
pLLG	Posterior lateral line ganglion
pLLN	Posterior lateral line nerve
pLLS	Posterior lateral line system
pLLP	Posterior lateral line placode
pSLO	Posteriores Seitenlinienorgan
POD	Peroxidase
PTU	Propylthiouracil
RT-PCR	Reverse transcriptase PCR
Sef	Similar expression of Fgf
SSC	Saline Sodium Citrate
Sox2	Sex determining region Y-box 2
SEM	Standard error
tracrRNA	Trans-activating crRNA
UTR	Untranslated region

11 Acknowledgements

Zum Abschluss dieser Doktorarbeit möchte ich von Herzen all jenen danken, die mich in all dieser Zeit unterstützt und zum Gelingen dieser Arbeit beigetragen haben.
Mein ganz besonderer Dank gilt Prof. Dr. Martin Bastmeyer, der mir die Möglichkeit gegeben hat, mich intensiv mit dieser wissenschaftlichen Fragestellung auseinanderzusetzen. Für diese Chance bin ich Ihnen sehr dankbar.
Weiterhin möchte ich Dr. Joachim Bentrop für die unzähligen fachlichen Diskussionen und theoretischen Inputs danken, von denen ich enorm profitieren konnte. Lieber Joachim, Deine Unterstützung war für mich von unschätzbarem Wert - nicht nur Deine fachliche Expertise, die mir bei so vielen Fragen weiterhalf, sondern auch Deine menschliche Art. Du hattest immer ein offenes Ohr für mich und hast mich in schwierigen Phasen aufgemuntert und ermutigt weiterzumachen.
Prof. Dr. Nicholas S. Foulkes danke ich für die freundliche Bereitschaft, das Zweitgutachten zu übernehmen.
Auch Prof. Dr. Holger Puchta möchte ich für die Möglichkeit danken, ddPCR-Experimente in seinem Labor durchführen zu dürfen.
Meinen Kolleginnen und Kollegen am Institut möchte ich für ihre stete Hilfsbereitschaft und die wunderbare, unterstützende Zusammenarbeit danken. Wenn mein x-tes PCR-Experiment mal wieder nicht wie gewünscht verlief, haben die gemütlichen Kaffee- und Kuchenrunden mich mit einer willkommenen Ablenkung und einem Energieschub wieder auf Kurs gebracht.
Vielen Dank an Lukas G.! Unzählige Male haben wir gemeinsam Themen durchdiskutiert - das war so oft ein große Hilfe.
Liebe Elisa und liebe Magdalena, Ihr beide habt mir nicht nur als Mitstreiterinnen, sondern auch als Freundinnen immer wieder Zuversicht und Ermutigung geschenkt, wenn ich sie brauchte. Eure Freundschaft und der ein oder andere Aperol gemeinsam mit Euch, haben mir in schwierigen Momenten sehr viel bedeutet und mir Halt gegeben.
Ganz besonders möchte ich mich bei Kerstin Weber für ihre unschätzbare Unterstützung bedanken. Liebe Kerstin, nicht nur Deine tatkräftige Mithilfe beim Genotyping, ohne die ich mit Sicherheit nicht so zügig vorangekommen wäre, auch die gemeinsamen Tratschrunden mit Dir als Labortischnachbarin oder im Fischkeller waren sehr wertvoll für mich.
Liebe Ramona, schon während meiner Masterarbeit hast Du an mich geglaubt - dieser Glaube hat sich durch die Doktorarbeit fortgesetzt. Danke für die wertvollen Diskussionen mit Dir und Deine große Unterstützung durchs Korrekturlesen, auch wenn Du die letzten Jahre schon gar nicht mehr hier am Institut warst.
Meinen Eltern Britta und Joachim danke ich von Herzen! Ihr habt mir in all den Jahren bedingungslos den Rücken freigehalten und mich in jeder Lebenslage moralisch gestärkt. Ihr habt mich in all meinen Entscheidungen unterstützt. Vielen Dank!
Auch meinem Bruder Philip möchte ich von Herzen für seine immerwährende Unterstützung und aufmunternden Worte danken. Philip, ich danke Dir von Herzen für die unzähligen Stunden, in denen Du mir beim Formatieren dieser Arbeit geholfen hast.
Zu guter Letzt möchte ich meinem Freund Florian für seinen bedingungslosen Rückhalt, seinen Beistand und seine Unterstützung danken. Ohne Dich an meiner Seite hätte ich all dies niemals erreichen können. Danke, dass Du immer an mich geglaubt hast.